Project No. 37869

Novel Mobility Solutions for Extreme Lunar Terrain

A Major Qualifying Project
Submitted to the Faculty of
WORCESTER POLYTECHNIC INSTITUTE
In partial fulfillment of the requirements for the
Degree of Bachelor of Science
Submitted March 22, 2024

Benjamin Cobb (AE)	Alexa Dahlquist (AE)	Michael Gouveia (AE)	Finnian Hamblett (AE)
Roman Henry (AE)	Joseph Kuchenmeister (AE)	Cristina Perez (AE)	

Report Submitted to:

Professor Nikhil Karanjgaokar, Advisor, WPI

This report represents the work of seven WPI undergraduate students submitted to the faculty as evidence of completion of a degree requirement. WPI routinely publishes these reports on its website without editorial or peer review.

Abstract

The goal of this project is to demonstrate the viability of a walking hexapod design as an alternative rover mobility method in the hopes of advancing research on more practical means of extraterrestrial exploration over difficult terrain. The polar regions of the Moon have become areas of great interest to scientists because they have not yet been explored and may provide valuable insight into the many scientific questions of the universe, including the survivability of life in space. However, because of its extreme temperature fluctuations, mountains, craters, permanently shadowed areas, and rough terrain, the Lunar poles are extremely harsh and difficult to explore, particularly with traditional four-wheeled rovers. NASA has been investigating new ways to explore these harsh terrains and more inaccessible regions on the Lunar surface through innovative mobility techniques. Our team aims to help expand this research by developing a 6-legged rover prototype to demonstrate the viability of this mobility method on the Lunar poles. We designed a proposed rover that can explore the Lunar terrain and constructed a simplified prototype to demonstrate the viability of the design as well as the control and navigational systems. The selected hexapod design provides the rover with enhanced rotational mobility and more stable positions. Ultimately, the team's novel mobility rover aims to expand the research on alternative mobility rovers with the hopes of making Lunar, and eventually Martian, exploration in difficult terrains much easier.

Keywords: Hexapod, alternative rover mobility, Lunar poles, harsh terrain, proposed rover, simplified prototype

Acknowledgements

The team would like to thank Professor Nikhil Karanjgaokar for advising this project and providing assistance wherever it was needed. Additionally, we would like to extend our thanks to Professor Zachary Taillefer for setting up and managing the lab space for the assembly of our prototype. We are thankful for the assistance and advice of Professor Adrianna Hera on simulation analysis through lessons on how to utilize ANSYS and COMSOL. The team would also like to acknowledge the valuable assistance of several WPI students and alumni including Kelli Huang, Zack Stahl, Taylor Frederick, Arjun Ramakrishnan, Max McCalla, and Toby Enoch, whose efforts made the construction of the prototype and development of the navigational systems possible. Finally, we would like to acknowledge the contributions of the entire WPI Aerospace Engineering faculty, as without the knowledge and skills learned throughout our time at WPI, we would not have had the opportunity or knowledge to undertake this research endeavor.

Table of Contents

List of Figures

List of Tables

Table of Contributions		
Subsection	**Primary Contributors**	**Secondary Contributors/Editors**
Abstract		
	Lexi	Finn
Acknowledgements		
	Mike, Finn	Lexi
Introduction		
1	Mike	Mike, Lexi
Mission Planning		
2	Lexi	Mike
Background		
3	Mike	Mike, Lexi, Finn
3.1	Mike	Mike, Lexi, Finn
3.1.1	Mike	Mike, Lexi, Finn
3.1.2	Joey	Mike, Lexi, Finn
3.1.3	Cristina	Mike, Lexi, Finn
3.1.4	Finn	Mike, Lexi, Finn
3.1.5	Roman	Mike, Lexi, Finn
3.1.6	Lexi	Mike, Lexi, Finn
3.1.7	Ben	Mike, Lexi, Finn
3.2	Mike	Mike, Lexi, Finn
3.2.1	Joey	Mike, Lexi, Finn
3.2.2	Finn, Roman	Mike, Lexi, Finn
3.2.3	Ben	Mike, Lexi, Finn
3.2.4	Lexi	Mike, Lexi, Finn
3.2.5	Cristina	Mike, Lexi, Finn
3.2.6	Mike	Mike, Lexi, Finn
3.3	Mike	Mike, Lexi, Finn
Methodology		
4	Lexi	Mike, Lexi, Finn
4.1	Mike, Lexi	Mike, Lexi, Finn
4.2	Ben	Mike, Lexi
4.21	Ben	Lexi
4.22	Ben	Lexi
4.23	Ben	Lexi
4.3	Lexi	Lexi
Proposed Rover Design		
5	Lexi	Mike
5.1	Lexi	Mike

5.2	Lexi	Mike
5.3	Lexi	Mike
5.4	Lexi	Mike
5.5	Ben	Lexi
5.51	Ben	Lexi
5.52	Ben	Lexi
5.53	Ben	Lexi
5.54	Ben	Lexi
5.55	Ben	Lexi
5.56	Ben	Lexi
5.6	Ben, Mike	Lexi
5.7	Lexi, Ben	Lexi
Prototype Rover		
6	Ben	Lexi, Mike
6.1	Ben, Joey	Lexi, Mike
6.2	Ben, Mike, Joey	Lexi, Mike
6.3	Joey	Lexi, Mike
6.4	Ben, Mike	Lexi, Mike
6.4.1	Ben, Mike	Lexi, Mike
6.4.2	Ben, Mike	Lexi, Mike
6.4.3	Ben, Mike	Lexi, Mike
6.4.4	Mike	Lexi, Mike
6.5	Mike	Lexi, Mike
Simulations		
7	Finn	Mike, Lexi, Joey
7.1	Finn	Mike, Lexi, Joey
7.2	Finn	Mike, Lexi, Joey
7.3	Ben	Mike, Lexi, Joey
Prototype Rover – Fabrication and Assembly		
8	Mike	Lexi, Joey
8.1	Mike, Ben	Lexi, Joey
8.2	Mike, Ben	Lexi, Joey
8.3	Ben, Joey	Lexi, Joey
Rover Navigation and Controls		
9	Roman, Cristina	Mike, Finn
9.1	Roman, Cristina	Mike, Finn
9.1.1	Roman, Cristina	Mike, Finn
9.1.2	Roman, Cristina	Mike, Finn
9.1.3	Roman, Christina	Mike, Finn
9.2	Roman, Cristina	Mike, Finn
9.3	Roman, Cristina	Mike, Finn

Validation		
10	Mike	Lexi
10.1	Mike	Lexi
10.2	Mike	Lexi
10.3	Mike	Lexi
10.4	Mike	Lexi
10.5	Lexi	Mike
10.6	Lexi	Mike
Broader Impacts		
11	Finn, Mike	Mike, Joey
11.1	Finn, Mike	Mike, Joey
11.2	Finn, Mike	Mike, Joey
Conclusion		
12	Finn, Roman, Mike, Lexi	Joey, Mike, Lexi

1. Introduction

The Moon has always been a source of great mystery and curiosity to astronomers, scientists, and anyone who has gazed upon the night sky. Its overarching influence on society and science can be seen as far back as early religion, the first philosophers, and ancient time keeping. As our technological capabilities have advanced, scientific interest in understanding the Moon and discovering the answers it may hold has only heightened. This desire for understanding has led to the implementation of observational missions to the Moon, rovers to explore the Lunar surface, and manned missions to expand the reach of humanity, all of which have enabled research and exploration of this celestial body to an extent that was once unimaginable.

It has been over 50 years since humanity has last stepped foot on the Moon. However, new technology and a restored interest in space exploration have led to the conception of plans to return in the 21st century (*Why Has It Been 50 Years Since Humans Went to the Moon*, n.d.). NASA's Artemis program is the modern project to send people back to the Moon, and it consists of at least three missions (National Aeronautics and Space Administration, 2020). Artemis 1, which was completed in 2022, was an unmanned orbital mission to the Moon intended to test the Orion spacecraft and launch systems, which will be used for later manned Lunar missions (*Artemis I - NASA*, n.d.). Artemis 2 is planned for 2024, in which NASA will send a crew to orbit the Moon in preparation for Artemis 3, during which humans will return to the Lunar surface, this time to its South Pole. The main goal of these missions is to establish a human presence on the Lunar surface and further explore its unknown regions (NASA, 2024).

These missions aim for a much more in-depth exploration than previous programs, which has inevitably presented scientists with a new set of challenges. One of these obstacles stems

from the desire to explore some of the more unique areas of the of the Moon such as deep craters, Lunar caves, and polar regions. Many of these environments consist of extreme terrain involving features like steep slopes, corrosive regolith, and permanent daylight or darkness, which makes exploration with traditional wheeled rovers difficult or even impossible (*Designing Rovers for the Moon's Extreme Environment*, 2022). As a result, engineers and scientists have been tasked with developing new rover mobility solutions to better explore these harsh terrains. In 2022, NASA turned to the nation's university students through the BIG Ideas Challenge to help research and develop new, innovative solutions to locomotion on extreme Lunar terrain (*2022 Challenge Summary: Extreme Terrain Mobility*, 2022). While the competition has since concluded, the WPI aerospace engineering faculty has decided to build upon the challenge through an undergraduate Major Qualifying Project (MQP) in order to further develop new solutions to rover mobility.

Our team of students from Worcester Polytechnic Institute has researched an alternative mobility rover concept under the guidelines of this challenge and designed a proposed rover, V.E.C.T.O.R (Vehicle for Exploring Challenging Terrain, Obstacles, and Regions), that would be capable of completing a Lunar mission assuming a budget suitable for such a construction. The team has also proven the viability of the design and systems by successfully manufacturing and testing a simplified rover prototype using the available resources.

2. Mission Planning

The team's developed rover, V.E.C.T.O.R., would serve as a secondary payload aboard a spacecraft destined for one of the Lunar poles. It could travel aboard a number of existing launch systems depending on their mass capabilities, secondary payload envelope, component compatibilities, and Lunar destination.

The team's proposed rover has a total mass of approximately 756.77 pounds (343.265098 kg) and takes up a volume of about 77500 cubic inches (1.26999746 cubic meters) in its stowed configuration as shown in Figures 1 and 2 below. These mass and volume calculations are discussed in more detail in later sections about the proposed rover. It contains no explosives that would interfere with any components on the selected launch system.

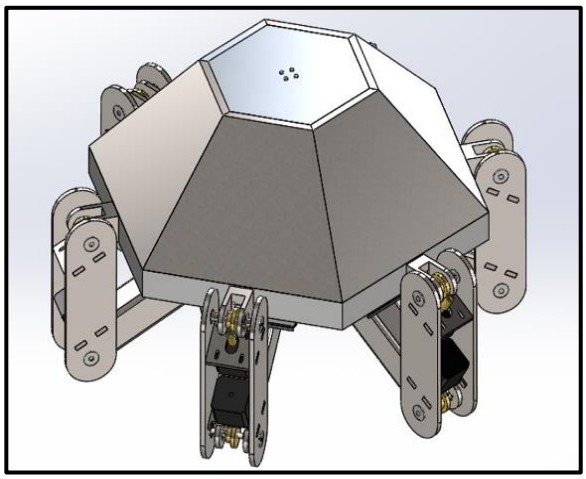

Figure 1: Isometric view of the rover in the stowed position

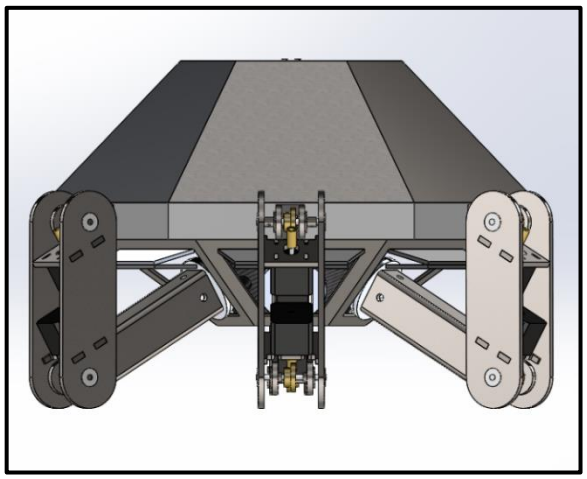

Figure 2: Side view of the rover in the stowed position

One example of a mission system that could be utilized by our team is NASA's Commercial Lunar Payload Services (CLPS), which "allows rapid acquisition of Lunar delivery services for payloads that advance capabilities for science, exploration, or commercial development of the Moon" (*CLPS Providers - NASA*, n.d.). There are currently fourteen vendors

working with NASA on this program for payload delivery including Astrobotic Technologies, Blue Origin, and Space X. The team's rover could be placed on any system that will be landing at either of the Moon's poles and has the capacity to carry a payload with a mass of about 345 kg and a volume of about 1.27 cubic meters. Some of the landers that fit these criteria are Astrobotic Technologies' Griffen Lander (*Lunar Landers | Astrobotic Technology*, 2024), Blue Origin's Blue Moon Mark 1 (Blue Origin, 2023), and Firefly Aerospace's Blue Ghost (Firefly Aerospace, 2024). Figures 3, 4, and 5 show each of these respective landers as computer generated models. The selection of the best CLPS system to transport our team's payload will heavily depend on the available budget and timeline of the project.

Figure 3: Griffin Lander (Lunar Landers, 2024). © 2024 Astrobotic Technology

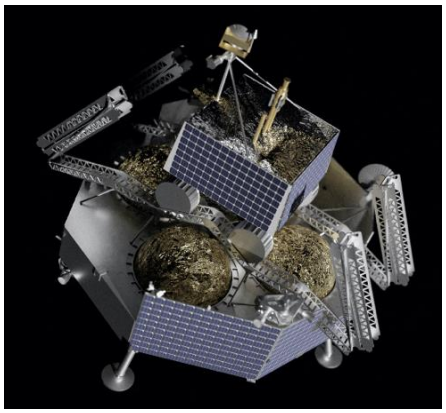

Figure 4: Blue Ghost (Firefly Aerospace, 2024). © 2024 Firefly Aerospace

Figure 5: Blue Moon Mark 1 (Blue Origin, 2023). © 2023 Blue Origin

V.E.C.T.O.R could also be transported to the Lunar pole through other projects like the Artemis missions, but the CLPS program is currently the most promising option for Lunar transportation for external groups. More time is needed for the CLPS program to develop and advance to the point where cargo and payloads can easily be sent to the Moon, but it will soon be ready to send projects like ours to explore the Lunar surface.

3. Background

Every Lunar rover has, so far, used wheels as the primary mobility method. This includes unmanned rovers from the USSR, China, and India as well as roving vehicles used by American Astronauts in 1971 and 1972 (Beck, 2021). With recently renewed interest in Lunar exploration, it has become vital to develop rovers that are able to explore more challenging Lunar environments to better explore the difficult and hard to reach regions of the Moon.

NASA's BIG Idea challenge in 2022 challenged university teams across the United States to develop new and innovative ways to explore the difficult environments present on the Moon. The Artemis Award, the competition's highest honor, was given to the team from Northeastern University for their rover COBRA: Crater Observing Bio-inspired Rolling Articulator, seen in Figure 6. This proposal was for a robotic explorer that could slither across the ground and tumble-down slopes.

Figure 6: Image of COBRA: Crater Observing Bio-inspired Rolling Articulator (NASA, 2022).

Other notable proposals included the University of Connecticut's Morphing Tank-to-Leg Modality for Exploratory Lunar Vehicles and the University of Maryland's TRAVELS rover. The rover proposed by the team from the University of Connecticut combined treads with legs, allowing the rover to roll on the treads or lift them vertically to use for walking. The rover designed by the team from the University of Maryland used legs with wheels on the bottom, allowing it to move its legs easily on flat ground. Both of these designs chose a quadruped configuration, which was common for proposals working with limited budgets. NASA has been developing a rover called, seen in Figure 7, which utilizes six legs for walking with a wheel on each for rolling, and is similar to the design proposed by the University of Maryland (*2022 Challenge Summary: Extreme Terrain Mobility*, 2022).

Figure 7: Image of NASA's Proposed ATHELE Rover Articulator (Collins, 2007). © 2007 NASA

The extra legs provide significant versatility to rovers in challenging terrain and increase overall stability but can cost significantly more money if the legs are complex, containing features such as multiple degrees of freedom. However, by utilizing legs with more degrees of freedom, ATHLETE would be able to handle steeper slopes than traditional, wheeled rovers without slipping.

These designs highlight a noticeable trend among modern rover designs; combinations of multiple mobility methods are often used to provide versatility for multiple types of terrain. The team sought to evaluate different mobility methods rovers can use for exploring Lunar terrain to establish which designs provide the most flexibility and how different methods can be combined. Combining multiple movement methods was not feasible within the constraints of our team's proposed rover but evaluating the mobility methods and terrain helped to develop the design and highlight areas for advancement.

3.1 Mobility Methods

Challenging terrain on the Lunar surface drives the need for novel mobility solutions that are more versatile than traditional wheeled rovers. In order to select the most suitable mobility method for challenging terrain, it is necessary to examine non-traditional mobility methods and compare the strengths and weaknesses of each. Many new designs for proposed Lunar rovers have incorporated multiple mobility methods to allow travel across multiple types of terrain. Research into many proposed rover designs resulted in seven non-wheeled mobility methods to be examined. Since our mission must not use wheels as the main source of mobility, the primary method for moving the rover must be one or multiple of the following: walking, slithering, tumbling, hopping, flipping, revolving gyroscopically, or grappling.

3.1.1 Walking

Walking is the most familiar non-wheeled mobility method and, as expected, has been used in numerous proposed rover designs, such as SpaceClimber (Bartsch, 2012). Walking provides the ability to traverse steep slopes and rocky terrain with ease. One downside of this method, specifically under the provided guidelines, is the costs associated with prototyping legs

containing multiple degrees of freedom. Adding more degrees of freedom to the legs will allow for a more versatile rover and will enable it to traverse difficult terrain more easily (Bartsch, 2012). However, this also requires the addition of more motors or actuators to drive the legs, thus increasing costs to prototype a viable design. A prototype could still be designed with fewer degrees of freedom to demonstrate movement in certain situations. Additionally, most proposed walking rovers utilize a hexapod design because it greatly increases the stability of the rover, but this can also increase manufacturing costs. Figure 8 below depicts an image of Boston Dynamic's walking robotic quadruped named Spot.

Figure 8: Boston Dynamic's walking robotic quadruped named Squat (Boston Dynamics, n.d.). ©2023 Boston Dynamics

3.1.2 Slithering

The slithering method is one of the most exotic, non-wheeled rover mobility methods. A rover that slithers would move in a similar manner to a snake and is most beneficial when soft robotics, the use of lighter, flexible materials, is desirable (Boston Dynamics, n.d.). This would likely result in a lower overall weight and cost, but the softer materials would not be suitable for the harsh Lunar environments. A slithering rover would be composed of several "modules" that are repeated to form a snake-like linkage system, each of which would need multiple actuators to

expand and contract, thus increasing cost (Boston Dynamics, n.d.). It is also difficult to accurately track the movement of the rover and correct the associated errors. Figure 9 below shows a rover that traverses the ground by slithering like a snake.

Figure 9: Example of a slithering rover with segments that expand and contract (NASA, 2022).

3.1.3 Tumbling

Tumbling rovers move by rotating their entire body to generate motion. When the external shell is strong enough, systems that rely on this method of mobility can traverse a wide range of terrains, including rough, rocky, or uneven surfaces, which traditional wheeled rovers tend to struggle with (NASA, 2022). Tumbling allows the rover to move in any direction, including sideways and upside down, which is useful for navigating obstacles or exploring small, complex spaces. Despite these benefits, this type of mobility requires precise control in order to navigate and land safely, particularly in low-gravity environments such as the Moon. It can be difficult to keep the rover's balance while falling and may cause vibrational harm to the sensitive internal components. The compact designs necessary for this would also limit the volumetric

space for scientific instruments and payloads. Tumbling and changing orientation both consume significant energy, which may limit the rover's overall operational time (NASA, 2022). Also, tumbling rovers may become stuck in a position where they are unable to regain mobility or communicate, which would render the mission ineffective.

3.1.4 Hopping

A rover that moves by hopping has been shown to work well with the Moon's low gravity. The most important consideration for a jumping robot is the balance required to stay oriented upright in midair because if the robot gets stuck on its back it may be helpless to right itself. Hills are specifically difficult for this mobility method because when the rover tries to bounce uphill, it can end up jumping at unintended angles and it is harder to get the traction required to hop up hills. Instructing the rover to hop to an extremely precise location is difficult for the operator, which can result in it hopping over the intended target, leading to inefficient movement toward the final objective (NASA. n.d.-c). The Lunar regolith can also slow rovers with this mobility type down significantly as dust covered components can prevent the ability to completely clear the ground. Also, the hopping mechanisms would require high bursts of energy to function and can cause vibrational harm to the rover’s internal (NASA. n.d.-c). One of the main advantages of this mobility method is that any minor obstacle, such as rocks or pits, can be easily circumvented by leaping over them. The downsides of this movement type can be significantly mitigated by using hopping as a secondary movement type to avoid obstacles that other mobility types cannot handle as well.

3.1.5 Slinky

The slinky mobility method is similar to hopping, but only the back legs initiate a jumping motion. The front legs always maintain contact with the ground, causing the robot to flip over in order to move. The back legs rotate to land, making these legs the new front legs of the system. This process repeats as the robot flips itself over continuously (see Figure 6). A benefit of this approach is that it allows the rover to maintain contact with the ground, and therefore is more stable than a hopping rover (NASA. n.d.-c). The shouldered joints required for this method mean that its legs would have enough mobility to land on extremely atypical, rough, and sloped terrain. Rovers utilizing this method still retains the ability to hop if it activates both sets of legs at once. However, it has similar downsides to hopping rovers in that it needs significant bursts of power for every movement, a potential issue depending on the discharge capabilities of the battery, it can easily become unstable in rough terrain, and it can cause vibrational harm to the components.

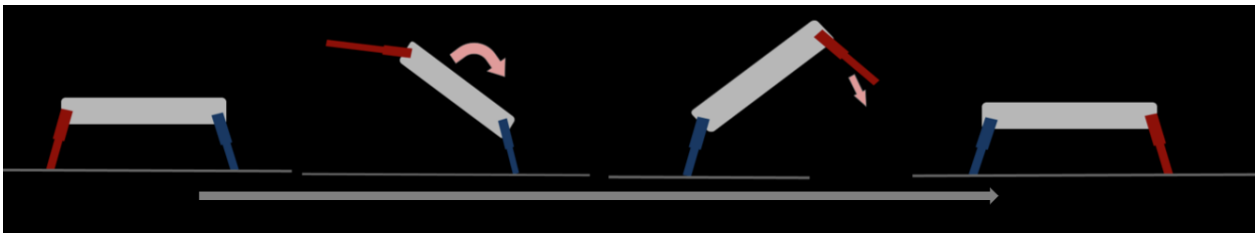

Figure 10: Diagram of how the slinky rover mobility method would function

3.1.6 Gyroscope

Gyroscopic mobility relies on the actuation of one or more centered wheels to propel and balance the device about its center of gravity (Figure 11). A rover driven by gyroscopic motion could be beneficial on the Lunar surface as it would be able to traverse the difficult terrain and avoid large obstacles easily. This type of mobility method requires a spherical body which is

beneficial because it can easily protect inner parts and electronics, maximizes available volume when compared to the surface area, and is good at counteracting the pressure in space (Kim Et al., 2020). There is a significant amount of research on gyroscopic driven robots, including ones designed for the Martian surface.

The incorporation of a gyroscope in the Lunar rover design inherently has the added benefit of stability in all positions and allows the rover to rotate freely in all directions, which would be helpful on the rocky terrain. Despite these mobility strengths, gyroscopic actuation presents many shortcomings when designed for the Lunar surface. It would require the use of powerful and expensive actuators that would take up a significant volumetric space. The spherical body in contact with the Lunar surface would make manufacturing, climbing steep slopes, and resisting slippery terrains all more difficult, and its ability to rotate in all directions would significantly complicate the control aspect of the rover. Overall, there may be some value in utilizing the spherical shape and gyroscopic stabilization as instrumentation in a rover, but its difficulty on slippery surfaces may interfere with its mobility function on the Lunar surface.

Figure 11: Inner workings of a gyroscopically propelled spherical rover (Kim Et al., 2020). © 2020 Springer

3.1.7 Tether/Grapple

Grappling is a method of movement that involves shooting a hook with an attached string and then using a winch to reel the rover toward the target location. The secondary mode of grappling is anchoring, which enables the rover to scale and descend from large objects as well as move horizontally (Kim Et al., 2020). The tether could also be attached at two different points, allowing it to move across the cord like a zipline. A main flaw of this system is that the parts for such a machine are complex and would require the hook/cabling to be easily reusable, thus increasing the overall cost of the rover. For instance, the launching mechanism would need to have high power parts capable of discharging quickly. It would also need to be resettable, such as with a spring-powered method. Grappling could also be friction and heat intensive, requiring significant cooling (Kim Et al., 2020). The grappling hook is intended to be used as a secondary mobility option with another method of translation serving as the primary method of movement.

3.2 Lunar Terrains

The ability of the rover to complete its exploration mission depends on its ability to traverse difficult terrain and many unexplored regions of the Moon. Any given design must prioritize the terrains that are most likely to be encountered when completing the mission but should also be able to traverse as many of the likely terrains as possible. The specific terrain and environmental classifications that are likely to be encountered on the Moon are icy regions, caves, steep slopes, rocky terrain, Lunar regolith, and dark environments. Analyzing these specific environmental challenges that a rover is likely to face helped the team in selecting a general design for the rover based on the compatible mobility methods for the most common terrains.

3.2.1 Icy Regions

Icy regions have been confirmed to exist on the Moon beneath the surface but are likely to only exist there because the Moon heats to over 250°F during the day (Sharp, *2023*). The areas covered in water ice are a vital resource for any human Lunar colonies as the water contained in these subterranean regions will allow astronauts to grow food, synthesize rocket fuel, and drink this necessary component of life. This water ice is much denser around the deep craters on the Lunar south pole, ranging from about 6.2 to 8.2 kilometers below the surface of the Moon where the sun never heats. These icy areas where the terrain can be slippery could pose major challenges to any robotic Lunar explorers. To be useful in such an environment, a system must be able to move across walls of deep Lunar caves and have enough traction on the frozen surface so as not to slip.

3.2.2 Lava Tubes / Caves

Lunar lava tubes are often cited as areas for humanity to set up bases on the Moon because of the thick layer of regolith preventing radiation and harsh temperature changes from damaging astronauts. These lava tubes were formed from basaltic lava flows that expanded through the Moon's surface until exposed to the open space. The cooling that resulted from this leaves a pit that can be more than a kilometer across at the entrance and stretch for miles under the surface of the Moon. (Figure 12) These tubes are unexplored by any astronaut or manmade rover, so scientists have little knowledge of the challenges often faced in this environment, other than what can be presumed. Darkness will be the first issue a rover has to contend with in a lava tube but extreme heat, large drops, uneven terrain, and more could lurk in the depths. On the other hand, that makes this location a valuable target for any explorer and scientist who wishes to learn about how our Moon was formed and continuously evolves.

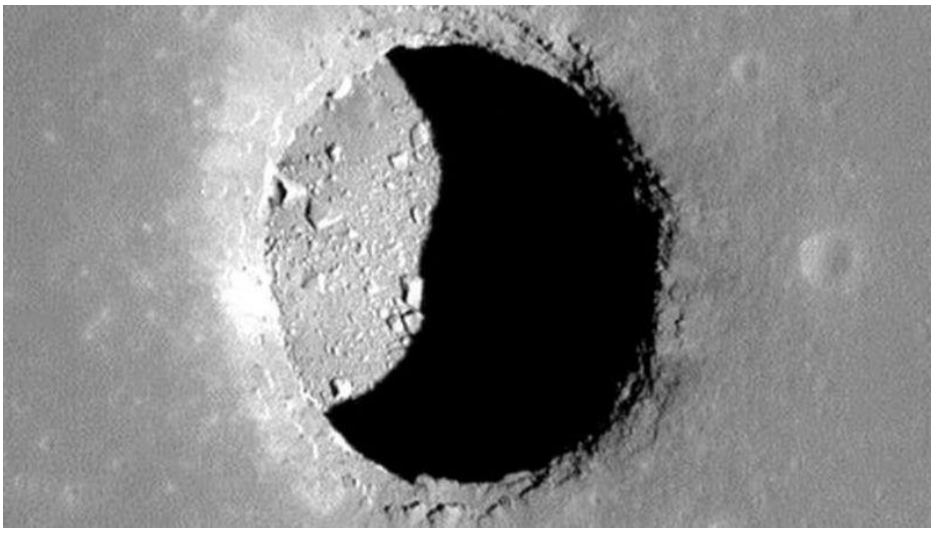

Figure 12: Image of a lava tube entrance on the surface of the Moon image (Rincon, 2015). © BBC 2015

3.2.3 Steep Slopes

With the numerous large craters on the Moon, there are naturally many steep slopes, which can be greater than 30°. This presents a significant problem for Lunar mobility, especially considering that these slopes are also covered in dusty regolith and small rocks. Maintaining traction and stability on these surfaces can become challenging, especially for rovers that use wheels or roll. Rovers that walk with legs need to be capable of retaining stability if regolith begins to displace and slide down the slope. This terrain is one of the most common and likely most detrimental to a rover if it causes the system to lose stability and topple over.

3.2.4 Rocky Terrain

The Lunar surface is covered in rocky debris, which must be considered when designing a Lunar rover, as it can interfere with both functionality and mobility. These rocks can range in size from boulders to grains of sand. They originated from asteroid impacts (Breccia), old volcanoes (Basalt), and solidified core fragments (Anorthosite) (NASA, 2023). Because of the variety in rocky obstacle sizes on the Lunar surface, a designed rover must be able to detect, maneuver around or over, and traverse effectively through fields of Lunar rocks and debris to successfully complete its mission.

3.2.5 Lunar Regolith

Regolith, also known as "Lunar soil," is a layer of loose, fragmented rock that covers the Moon's surface, and was likely formed as a result of continuous meteoroid impacts (NASA, 2003) "Lunar dust" is another term used for the finer particles of regolith. The Lunar maria are vast, dark plains where regolith can extend up to 5 meters down. The regolith in the Lunar highlands can reach depths of up to 10 meters, and even 15 meters in the older highlands.

Natural weathering on the Moon is impossible due to the lack of an atmosphere and flowing water. As a result, the regolith is very abrasive and sharp. This is problematic for electronics and spacesuits and can tear through or corrode many manmade components or materials.

3.2.6 Dark

While darkness itself is more of an environmental factor, not a terrain, it presents a unique set of challenges that must be overcome similarly to any of the terrains discussed. These darkness challenges are present alongside the challenges of the terrain in which the darkness occurs. Some of the terrains discussed will require a rover capable of operating in dark environments, such as caves or craters, but darkness could also be an inherent challenge of surface locations that have long periods without sunlight. The primary challenges presented by dark locations pertain to power. Because solar panels would not be a viable option, there may be navigation difficulties due to the limited visibility, communication problems due to the difficulty of clearly sending signals, and complex control requirements because the rover may not be able to communicate externally to receive new instructions.

The first of these problems mandates the use of either local power generation without solar panels, likely limiting the possibilities to a radioisotope thermoelectric generator, or batteries, which would require a power generation hub for the rover after completing a given mission. The benefit of the battery option is that it could also solve some of the secondary problems with navigation, communication, and control because it would likely improve the ability to communicate with the rover. This would, in turn, allow the control scheme to utilize less automation, and could potentially enable external communication to assist with navigation. However, because the rover's mission is exploration, it would likely be operating in areas that are not mapped in the level of detail required for navigation to be predetermined. This implies

that a realistic rover would need a method of gathering information locally to assist with navigation. Given the anticipated lack of natural light, any instrument intended to gather navigation information would need to either operate in darkness or generate its own light. One proposed solution to this is a cost-effective method of terrain mapping that utilizes light striping to identify obstacles, which was developed by the Robotics Institute at Carnegie Mellon (Haidar, 2020).

3.3 Conclusion

When considering the information above, it becomes clear that the mobility method and terrain challenges are inevitably linked. Any chosen rover design must use the mobility method, or methods, that allow it to overcome the most likely terrain challenges with ease. This is further constrained by the design limitations pertaining to budget and time, both of which are low for this project. With this in mind, the team chose a mobility method that could be executed within the given design constraints while retaining the ability to overcome as many terrain obstacles as possible. The team selected the walking mobility method because it is extremely versatile and can traverse many different types of terrain. This enabled the greatest flexibility in exploring the various unique regions of the Moon that are more difficult for traditional wheeled rovers.

4. Methods

In order to successfully complete this project, the team followed the engineering design approach outlined in Figure 13 below. As stated in the introduction and the background sections of this report, the team began by researching the problem at hand including rover history, mobility methods, and Lunar terrain and identifying the defining constraints of the project including budget, time, and mission goal. The team, after learning about the terrains and mobility types began brainstorming how to create a rover within the specified budget and time constraints. Multiple initials designs were considered including, but not limited to, a hopping rover that would rely on charged springs to a rover that used a tether with a sled-like bottom to glide on the Moon's surface. From here, the team finalized a viable design and began constructing a prototype rover with the available resources. Once completed, we added navigation and controls systems and tested our prototype, making improvements as needed. The following sections outline how the mobility method was selected and how the final rover idea was ultimately designed.

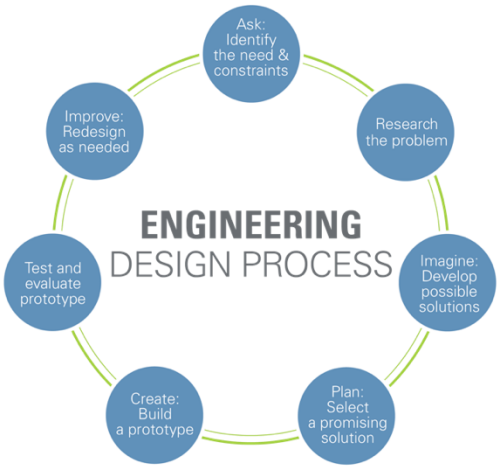

Figure 13: The Engineering Design Process followed by the team to create the rover (TeachEngineering, n.d.). © TeachEngineering

4.1 Mobility Method Selection

Before designing the rover, the team needed to select a general mobility method (or methods) that would be viable given the project's budget, time, and physical constraints. The team had only six months to design, fabricate, test, and validate a rover design, and the budget was relatively small for a project of this size at around $1,700. In addition, the project guidelines stated that the rover could not use the conventional wheeled design. These constraints along with a definitive mission goal were used to narrow the mobility selection process. We decided that the rover's mission would be to would be to explore one of the polar regions of the Moon, so it would need to be able to withstand cold, icy, and dark conditions along with the other terrain features found there like regolith, rocks, and steep slopes. Some general information that was considered when deciding upon a main mobility method can be seen below in Table 1 below.

Table 1: Color Coded Mobility Methods Cost-Benefit Analysis

Mobility method	Cost	Pros	Cons
Walking	Moderate	Simple movement, versatile over many terrains	Expensive for high DOF, inefficient on flat ground or shallow downhills
Slithering	High	Unique mobility method	Very expensive, complex movement, limited terrain advantages
Tumbling	Low	Simple movement, cost efficient	Complex control system, difficult survivability, limited terrain advantages
Hopping	Low	Cost efficient	Complex control system, difficult survivability, limited terrain advantages

Slinky	Moderate	Unique mobility method	Limited advantageous terrains, could be difficult to control
Gyroscope	High	Efficient mobility method	Expensive, difficult to design, complex control system, minimal versatility
Tether	High	Useful in extreme terrain	Expensive, difficult to design, minimal versatility, inefficient

Table 1 lists all the mobility methods considered for the team's rover and compares their cost, advantages, and disadvantages, which made the final selection process much easier. The cost column is color coded so that a higher cost is in red (less advantageous), and a lower cost is in green (more advantageous), with moderate cost in yellow (neutral). For the advantages column, the darker the shade of green the more beneficial these features are to the rover given the project constraints. For the disadvantages column, the darker the shade of red, the more detrimental the features are to the rover given the project's constraints. The information and color scheme in this table were generated by the team based on the mobility research found in the previous sections and the project guidelines.

As seen in Table 1, there were four mobility methods that the team estimated would have a moderate or low cost for developing a prototype, which was one of the main driving factors for the team's selection. Of these, the two lowest cost solutions, hopping and tumbling, were expected to have the lowest utility in the challenging terrain present on the Moon. Of the two moderately priced methods, walking and slinky, walking was deemed to have the highest versatility because of its ability to traverse slopes and uneven terrain. The other moderately costly option, slinky mobility, was expected to be difficult to control on uneven terrain. Since most missions to the Moon in the near future will likely be focused on exploration, the team believed that versatility was one of the most important features that our rover could have because

it would allow it to continue exploring regions of the Moon that could hold vital resources or scientific value.

The team's primary objective was to design a rover that could have a prototype built within budget and time constraints. Since the moderately priced walking mobility method appeared viable, the team decided to rule out the more costly and complex mobility methods of slithering, tethers, and gyroscope. These eliminations and clear advantages enabled the team to confidently select walking as the primary mobility method for the rover. The team also chose this with the knowledge that several other mobility methods, including wheels, could be added to a walking rover to extend its adaptability and versatility.

4.2 Design Methodology

In order to design the rover, the team began by outlining the primary challenges it would face maneuvering on the Moon and testing on Earth and used this information to build up the system requirements. As outlined in the background research, the challenges were primarily driven by terrain-based requirements as it would need to operate amidst regolith, steep slopes, rocks, darkness, and ice. Operating in and around such terrain requires a robust design capable of handling complex and diverse obstacles.

As previously stated, walking was determined to be the most feasible mobility method for operation in these environments due to its moderate cost, high versatility, and the relative system simplicity system. The primary design considerations specific to a walking rover were determined to be maneuverability, stability, and ability to navigate, although speed and ground clearance were also considered. After outlining these considerations, designs for specific rover components were made so that they would mitigate the expected disturbances or problems and

evaluated based on their manufacturability. This proposed design was then simplified so that a prototype could be built given the team's resources and budget.

4.2.1 Maneuverability

For a walking robot to be capable of locomotion, legs with multiple degrees of freedom are required. Selecting the number of degrees of freedom has a direct impact on the maneuverability of the rover as the more degrees of freedom used, the more robust the system can be. However, both the cost and complexity of the system increase substantially with more degrees of freedom. Considering this, the team determined that the minimum degrees of freedom required for a functional walking robot's leg should be selected.

A single degree of freedom leg does not have the required articulation to enable walking as a single appendage would simply sweep in an arc. The appendage would only contact the ground in one place and be unable to move. A two degree of freedom leg improves upon the single degree as it provides the ability to walk in a straight line because it allows for the adjustment of foot placement forward or backward. Despite this, it does not allow for any turning motion without dragging feet or legs across the Lunar surface in a pivoting maneuver. Such a maneuver would abrade the feet of the rover while also reducing its stability. To combat this, a third motor was added to allow for rotational motion without these consequences. This third degree of freedom allows the legs of the rover to pivot at the joint on the main body, allowing for turning actions to be completed either while walking or standing in place.

4.2.2 Stability

The rover will be required to traverse terrain in which steep slopes covered in regolith will likely be present. This means that the feet could be prone to slipping and that the rover must

prevent itself from tumbling. To protect the rover from tumbling and increase its overall stability, it needs to have a relatively low center of gravity and wide base. However, a rover with a center of gravity that is too low can prevent ground clearance and a rover whose base is too wide can be too large to maneuver easily. Reconciling these issues requires determination of the desired maximum obstacle size and slope for the rover to be capable of traversing. For the proposed rover, the system will be required to traverse obstacles of 30cm in height or less. For the prototype, the rover will be required to traverse obstacles of 15 cm in height or less without needing to circumvent them. This led to the determination of acceptable base and ground clearance specifications. Allowing for a 45° angle of the upper and lower legs with the ground, and a minimum 10 cm of clearance as a safety factor, led to a minimum combined leg length of 25 cm.

To protect from slipping, the rover requires feet which penetrate into the Lunar surface. To this end, spiked feet were attached to the legs in the proposed rover design but were not compatible with testing for the prototype due to a limited budget for test regolith. In addition to the wide base and spiked feet, 6 legs oriented in a hexapod configuration were decided upon for both the proposed rover and the prototype. This gives the option of having 5 stable legs in contact with the ground at any given time on treacherous terrain, further improving stability.

4.2.3 Navigation

For the rover to be able to navigate the terrain, digital mapping technology is required. One option for this is a visual reference database with image recognition software. This method requires advanced computing software as well as high resolution satellite imagery of the intended exploration area and was therefore excluded from consideration. Another option was using direct visual mapping using digital imagery. This method requires complex computational

methods as well as an onboard lighting system for use in dark regions. The computational complexity was ultimately deemed prohibitive for the purposes of this design. The final method considered was LiDAR point cloud mapping. Using a LiDAR sensor, a 3D point cloud rendering can be made of the terrain through which the rover is navigating. This method of navigation requires comparatively simple computational methods and is significantly more accurate than the other two methods. The major requirement of this system is the cost of the sensor itself. Ultimately, the ease of implementation and the improved accuracy led us to select LiDAR as our primary navigation method, despite the larger upfront cost.

4.3 Initial Designs

Based on the team's research and the project guidelines, we developed a few initial design concepts, the most promising of which being a rover with a hexagonal shelf, six protruding legs, and a protective shell. The team also discussed the possibilities of perusing a spherical rover, which was deemed incompatible with modern manufacturing and the limited budget, and a rover with four legs, which was ruled out for stability concerns given the likelihood of imperfect machined parts. A rudimentary CAD model of the decided upon walking hexapod design is shown in Figure 14 below. A more detailed version of the rover's shell is shown in Figure 15.

The team initially intended to design a rover where the legs could fold up inside of the body, which ultimately drove the size and design of the leg structure as well as its location on the rover body. In order for the legs to effectively fold up into the body, there needed to be space within the leg structure itself for one half to fold into the other half. This concept led to the initial design of the legs shown in Figure 16. One of the possible designs to support the folding functionality was making a portion of each leg also part of the exterior shell as shown in Figure

17. This would enable the rover to fold in its legs without taking up too much room inside of the shell but would also leave a gap that needed to be taken into consideration when the legs are not folded. The team also discussed the possibility of a foot swapping mechanism where the rover would be able to change out its feet depending on the terrain it encounters. Some initial mockups of this idea are shown in Figure 17.

It was eventually decided that this feature could reasonably be incorporated into the proposed rover design, but due to budget and time constraints, it could not reasonably be incorporated into the team's prototype. Ultimately, the basic ideas present in each of these initial concepts drove the overall final design of both the team's proposed and prototype rovers, but as new problems and ideas came to fruition, some of the designs had to be changed. Firstly, the lower shell of the rover was deemed inhibitive to the motion of the legs and had to be removed. Secondly, the requirement to implement a gearing system changed the position of the motors in the legs and removed the folding capability. Thirdly and finally, the design of the prototype rover needed to be simplified due to budget constraints and the foot wheel had to be removed from it. The wheel remained in place for the final proposed rover.

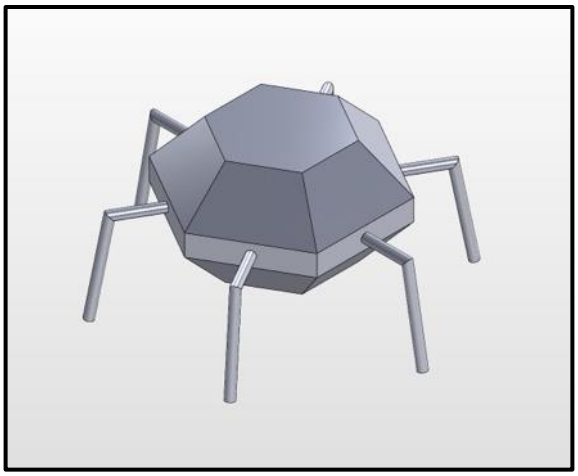

Figure 14: Basic CAD model of the initial hexapod design

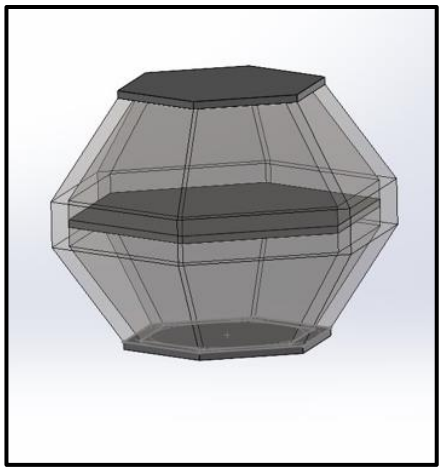

Figure 15: More detailed model of the rover shell

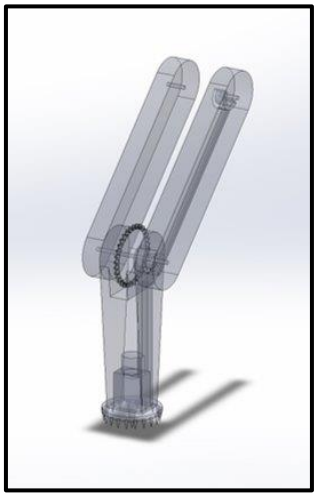

Figure 16: Initial leg design with room in the upper section for the lower section to fold into

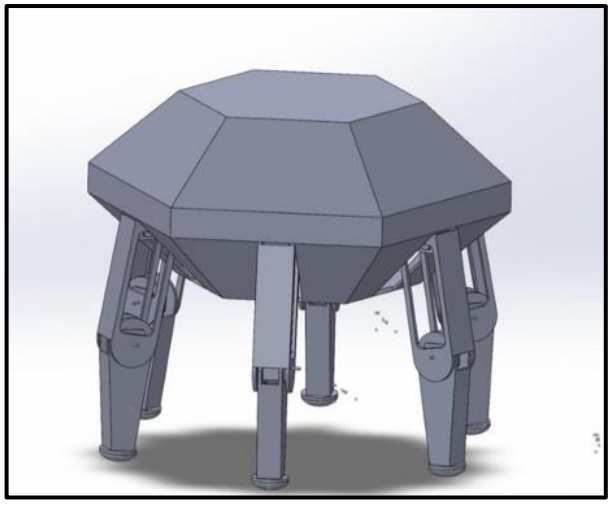

Figure 17: More detailed version of the initial rover design

5. Proposed Rover

With both the Lunar conditions and mobility solutions carefully considered, the team designed the body, legs, and feet that would best suit the rover and added the desired scientific and maneuverability features. This proposed design includes a hexagonal body with six legs total, each placed on the midpoint of a hexagon side as shown in Figure 18. The components exposed to the harsh Lunar conditions will be covered with a protective and radiation-resistant sheath that is not depicted in the CAD models. The upper panels of the body can hinge open to expose the inner solar panels as in Figure 19.

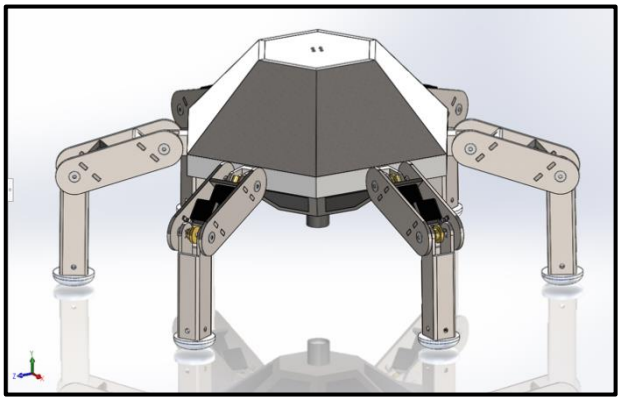

Figure 18: Isometric view of the proposed rover

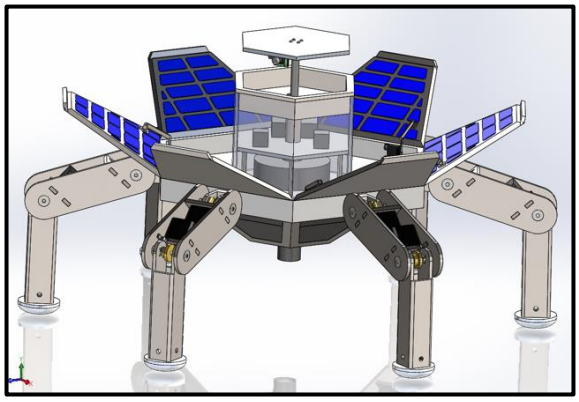

Figure 19: Isometric view of the proposed rover with upper panels open

At the top of the rover is a rotating, linearly actuated periscope containing a LiDAR, two low resolution cameras, and one high resolution camera as shown in Figure 20. With this periscope, the reflective material, and the sheath, this will form a relatively round high gain antenna dish that can be used for communication. There is a separate compartment on the bottom of the base (Figure 21) that contains a rotating wheel, into which the rover can insert its legs and swap out feet (Figures 22 and 23). This allows for the variation of feet textures for different terrains that may be encountered on the Moon. Each of these features and components will be described in greater detail in the sections below.

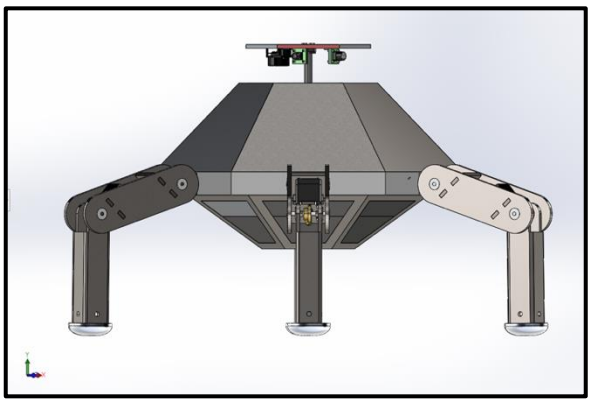

Figure 20: Periscope on the proposed rover

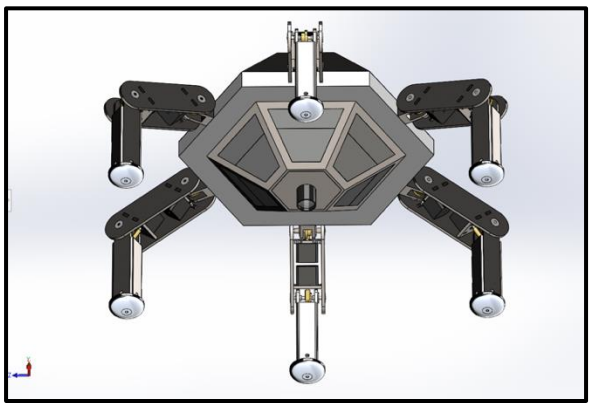

Figure 21: Bottom of the proposed rover

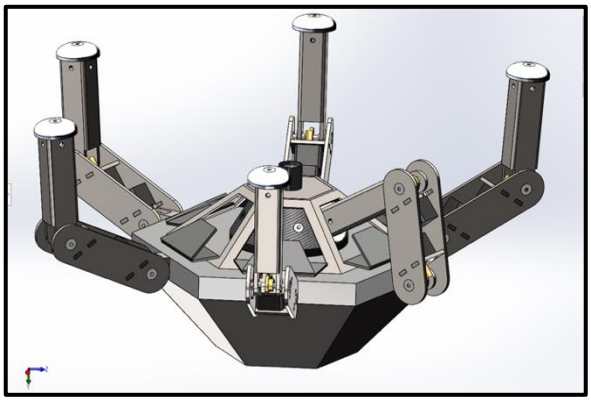

Figure 22: Bottom view of the proposed rover

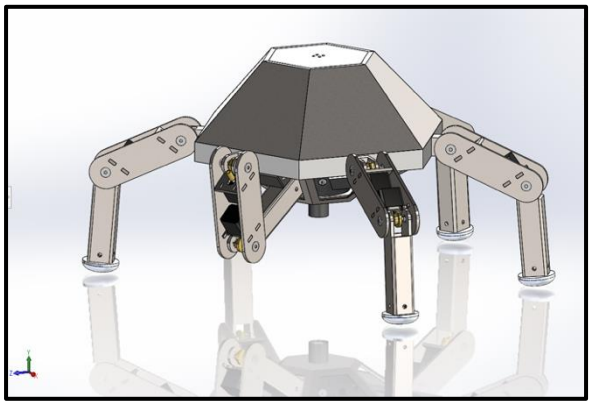

Figure 23: Proposed rover foot swap

5.1 Body

The body, shown in Figure 24, utilizes a symmetric hexagon divided into an upper and lower half. The shelf for the body, shown in Figure 25, which contains the interior components is made out of titanium and contains a number of bolt holes to attach the panel actuating motors and the central column. This part has a mass of about 126.44 pounds (57.3522192 kg) and has a surface area of 2730.13 square inches (1.76137067 square meters). The upper shell is comprised of 6 individual panels (Figure 26) that are able to hinge open. There is a tight seal between each (not pictured in Figures) in order to protect the internal components. The panels are made of titanium, and each have a mass of about 22.16 pounds (10.0516069 kg) and a surface area of about 467.91 square inches (0.30187682 square meters).

The team decided to place a series of thin, custom solar panel grids on the interior of each of the six panels to use for battery recharge and power (Figure 27). These would be purchased from an outside source and would vary in specific materials depending on the vendor chosen but would most likely be made out of gallium arsenide cells covered in thin glass. As an estimation, each grid would have a mass of about 1 pound (0.45359237 kg) and a total surface area of about 255.75 square inches (0.16499967 square meters).

As shown in Figure 28 there is also a shell attached to the bottom of the rover's shelf that houses the rotating foot carousel. This component has a frame and six foldable hinge flaps that open to allow the legs to enter. The frame of this system is made of titanium and has a mass of about 27.47 pounds (12.4601824 kg) and a surface area of about 889.62 square inches (0.57394724 square meters). Each panel is made out of 6061 aluminum alloy to reduce the weight that will be lifted to expose the wheel. They each have a mass of about 2 pounds (0.90718474 kg) and a surface area of about 154.60 square inches (0.0997417 square meters).

There are 6 industrial servo motors that control the opening and closing of the upper panels, which can be doubled in number for the sake of redundancy in the case of motor failures. There is also significant hardware in the body which includes motor mounts, hinges, pins, servo arms, spacers, bolts, nuts, and more. The details about the periscope that sits on top of the rover body are discussed in the next section. There is also a column of electronics surrounded by a radiation resistant shroud located in the center of the body, which will be further discussed in the electronics section.

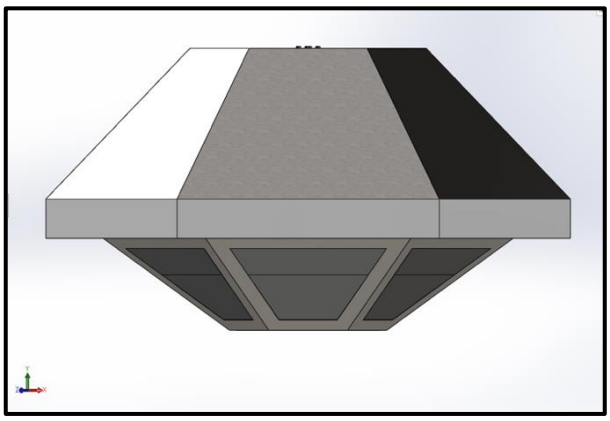

Figure 24: Body of the proposed rover

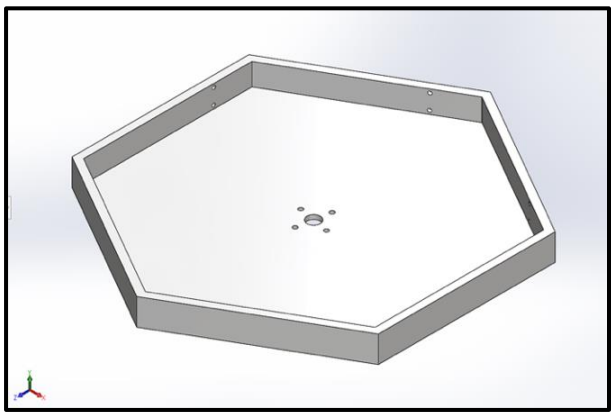

Figure 25: Shelf of the proposed rover

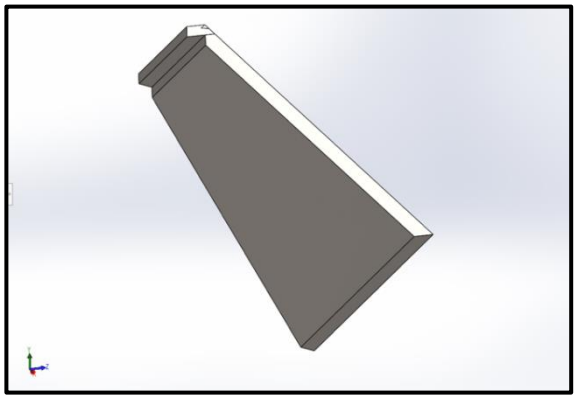

Figure 26: Upper panel for proposed rover

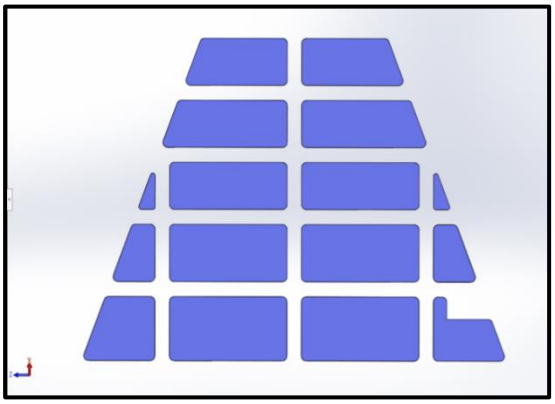

Figure 27: Solar panels for proposed rover

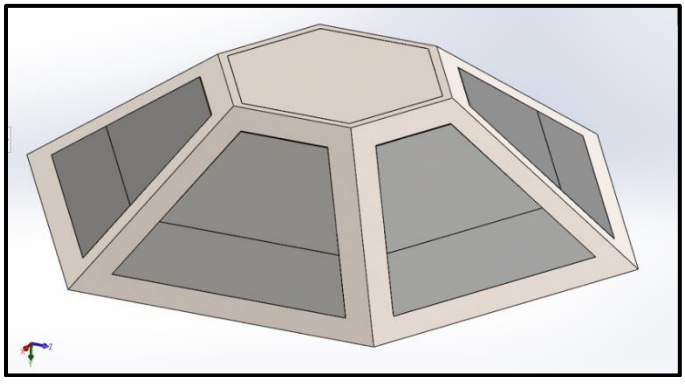

Figure 28: Bottom shell of the proposed rover

5.2 Periscope

The periscope system (Figure 29) sits at the top center of the rover body and is linearly actuated through the central column (Figure 30). Mounted underneath the periscope is the LiDAR, the high-res camera, and the low-res cameras, which will be discussed in further detail in the electronics section below. The hollow central column is used to mount components and to aid the linear actuator for the periscope (Figure 31). It is made out of titanium, has a mass of about 9.45 pounds (4.28644789 kg), and a surface area of about 196.15 square inches (0.12654813 square meters). The containment module (Figure 32) is a dish that encases the periscope and its electronics when the system is closed. It is made out of 6061 Aluminum Alloy, has a mass of about 16.15 pounds (7.32551677 kg), and a surface area of about 693.38 square inches (0.44734104 square meters). An aerospace grade linear actuator would be used to raise and lower the periscope and a servo motor would be used to rotate it. There is also significant hardware in the periscope system which includes mounts, bolts, nuts, and more.

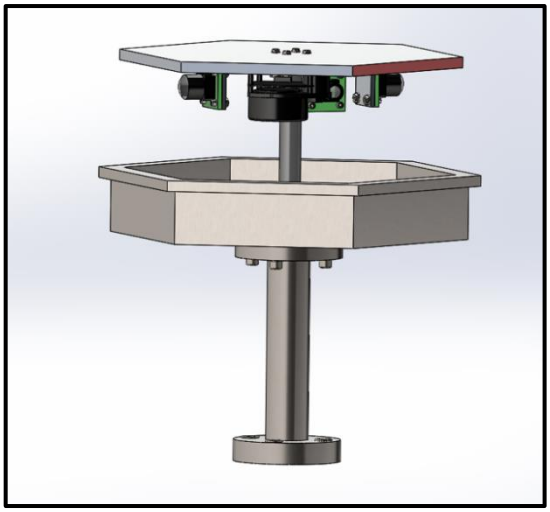

Figure 29: Periscope system on proposed rover

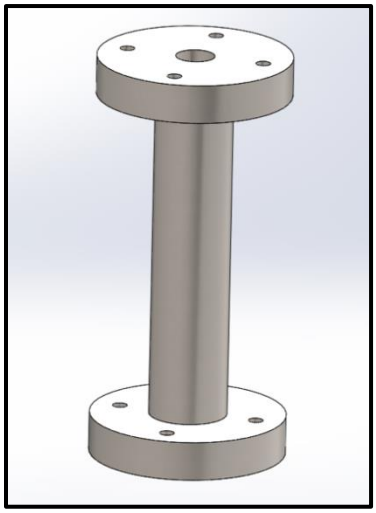

Figure 30: Central column for proposed rover

Figure 31: An example of a linear actuator that could be used on the proposed rover (Bullet Series 35 Cal. Linear Actuators, n.d.). © Firgelli

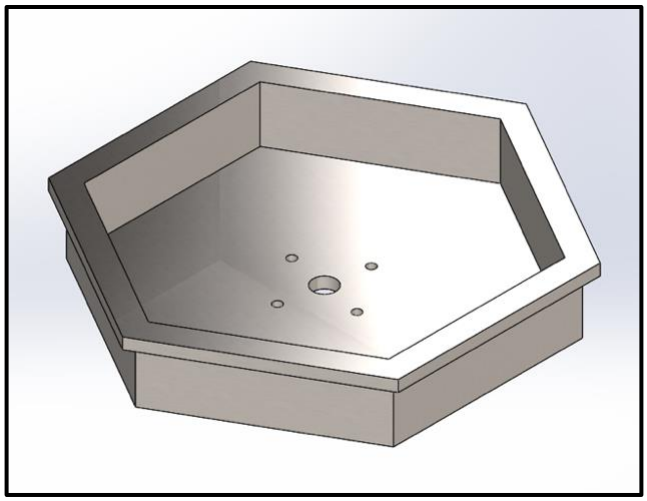

Figure 32: Containment module for the proposed rover

5.3 Legs

Each of the six legs are composed of an upper section, a lower section, a shoulder, and a foot. More details about the foot are discussed in the next section. One full leg system is shown in Figure 33 below. The lower section is simply one machined titanium part (or a collection of machined parts to form a unit) as shown in Figure 34. It is hollow so that electronics and magnets can run through the system to support the foot swapping mechanisms at the bottom. One lower section has a mass of about 12.45 pounds (5.647225kg) and a surface area of about 342.98 square inches (0.22127698 square meters).

The upper section consists of two titanium side plates and two 200:1 gear box systems, represented in the CAD models as a stepper motor, an axel, two flanges, a set of worm gears, and two bearings. These gear boxes would be outsourced from an external vendor to improve accuracy and reduce moto slippage. Figure 35 below shows the upper section of one of the proposed rover's legs. The lower gear box of this section controls the outward swing of the "knee joint" and the upper gear box of this section controls the vertical motion of the "shoulder joint." Each of the titanium side plates have a mass of about 6.15 pounds (2.78959307 kg) and a surface area of about 186.38 square inches (0.12024492 square meters). Each gearbox will vary in mass depending on the selected vender but will likely have a mass of around 0.374 pounds.

Figure 36 shows the shoulder joint component, a custom machined titanium part, located at the top of the leg, which controls the side-to-side motion of the system. This combination allows the leg to rotate 360° in order to generate a full step of the system. The side wall of the rover body needs to be made out of a flexible material to allow for the rotation of the shoulder. Since a solid wall would have supported a significant load here, the flexible material would need to be paired with a support structure capable of moving with the joint, using a roller system.

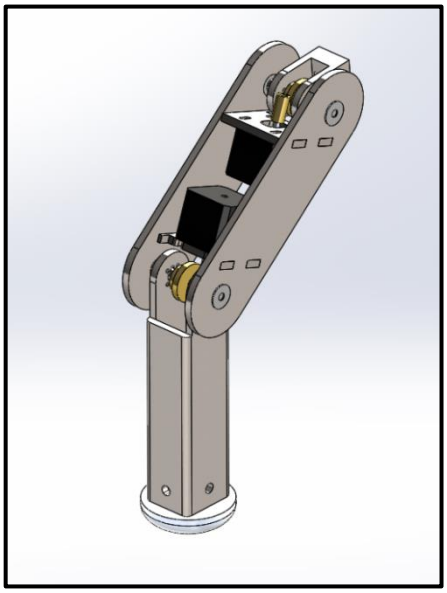

Figure 33: One full leg system of the proposed rover

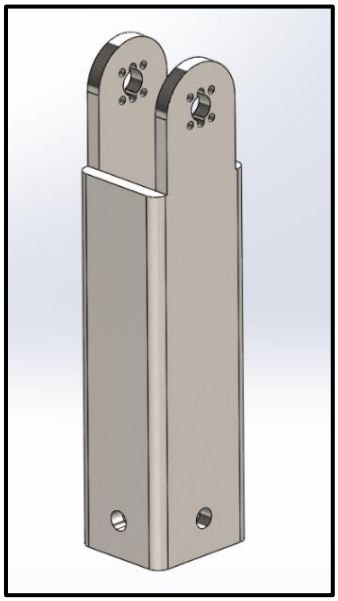

Figure 34: Lower section of one leg for the proposed rover

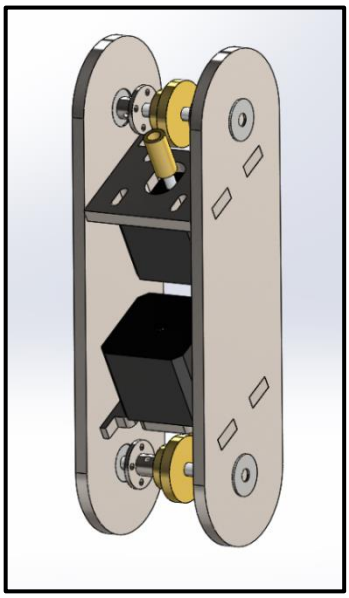

Figure 35: Upper section of one leg of prototype rover

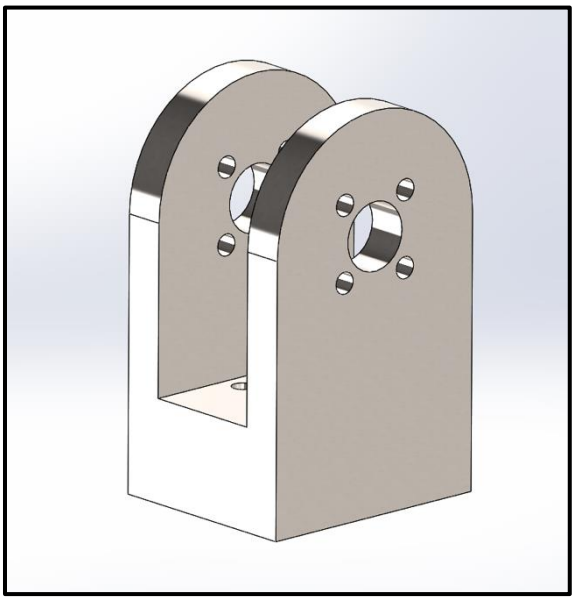

Figure 36: Upper shoulder joint of prototype rover

5.4 Feet

As stated in the previous section, attached to the bottom of each leg is a rounded foot (Figure 37) to help improve foot placement on non-flat surfaces like those typically found on the Moon. Each foot is made out of Aluminum 6061 to support the weight of the rover, has a mass of about 4.36 pounds (1.97766273 kg), and has a surface area of about 95.55 square inches (0.06164504 square meters).

One of the most unique features of the team'sproposed rover is its ability to change foot texture. This mechanical substitution of multiple foot variants allows the rover to adapt to different environments to improve stability and traction in the Lunar environment. At the bottom of each foot is a small hole, which would be covered in the case that there is no additional foot texture added to prevent regolith infiltration. This "changeout" is accomplished through the help of a rotating foot wheel located inside the lower shell of the rover.

This wheel is shown in Figure 38 below and houses all of the stored foot textures like extra spikes. It is made out of Hexcel AS4C (3000 Filaments) coated in a protective film, which has a mass of about 46.42 pounds (21.0557578 kg), and a surface area of about 629.12 square inches (0.40588306 square meters). The leg would fold into this lower shell after the corresponding flap opens, as shown in Figure 23 above. If there is already a texture on the foot, it would first align with an empty slot and the electromagnet system would be used to repel the old texture into the casing, then the wheel would rotate so that the foot aligns with a new texture. The electromagnet system would then be used to attach the new texture to the foot so that it can return to the surface. The foot would be secured in place via a permanent magnet and detached by powering on an electromagnet within the rover leg. This electromagnet would be polarized to repel the permanent magnet and release the foot from the leg housing. This design can easily be

extended to allow for instrumentation to be attached to the legs as well, providing the capability to precisely direct scientific instruments remotely.

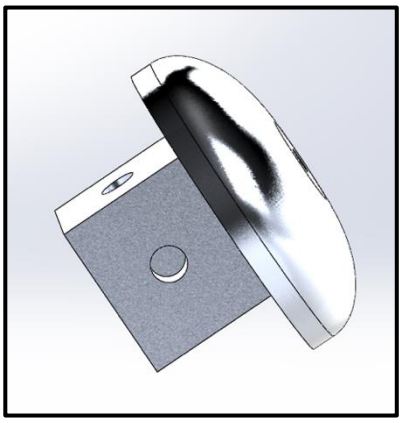

Figure 37: Foot for the proposed rover

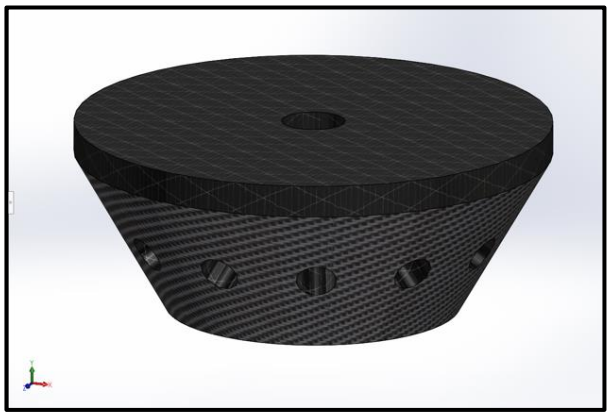

Figure 38: Rotating foot wheel for the proposed rover

5.5 Electrical

For the proposed rover, the electrical system consists of five primary subsystems: actuation, sensing, computation and control, thermal management, and power. These are discussed in the subsections below.

5.5.1 Actuation

Actuation includes the ability to attenuate every mechanical component on the proposed rover, including the periscope, shell, legs, and foot-wheel. The legs include 18 stepper motors and 18 rotary position sensors. Both the periscope and foot-wheel also require their own stepper motor and rotary position sensor. The periscope also requires a linear actuator so that it can be raised or lowered. Finally, the shell requires 6 servo motors to open and close as shown in Figure 20.

To ensure the motors do not experience over-torquing issues, high torque, Nema 24 stepper motors were selected for all 20 of the onboard stepper motors, and PST 360s were selected for the corresponding rotary sensors, which can provide accurate positioning of the stepper motors within 1% of actual position (Piher Sensing Systems, n.d.). Given the large 200:1 stepdown of the associated gearboxes, this would lead to a positional accuracy on each leg angle of 0.005% in either direction. The motors themselves are rated for 20-50V and 4A per phase (Applied Motion Products, 2024).

The linear actuator for the periscope needs to be powerful enough to lift it smoothly and repeatedly throughout its life. A bullet series 35 cal. linear actuator with a stroke length of 24 inches and a maximum loading of 270 pounds was selected for this purpose (Bullet Series 35 Cal. Linear Actuators, 2024). This provides ample weight capacity and will not wear quickly during operation. It is also dust rated, further protecting it from the Lunar environment. This is a 12V, 3.8A actuator.

Finally, the servo motors for the shell do not require large torque capacities like the rest of the rover. As such, we selected the BETU 50 kg servo motors, which are rated at 10-15V and 5.5A at max draw, but only 0.32A stationary draw (Applied Motion Products, 2024).

5.5.2 Sensing

The rover payload consists of two primary sensor types; cameras and LiDAR. A total of 3 cameras are included in the design on the underside of the periscope. The first camera is a high-resolution optical camera which can be used to take either video footage or still images in the direction the periscope is facing. The camera tentatively selected is a GS3-U3-89S6C-C 1” high performance color camera with an 8.9 MP resolution and a frame rate of 43 frames per second (fps) (Edmund Optics, 2024).

The second two cameras are both lower resolution cameras with wide angle lenses providing 185° overlapping view fields to allow for a total 360 degree view around the rover at all times. These cameras were selected to be the GS3-U3-23S6C-C 1/1.2" high performance color cameras with a 2.3 MP resolution and a frame rate of 162 fps (Edmund Optics, 2024). They were additionally equipped with an Edmond's Optics fisheye lens to provide the desired field of view. All 3 cameras are USB powered and can be connected directly to the rover's computer core for image handling.

The LiDAR sensor chosen is a Velarray M1600 due to its wide field of view (32° vertical view field and 150° horizontal view field) and good perception range (0.1 to 30 meters), providing all the 3D mapping capabilities required for the rover (Velarray M1600, n.d.)

5.5.3 Computation and Control

To control the rover, a Unibap AB SpaceCloud iX5-106 computer is used. The price data for space system's onboard computer modules is not published, but we estimate roughly $25000 based on similar models and functionality price rates. In terms of performance, the computer provides I2C and SPI addressing to allow for the control of multiple systems on the rover. It also has 5 separate serial ports for gathering data from sensors such as the cameras and LiDAR. Additionally, the computer has redundant 120 GB solid state hard drives and 2 GB of DDR3 ram, allowing for significant onboard processing and storage.

For motor control, a bank of 20 DM556 stepper motor drivers were selected to operate the stepper motors. Each driver is rated for motors of up to 48V and 5.6A per phase, making them perfectly suited for the selected stepper motors. Additionally, each driver has built in overvoltage and overcurrent protection (AutomationDirect, 2024). These electronics as well as

some mentioned in the following sections will be stored in the central column of the rover (shown in Figure 39 below), which is protected by a radiation resistant shroud.

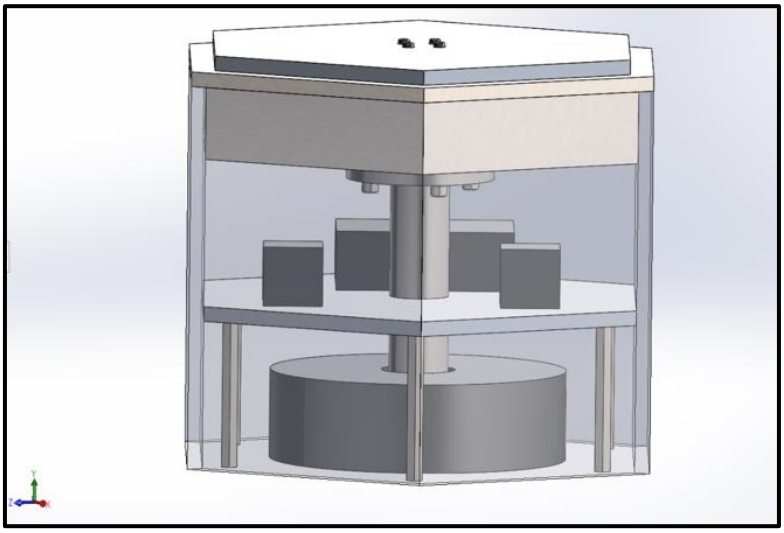

Figure 39: Central column of the rover where most of the electronics will be stored

5.5.4 Thermal Management

This system will include a heater to keep the electronics within safe operating temperatures. It will heat the top half of the rover interior, which will be insulated from the exterior and from the bottom of the rover interior. The heaters are unnecessary during sunlight hours on the Moon, but during the nighttime hours, a total heat generation of 50 watts is required to keep the rover's electronics within a safe operating range (as shown in thermal simulations).

5.5.5 Power

The power system is composed of the solar arrays and the custom "donut" shaped battery located on the base of the rover's main body. The battery needs to provide power to 18 stepper motors, 6 servo motors (as holding power), and the computer simultaneously. Given the voltage and amperage of the stepper motors, they require 160 W per motor. The servo motors require 4.8

W per motor, and the computer requires as much as 30W. The cameras and LiDAR sensor don't have published wattages, but we have a max estimate of 30W each based on similar products. This provides a total wattage requirement of 3.03kW. Given a 12 kWh battery, the rover would have a 4 hour range during nighttime operations if all motors are running simultaneously. In nominal operations under a tripod gate condition, only 3-9 motors would run simultaneously for most of the movement, with roughly a 5 motor average. This would provide a significantly reduced wattage requirement of 950 W, allowing for a 12.6 hour range during nighttime operations.

The solar array spans the internal surface area of the upper shell (see Figure 20), covering a total of 0.990 m^2. Using Gallium Arsenide panels, which have a maximum production efficiency of 46% (Papež Et al., 2021), and given a solar energy flux of 1367 W/m^2 on the Moon in full sunlight, the panels have a maximum power generation of approximately 480 W. This would reduce the load on the battery substantially, increasing the range to 4.71 hours with all motors in full operation and 25.5 hours with the 5-motor average during daytime operations in full sunlight. Additionally, by reducing the power to only computer operation, the rover would only have a 30 W power draw during daytime operations at rest, allowing it to recharge its battery fully in 26.7 hours.

5.5.6 Electrical System Summary

The electrical system of the rover consists of a total of 27 actuators, 20 motor controllers, a computing unit, a large solar array, and a sizeable battery. Given this design, the rover is capable of semi-autonomous missions ranging several hundred hours from the base station during the day, and 6 hours from the station during nighttime operations.

5.6 Communications

Communications are an essential component for most aerospace applications to relay data or to facilitate operation. This system is made far more difficult for the team's proposed rover because we would need to rely on additional resources for communication with Earth. Considering the proposed rover's mission, VECTOR would need to rely on preexisting Lunar orbiters to assist with communication to Earth. This presents the additional challenge of coordinating data transfer with an orbiting satellite. The communication system would need to use software tools to solve this issue and ensure that selected hardware could enable sufficient data transfer rates.

The communications software onboard the proposed rover would need to account for the limited time periods during which communication to the orbiter was possible. This means that communications would need to be batched. The specific method used to batch data for transfer would depend on the user's preferences but would need to consider the amount of data to be transferred in a given period and the priority of data. In order to determine the data to be transferred, the on-board computer would need to perform some preprocessing. Additionally, the amount of data that could be transferred may vary depending on the orientation of the Lunar orbiter or whether other tasks were being performed on either the orbiter or rover. Given the mission plan for VECTOR, one potential orbiter is the Lunar Reconnaissance Orbiter (LRO), which is shown in Figure 40 below. LRO entered a polar orbit in 2015 and would be capable of communicating with a rover on the surface (NASA, n.d.-a). Depending on specific instrumentation, additional orbiters may be desirable to allow specific data transfers.

Figure 40: The Lunar Reconnaissance Orbiter (NASA, n.d.-a). © NASA

Communications on the rover would be performed by an antenna. The team determined that the solar array could also be used as a semi-parabolic dish for a high gain antenna, with the underside of the periscope acting as the signal receiver. To accomplish this, the solar array could be coated with a dielectric coating. Dielectric coatings can be tailored to be reflective to specific wavelengths (Online, 2023). This would allow the primary wavelengths of light used for power generation to pass through the coating and be absorbed by the array, while the waveband selected for communication would be reflected from the surface and redirected to the receiver. Due to the flat shape of the panels the dishes would not be as effective as a true parabolic antenna, however they could approximate the shape and improve range of communication to a low Lunar orbit, if not further.

5.7 Cost analysis

Table 2 below shows a calculated cost estimation for the proposed rover. Most of the estimations for manufactured parts are based on the current cost of the corresponding material per pound, but not that as the materials' market values change, the cost of the rover will also

fluctuate slightly. There are also some estimates made based on unit prices for components that will likely be sourced externally. The hardware and manufacturing costs are a very rough estimation based on experience, the design, and general costs, but may vary significantly by vendor, issues, and changes. Ultimately, the overall total estimated cost for the proposed rover is about $60,894.19 but may vary based on the factors previously described.

Table 2: Cost estimations for the proposed rover based on component

Proposed Rover Cost Estimate					
Component	**Material**	**Price**	**Unit Value (mass, W)**	**Quantity**	**Estimated Cost**
Shelf	Titanium	$ 22.50/lb	126.44 lbs	1	$ 2,844.90
6 Panels	Titanium	$ 22.50/lb	22.16 lbs	6	$ 2,991.60
Solar Panel Grids	Gallium Arsenide	$0.60/W	80 W	6	$ 288
Bottom Frame	Titanium	$ 22.50/lb	27.47 lbs	1	$ 618.08
Bottom Panels	Al 6061	$ 1.00/lb	2 lbs	6	$ 12.00
Central Pole	Titanium	$ 22.50/lb	9.45 lbs	1	212.63
Containment Module	Al 6061	$ 1.00/lb	16.15 lbs	1	16.15
Linear Actuator	N/A	$189/component	3.7 lbs	1	$189
Lower Leg Section	Titanium	$ 22.50/lb	12.45 lbs	6	1680.75
Upper Leg Pannels	Titanium	$ 22.50/lb	6.15 lbs	12	1660.50
Foot Wheel	Hexcel AS4C (3000 Filaments)	$53/lb	46.42 lbs		242.421
Feet	Al 6061	$ 1.00/lb	4.36 lbs	6	$26.16
Foot Textures	Many	Many	N/A	Many	$200
Servo Motors	N/A	$422	1.2	6	$2532
Stepper Motors	N/A	$205	3.1	18	$3690
Gearboxes	N/A	$685	0.374	18	$12330
Hardware	N/A	N/A	N/A	N/A	$500

Manufacturing Cost	N/A	N/A	N/A	N/A	$15000
Motor Controller	N/A	$43	N/A	20	$860
Computer Module	N/A	$25000	N/A	1	$25000
Total	N/A	N/A	N/A	N/A	$70,894.19

6. Prototype Rover

Due in large part to the significantly high cost of producing the proposed rover, a simplified prototype was developed to demonstrate the feasibility of the rover and its systems within the confines of the team's budget. This led to redesigns, mainly simplifications, of all the major components within the rover to aid in cost effectiveness and manufacturability. It also resulted in the removal of several key features of the proposed rover for the prototype. With the significant budget constraints, it was simply not possible for many features of the proposed rover to be built or tested on the prototype. With this in mind, the goal of the prototype was to create a hexapod rover capable of walking independently across various types of terrain. This would demonstrate the viability of the general design elements without complex hardware and prove that the software elements required for an actual Lunar rover could be implemented with realistic hardware. Figure 41 shows a SolidWorks model of the designed prototype rover.

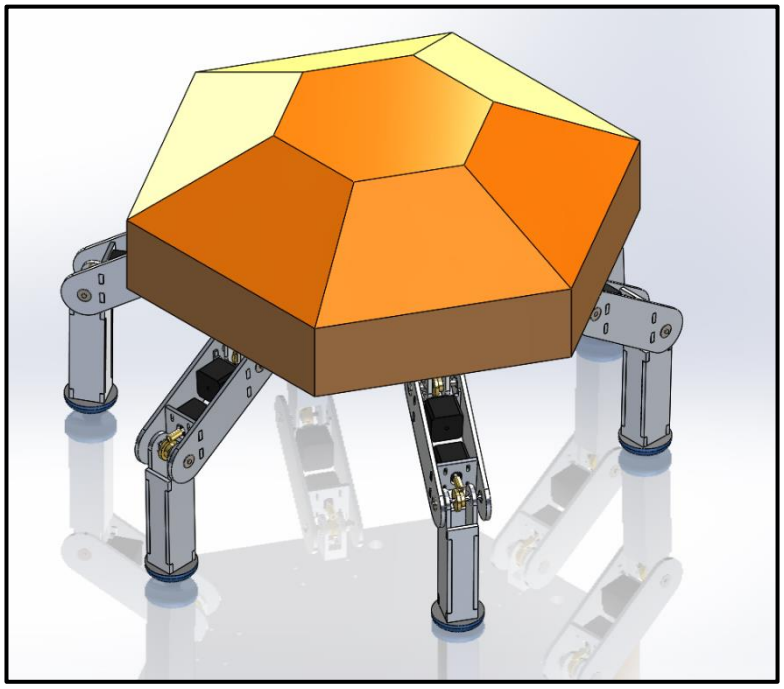

Figure 41: Isometric view of a CAD model for the prototype rover

6.1 Body Design

For the body of the rover, the team determined that the shape should be a symmetric hexagon, much like the proposed design. This allows for a wide base and a center of gravity that coincides with the center of the system. Additionally, the symmetry allows for a simplified control structure and an easy leg modification/reduction system. It is also easier to manufacture a hexagonal shape than a perfect circle in smaller machines.

Once the hexagonal shape of the rover was established, the housing and placement of the rover's primary components could be considered. First, the team determined that a central plate, or shelf should be made to mount all the rover's components. This plate is made of two trapezoidal sheets of ¼-inch acrylic reinforced with two 4-inch wide, 1/16-inch-thick aluminum brackets to join them. Additionally, to maintain symmetry of movement and control, the legs of the rover were each placed at the midpoint of the plate's hexagonal edges. Figure 42 shows the CAD model of this shelf with the holes for motor mounts and leg positioning.

Initially, it was determined that a shell in the shape of a truncated hexagonal pyramid would be placed on top of the acrylic plate. The upper shell's purpose is to protect the batteries, control boards, and other internal components of the rover from damage caused by exposure to regolith, radiation, and other hazards and would serve more as a representational feature on the prototype than a functional feature. This is similar to the petal-shaped shell used by the proposed rover, with the primary difference being that it does not open for either communication or solar collection purposes.

The lower shell of the proposed rover was initially intended to provide a storage space for the legs of the rover to fold and store, as well as to provide storage for the changing of the foot appendage on each leg when swapping between different configurations. The foot changing

mechanism, as discussed in section 6.3, was removed from the prototype due to complexity and budget constraints. Without this feature, the lower shell was removed from the design to improve ground clearance and reduce the prototype's overall weight and complexity. Figure 43 shows SolidWorks model of this shell.

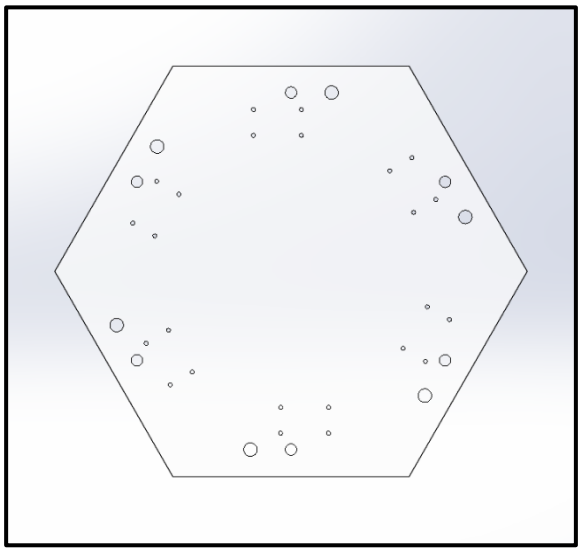

Figure 42: CAD model of the acrylic baseplate for the prototype rover

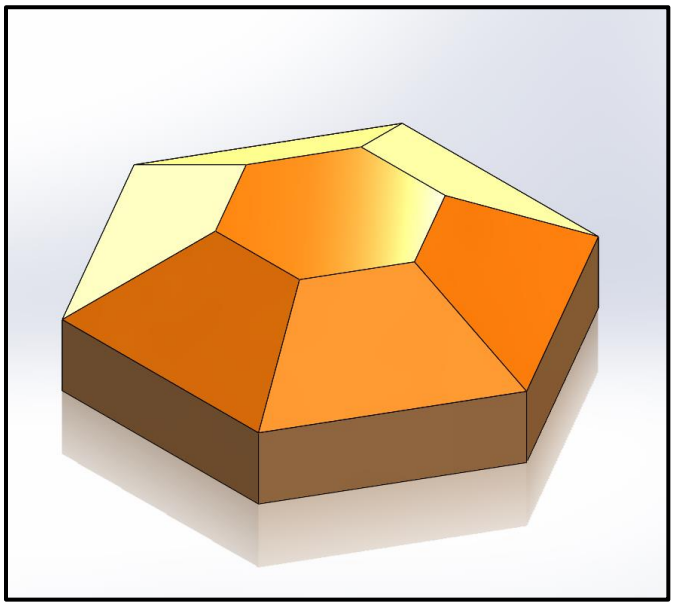

Figure 43: CAD model of the prototype rover's upper shell

6.2 Leg Design

The rover's legs underwent multiple changes throughout the design process from concept to proposed rover to prototype primarily to reduce the system's weight. Initially, dual shafted stepper motors were to be installed for the lower two motors between the linkages, and a single shaft motor was intended for upper motor. Due to the large weight of the stepper motors (0.454 kg each), the overall mass of the rover would have generated levels of torque in the range of 15-20 Newton-meters, greatly exceeding the 0.45 Newton-meter limit that the motors were rated to handle. To combat this issue, 60:1 worm gears were used with single shafted stepper motors. This provided a large torque increase at the cost of considerable joint actuation speed. It also provides high resolution of leg movements, with the minimum joint actuation angle being 0.03° for single steps and 0.015° for interleaving.

The final design of the legs can be considered as an assembly of multiple components, including the lower leg linkage, the upper leg linkage, and the shoulder. Figure 44 shows a SolidWorks model of the overall system of one prototype leg. Note that the leg looks the same as in the proposed rover because in the latter, the same components were used to represent a gearbox that would be used.

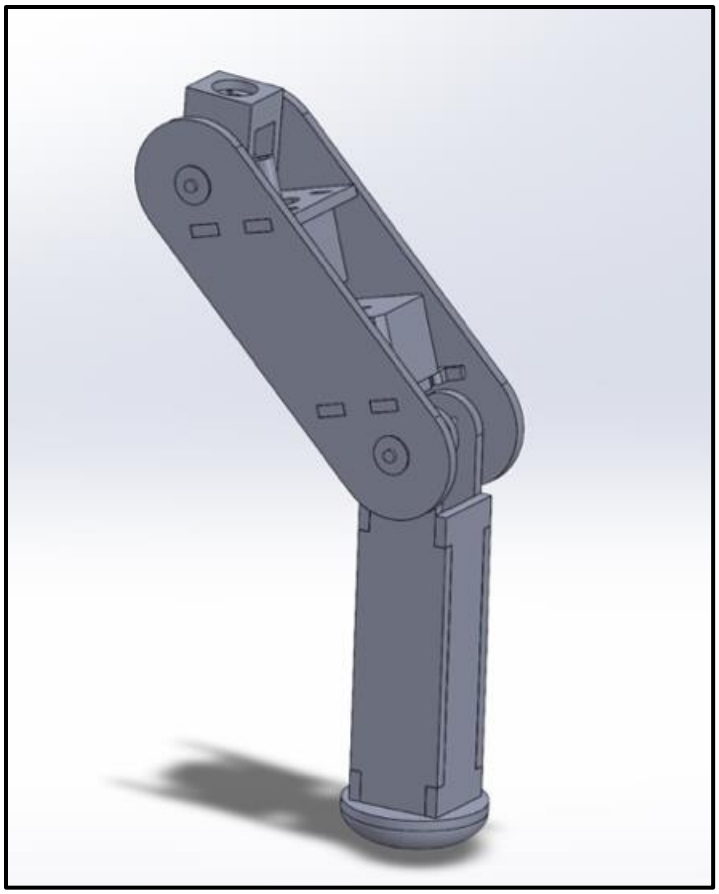

Figure 44: CAD model of the prototype leg

The lower leg linkage consists of four 6-mm aluminum plates, two on the sides to support the axles and one on both the front and the back for support. The hollow center of the leg provides a mounting location for the rover's foot, as well as a route for future wiring should any of the attachments become controllable (as either instruments or actuators). Figure 45 below shows a SolidWorks model of the leg's lower section.

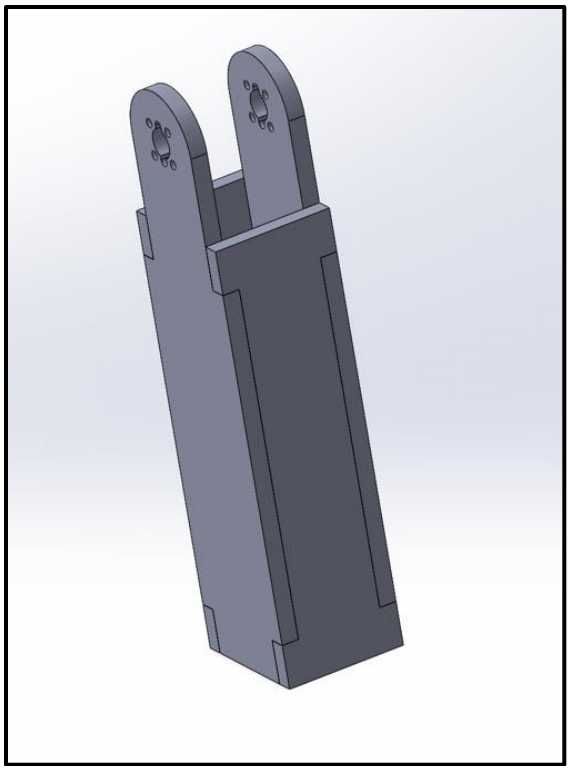

Figure 45: CAD model of the prototype's lower leg section

Like the lower leg section, the upper leg linkage also consists of four 6-mm aluminum plates. Two of the plates, with radial bearings at the top and bottom of each plate as well as slots for attaching the two central plates, make up the sides of the linkage. These central plates fit between the two side plates, and both add stability to the structure and provide a mounting location for the stepper motors. The cylindrical worm gears are fitted onto the shafts of the stepper motors and adjusted close to the worm wheel that is attached to the axles. Housed at the top of the upper leg linkage is the lower shoulder motor. Made of machined aluminum, this component fixes the top of the leg to the rover body via a vertical shaft, allowing the leg to be rotated using another stepper motor housed inside of the rover body. This stepper motor and shaft combination is equipped with a set of worm gears in the same manner as those within the upper leg linkage. Figure 46 below shows a SolidWorks model of the upper leg linkage.

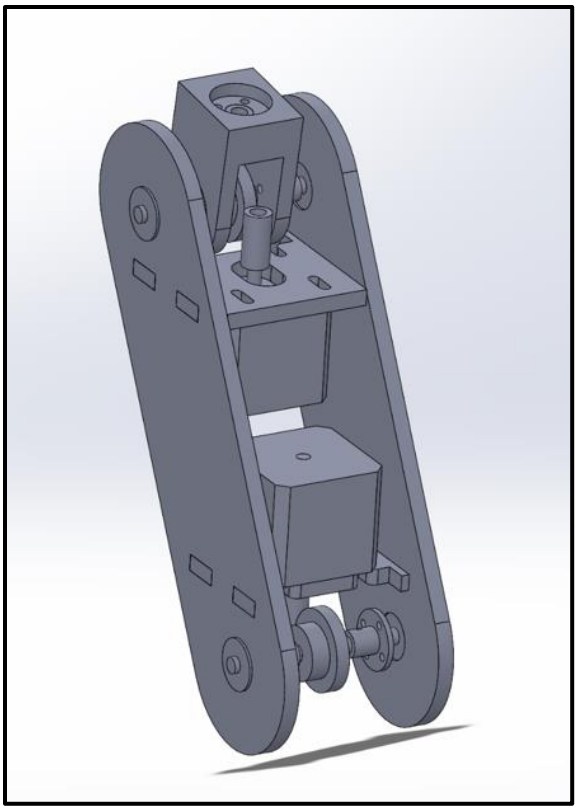

Figure 46: CAD model of the upper leg linkage

As an assembly, the rover legs are fully articulated. There are two "joints," a shoulder joint and a knee joint. The shoulder joint is composed of the upper shoulder motor and the lower shoulder motor, and the knee joint is made of the knee motor. There are two imaginary planes in the leg system, a primary rotational plane and a secondary rotational plane, both of which are parallel to the rover's shelf The primary rotational plane passes through the lower shoulder motor's motor axle and the secondary rotational plane passes through the knee motor's axle. The leg's upper shoulder motor controls the yaw orientation in the primary rotational plane, the lower shoulder motor controls the pitch orientation with respect to the primary rotational plant, and the knee motor controls the pitch orientation with respect to the secondary rotational plane. Figure 47 displays these orientation concepts. This nomenclature will be used throughout the report when referring to the joints and the motors in the prototype.

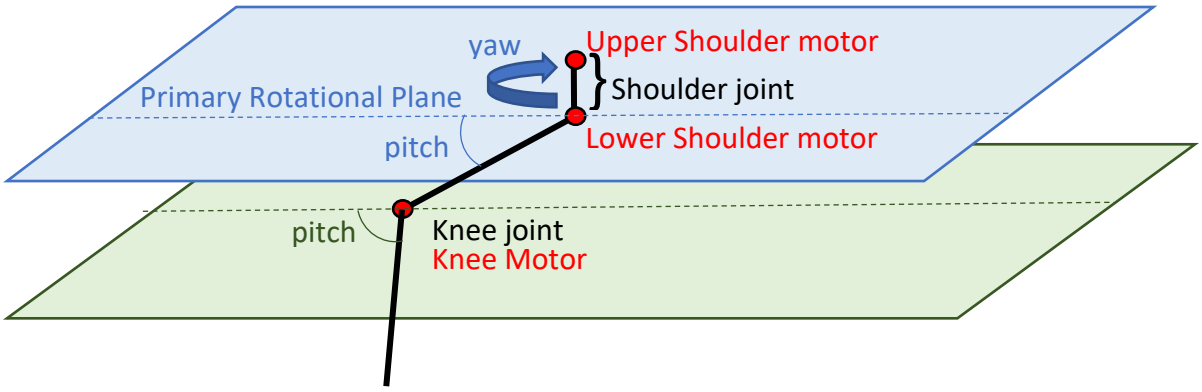

Figure 47: Diagram for the prototype's leg orientations and nomenclature

This combination of joints and motors allows each leg the freedom to rotate 360° and fold/extend over a range of 180° for the lower shoulder, and 230° for the knee, thereby providing ample range of motion for each leg to actuate. Given that all components are generally hollow and are made of aluminum alloy, they are very lightweight while still being reasonably strong. The overall largest contribution to the weight of each leg is therefore the stepper motor housed within it.

6.3 Foot Design

Attached to the bottom of each leg is a foot to improve stability and traction one the Lunar surface. While the proposed rover design is intended to allow for the mechanical substitution of multiple foot variants, it presented significant challenges for the prototype given the team's budget and time constraints. Implementing either an electromagnetic attachment system or robotic tool changers would be extremely expensive, and the inclusion of the attachment wheel provided additional technical and weight challenges. Ultimately, the design of the mechanical substitution system was deemed to increase the complexity and required budget of the rover beyond the scope of this project.

6.4. Electrical System

The electrical system for the prototype rover includes all components needed for mechanical motion (motors, controllers, etc.), systems needed for navigation (cameras, LiDAR, computer, etc.), and mechanisms of thermal management. The computational and sensory components of the rover include the Raspberry Pi, which can be controlled remotely and is powered directly by a small 5V external battery pack; the motor control boards; LiDAR, which includes IMU; and camera. See section 6.5 for more detailed information about the LiDAR, IMU, and camera sensing systems. The specifications for each of the electrical components are listed in Table 3 and described in further detail throughout the following electrical sections.

Table 3: Specifications for electrical components on prototype rover

Component	Quantity	Voltage	Current draw	Power Source
Raspberry Pi Model 4B	1	5.1V	3.0A	Small Battery
Stepper Motors	18	13V	2.4 A (1.2 A per phase)	Batteries
Motor Controllers	9	3V	4.8 A (1.2 A per phase)	Raspberry Pi
LiDAR	1	12 V	1 A	Batteries
IMU	1	N/A	N/A	LiDAR
Camera	1	5V	N/A	Raspberry Pi
Resistors (4 Ω, 50W)	11	N/A	N/A	Batteries

6.4.1 Motors and Motor Control

There are a significant number of components incorporated into the motor control system because of the hexapod design and the three degrees of freedom for each leg. Each degree of freedom requires one Nema 17 2 phase step motor bipolar 1.5A 59.5oz.in(42Ncm) 42x42x38mm stepper motor (Figure 48). In total, this resulted in the need for eighteen motors to control the

legs. All eighteen motors are identical single shaft stepper motors. These stepper motors have a range of operating voltages, but are run at thirteen volts each and are controlled using TB6612FNG FeatherWing motor controls boards (Figure 49). These boards can each control two motors, which means there will be nine total control boards for all the necessary motors. The motors require approximately 1.2 amps per phase, requiring 43.2 amps total for all motors to operate at full power simultaneously. This was achieved using two 12.8V batteries, each having twenty amp-hours. The FeatherWing control boards also require logic power, which was satisfied using the Raspberry Pi's (Figure 50) 3V power output. The specific method for controlling motor movements will be discussed later in the software section. In-line with each motor connection was a 4Ω, 50 W resistor (Figure 51), placed to protect the motor controllers from overcurrent damage.

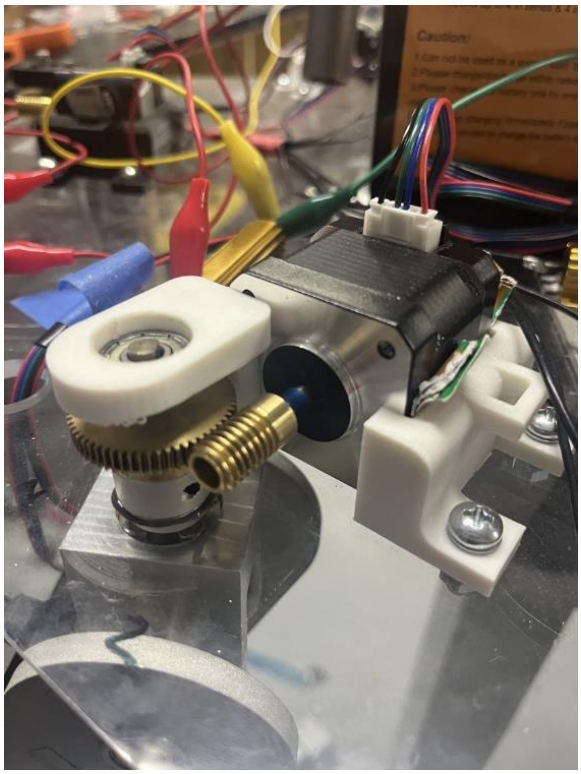

Figure 48: Motors used for the prototype rover

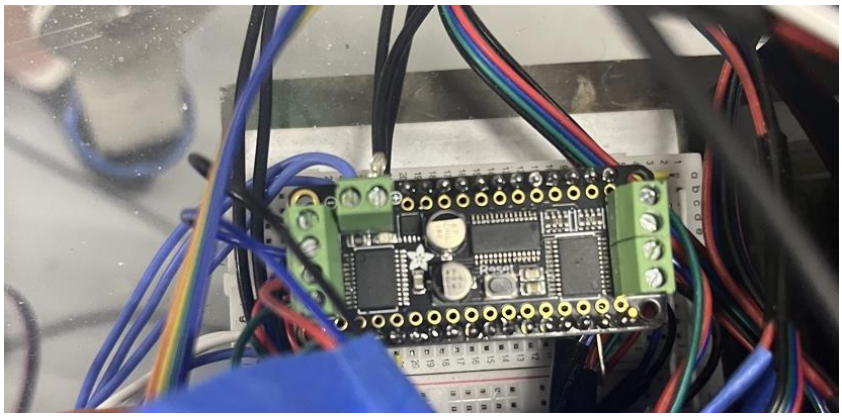

Figure 49: Motor control boards used for the prototype rover

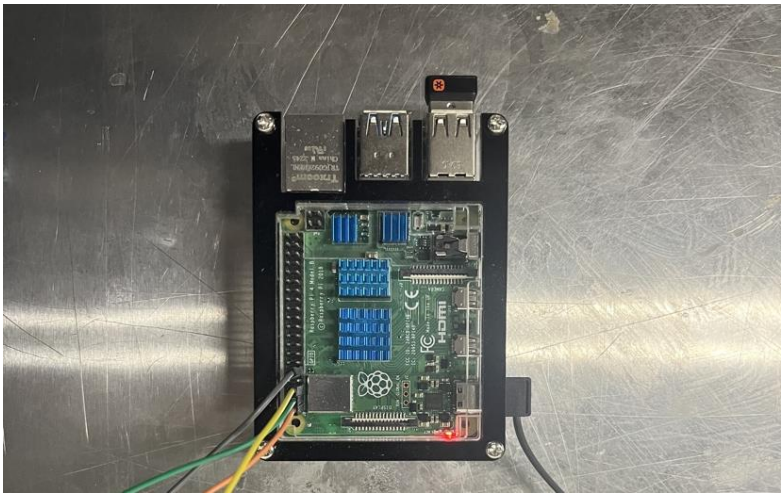

Figure 50: The Raspberry Pi used in the prototype rover

Figure 51: Resistors used in the prototype rover

6.4.2 Power

Power is supplied by a pair of 20 Amp (max current), 12V batteries (Figure 52), which were chosen to ensure the maximum required system amperage could be achieved. The batteries the team used are shown in Figures 52 and 53 below. The batteries were connected to a bank of motor control boards which directed the current to the appropriate motors. As shown in Table 3, the camera is powered directly by a Raspberry Pi, while the LiDAR is powered in line with the main batteries. As stated above, the motor control boards are directly connected to the batteries as well, but they are not powered by them. Instead, all the logic functions of these boards are powered directly from the 3.3V output power on the Raspberry Pi. The Motors can be powered with a simple set of batteries that are within the limits of both the motors and the control boards. The Raspberry Pi needs a much smaller power supply, which will also power other small components, such as the motor control boards, the inertial measurement unit, and the camera

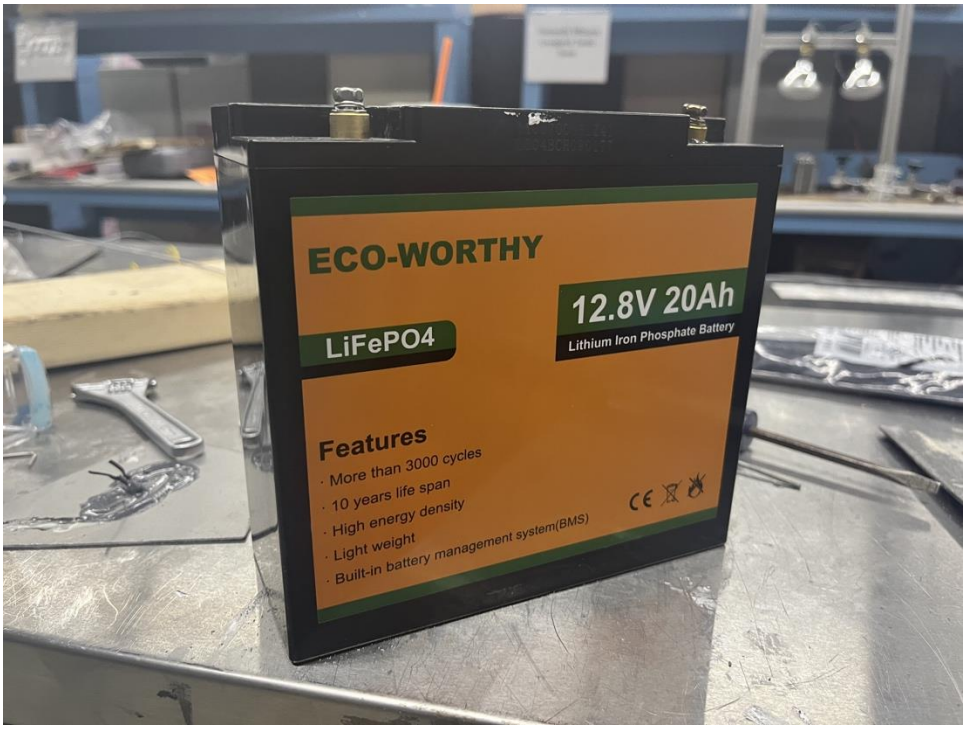

Figure 52: The batteries used for the prototype rover

Figure 53: Small battery used to power the Pi and motor control boards on the prototype rover

6.4.3 Thermal management

The resistors were clamped to a metal bracket that attached two large aluminum heat sinks (Figure 54) to dissipate the heat. Additionally, two fans (Figure 55) were installed, pointing at each radiator, to improve airflow and maximize off-heating capabilities. To ensure that the cooling features were sufficient, an IR temperature sensor was used during testing. The control boards remained just above room temperature, while the resistor banks stabilized at 54° C. This is safely below the 70° C the resistors are rated for. Because the rover generates large amounts of heat on its own, and the testing conditions never cause it to grow too cold, the heaters included in the proposed rover were deemed unnecessary for the prototype and were not included.

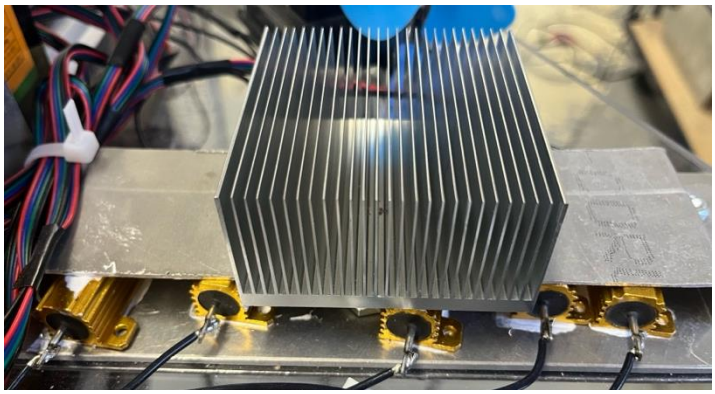

Figure 54: Bracket with heat sink used in the prototype rover

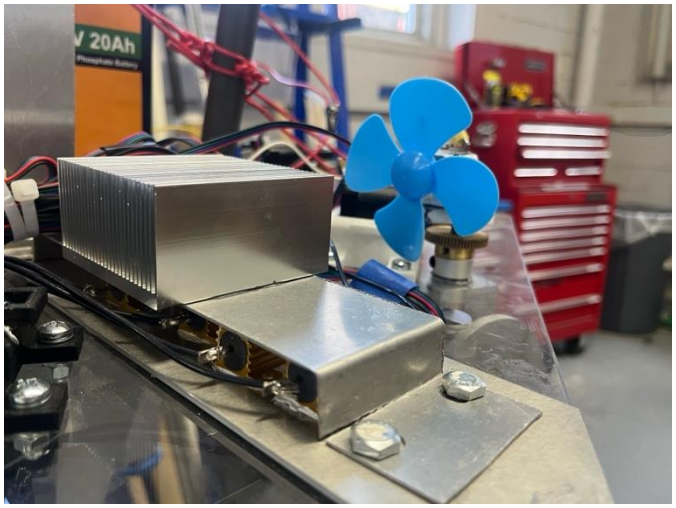

Figure 55: On board fans used on the prototype rover

6.4.4 Sensors

The prototype rover incorporates multiple sensors to navigate and gather data during operation. This is done using a three-hundred sixty-degree three-dimensional LiDAR sensor (Figure 56) and a camera (Figure 57). The LiDAR sensor generates a set of points in three-dimensional space representing the location of obstacles. This includes additional information such as the signal intensity and ring index. Additionally, the LiDAR sensor includes an inertial measurement unit (IMU). This IMU outputs both acceleration data and a quaternion indicating

the orientation of the sensor. This accelerometer data is used to obtain the rover's position over time. In cases where a rover was run using a closed-loop controller, the position data would be run through a Kalman filter. The specific method for implementing a Kalman filter will be discussed later in the Navigation and Controls section of this report.

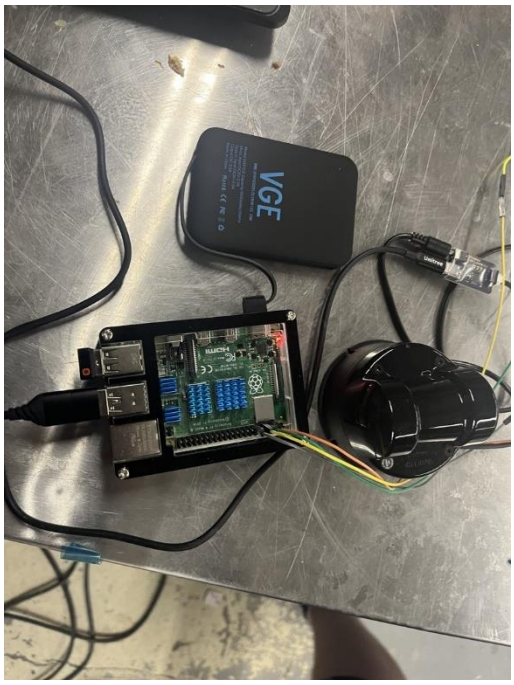

Figure 56: The LiDAR used in the prototype rover

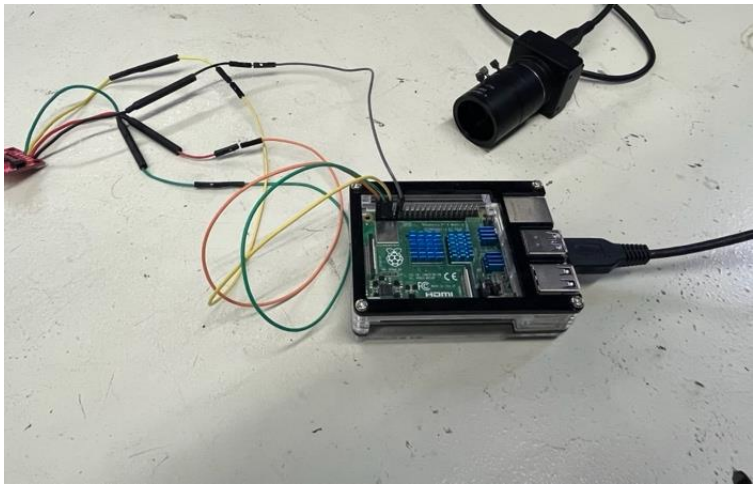

Figure 57: The camera used in the prototype rover

Overall, the rover's complete electrical system consists of 18 stepper motors, 9 FeatherWing motor control boards, 2 (12V) DC batteries, a (5V) DC battery, a LiDAR, a camera, and a Raspberry Pi to control it all. The Raspberry Pi uses I2C addressing to send commands to the stepper motor control boards, each of which controls 2 of the 18 stepper motors.

The majority of electrical components were purchased, with the only fabricated part being the 12V power harness connecting the two larger batteries to each of the FeatherWings. This harness was created by splicing 14-gauge wire into 9 smaller 18-gauge leads. Each of the leads feeds into an individual FeatherWing, while the 14-gauge end connects to the two batteries. Two of these connectors were fabricated, with one serving as the power positive and the other as the negative lead. The 14-gauge wire was used to handle the peak amperage of 43.2 Amps pulled from the battery bank. Each control board draws a maximum of 4.8 Amps on its own, and therefore did not require the same gauge of wire to handle the load.

Additional processing was required to configure the FeatherWings to fit within the rover as well. Stacking headers were soldered onto each of the boards so they could neatly stack on top of one another (Figure 58). This greatly simplified wiring because the Raspberry Pi could connect to all of them simultaneously. This connection was made with the pins for ground, 3.3V power, SDC (serial clock), and SDA (serial data).

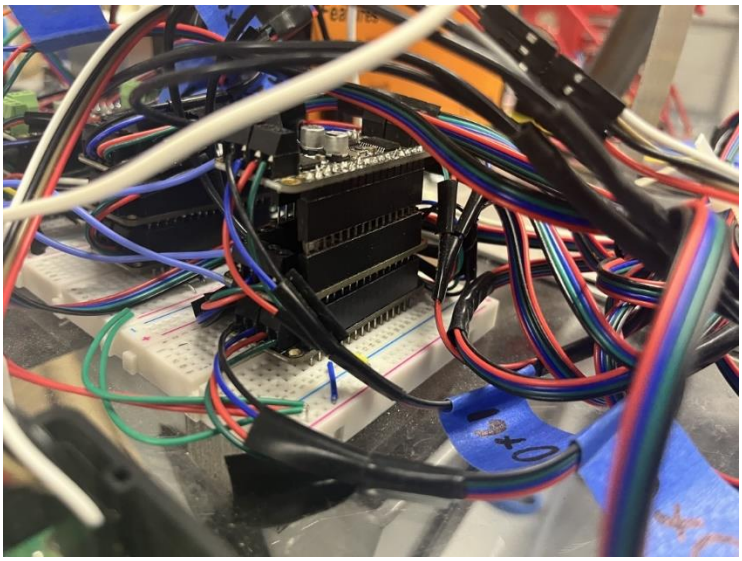

Figure 58: Image of the motor control boards stacked together for the prototype.

The motors were then connected to the FeatherWing boards using built in connectors on each motor and screw-clamp connectors on the FeatherWings. For the motors inside the legs, the wiring harnesses were routed through a small hole in the rover's shelf 5-cm away from the leg attachment point. Altogether, the dual power sources provide the motors with enough power to run effectively while still being able to operate the Raspberry Pi within its specifications.

6.5 Software

In order to operate the rover, the team created code to operate the motors and gather sensor data. The code was written in both Python and MATLAB. MATLAB was used for basic calculations since the team was far more experienced in this software. Python was used to operate the motors on the Raspberry Pi. Communication between MATLAB, which was run on a laptop, and the Raspberry Pi was done using the Secure Shell, SSH, protocol and the Secure Copy, SCP, protocol. These are standardized protocols that allow for remote connection and file transfer between computers over Wi-Fi. In this case, SSH and SCP were implemented in separate

Python scripts since the team was not able to use MATLAB's functionality to perform it directly. Instead, bash commands were executed from MATLAB to run the Python scripts responsible for SSH and SCP commands. The team recognizes that the use of Wi-Fi is unrealistic for any real rover, but decided that avoiding the issue of communications on the prototype would allow more time for running tests.

In addition to operating the motors, the team gathered data from a LiDAR sensor and a camera. This was done on a separate Raspberry Pi because the original IMU that the team planned to use operated over I2C addressing, the same protocol that was used to operate the motor controllers, and was conflicting with the control of the motors. Due to this issue, the team chose to use a second Raspberry Pi for sensors. Additionally, the prototype's speed depended heavily upon the speed at which the Raspberry Pi could send commands. Operating sensors on the same hardware would have resulted in slower execution of the motor code and a reduced rover speed. The operation of the sensors was similar to that of the motors, in the sense that scripts were run on the Raspberry Pi over SSH and data was collected using SCP. However, the LiDAR operation was performed using a previously compiled C++ executable because the software development kit from the LiDAR manufacturer was written in C++. The original software package for the LiDAR was built only for Windows so data had to be collected using custom C++ code. This also meant that the point cloud results would have to be plotted separately since the LiDAR software was only configured to use a serial data stream from the sensor.

The motor control code was written in Python which served as the basis for the rover control. This code reads commands from a text file and reads specific motor movements from a comma-separated value (csv) file. The motor movements were formatted as an n-by-twenty

matrix. Within this matrix, the first two columns were informational and the next eighteen contained the number of steps that a specific motor needed to run. Negative step numbers were used to represent backwards steps on a motor. Wait times were included because the motors need a certain amount of time to execute instructions sent over I2C addressing. Wait times that were too low resulted in the stepper motors failing to step properly. The specific value used for wait time varied throughout the project based on what was needed. See the validation section for more details on how wait times were tuned. This motor code worked well for executing large numbers of steps but was only good for moving motors to the specified location and not moving them at the desired rate.

In order for a rover to walk properly, the motors must run at prescribed rates. The need for this becomes apparent when considering that the inverse kinematics that are used to calculate angle changes for a desired movement are done in discrete times, so if one motor must move by ten degrees and another must move twenty degrees in a given time step, the second motor must move at twice the rate, rather than both moving ten degrees then the second motor moving another ten degrees. This requirement was fulfilled before sending the instructions to the Raspberry Pi by running a given set of calculated motor instructions through a rate filter. This rate filter was made in MATLAB, since MATLAB was used for the inverse kinematics, which will be discussed further in the Navigation and Controls section. The rate filter functions by using the lowest number of steps for a given movement phase, a term the team uses to refer to a single set of calculated instructions over a discrete time period, as the baseline and calculating the ratio of every other motor's instructions to this baseline. When the ratio was a decimal value, rounding was performed, and remainders were tracked. These remainders were accounted for in the next line of instructions. Then, the rate filter generates a new, significantly larger matrix of

the ratios and remainder values. This resulted in each original movement phase being divided into many lines of instructions with smaller values. This slowed down the rate of motor operation, but, due to the design of the motor execution code, it allowed the team to reduce the wait time and did not significantly impact run time.

One of the original design goals for the prototype was to demonstrate wireless operation. This is possible by remotely sending the instructions to the Raspberry Pi for motor control over SCP and then remotely calling the Python and C++ scripts using SSH commands. This worked well for running a set of instructions that did not need to change. However, as will be discussed later, testing showed that there was a need to interrupt motor execution to apply adjustments. This led to the creation of a new version of the motor execution code that would read additional commands from a text file, allowing it to be paused and stopped.

Additionally, this new code could be given precise adjustments while paused, which would be concatenated with the remaining motor instructions and then both would be executed in turn. This can theoretically be run remotely since it is very similar to the original code, however, due to limitations of MATLAB, it was not practical to execute it remotely, as intended. This was because the remote implementation required the terminal command to be sent to run the Python script while allowing the user to input new commands at the same time. In many programming languages, such as Python, this is done using explicit multi-threading. However, MATLAB's thread-based environment has a limited set of functions that can be used during parallel execution. This list does not include any method for running terminal commands, of which there are many, or any method of taking rapid user input. Since neither of these could be done in MATLAB's thread-based environment, it was not possible to run the prototype remotely with this version of the code. Despite this complication, the capability to run the rover remotely has

been demonstrated, even though testing was often run directly on the Raspberry Pi to maintain more precise control. All of the code written for this project will be included in a GitHub repository that can be found in Appendix A.

7. Simulations

Before the designed rover can be fabricated, simulations must be performed to confirm the feasibility of our design. Structural and thermal simulations are the primary concerns of this project before manufacturing can begin since failure in either of these areas would call for major design changes. The team decided to use ANSYS a Finite Element Analysis (FEA) program to create static structural simulations of the rover standing and dynamic simulations of the rover being dropped. COMSOL Multiphysics was used to create thermal simulations to determine the insulation and radiation needed to protect the rover from the harsh space environment. These simulations were run on simplified models of the proposed rover and the prototype to reduce the complexity and to ease the load on the computers. Both the drop test and statics simulation were run twice, once on our proposed rover and once on our prototype model, while COMSOL was only used to create a simulation of our proposed rover. However, given the budget constraints and the goals for the prototype rover, an implementable Lunar thermal management system will not be included, so instead a mass was added to ensure the model could lift such a system. The power budget for the proposed rover will still account for thermal management and the design will accommodate any hardware required for thermal control. All types of these simulations are instrumental to the success of both rovers.

Table 4: Structural, Dynamic and Thermal Figures.

	Structural	Dynamic	Thermal
Prototype	Figure 59-61	Figure 65-67	N/A
Proposed	Figure 62-64	Figure 68-70	Figure 71-72

7.1 Structural Simulations

During the structural simulations of both the prototype and proposed rovers, efficient use of the ANSYS statics program is critical for accuracy and speed of simulation. It is important to simplify the models used during this process. The designs were simplified to run the simulation faster by removing unnecessary details, such as flange shafts screws and other smaller components. The remaining parts were classified as bonded together, the gears were assumed to always be in contact with no slippage, the feet were considered anchored to the ground, and the gravitational force was applied directly to the surface of the lower shoulder joint.

Structural simulations are vital to the early rover design process because they will determine if the designed system can physically do what is intended. To create these structural simulations, only one leg of the rover was imported into the system for simplicity and computational speed. The model is then assigned a material giving it properties of, in this case, wrought Aluminum 6061. This foot model is then assigned connections for the rover. The joints of the leg were all considered bonded due to the gears in the real design actively resisting any vertical forces applied to them. The bottom of the model's foot was connected to the floor ensuring it would not move when exposed to a weight force. The weight force on the foot is expected to be a force of 160 Newtons, which is equivalent to the mass of the rover multiplied by the acceleration due to gravity, which is then divided over three legs. A factor of safety of two was also multiplied. Before the test could begin, a mesh was created which discretizes the leg model's complex geometry into smaller recognizable pieces that enable computation. After the mesh was fitted the simulation was ready to run. A force of 160 Newtons was then applied to the leg at the shoulder joint. This was done to evaluate whether the leg would fail or deform under the expected conditions.

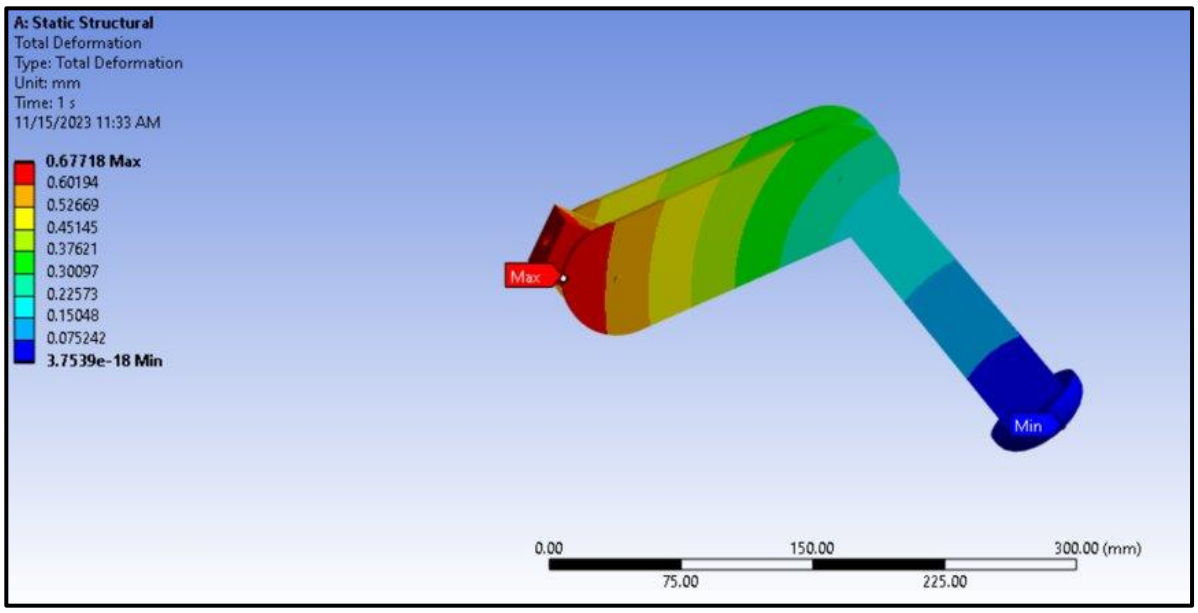

Figure 59: The prototype leg under 160 Newton force and the deformation that results

As demonstrated in Figure 59 above this simulation showed that the leg will not fail under the expected loads and would experience a maximum deformation of about 0.67 mm. This is within the design goal of no more than one millimeter of deformation when standing in a tripod configuration. Low levels of deformation ensure that the material remains in the elastic regime and does experience plastic deformation, which would remain even after the load is reduced. As demonstrated in Figure 59, the deformation is largest closest to the shoulder joint and as the force is spread out over the rest of the structure the deformation decreases as it approaches the foot, where it is insignificant. The team also used this simulation to examine the stress and strain throughout the prototype's legs, which can be seen below.

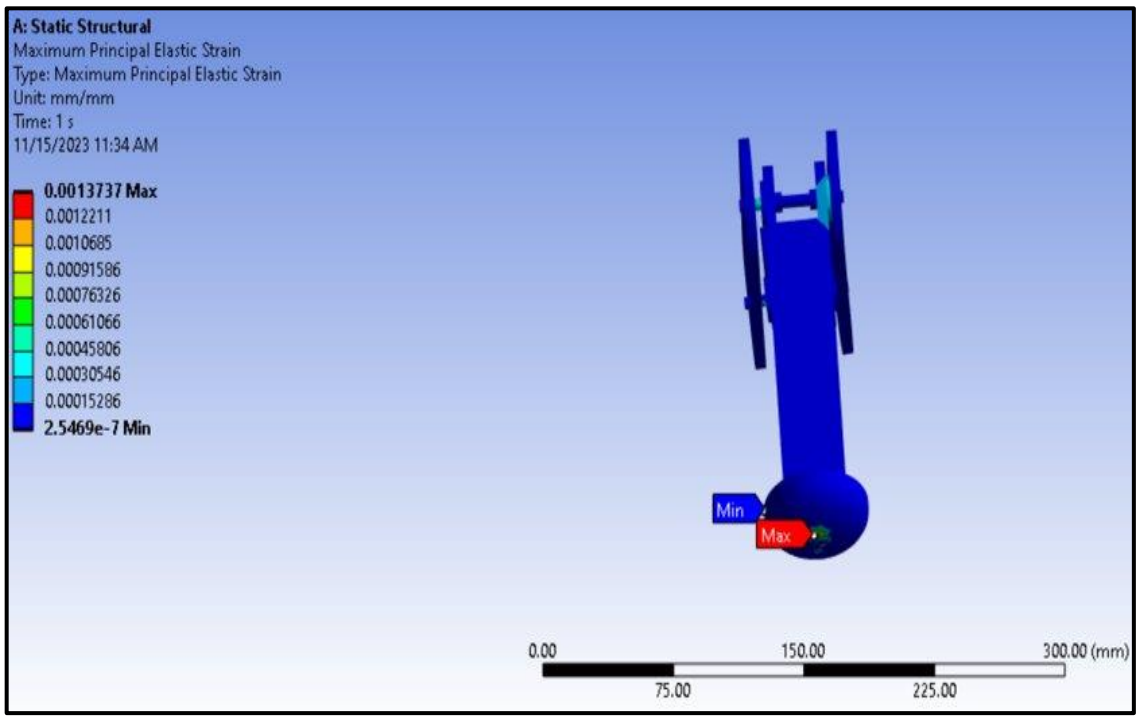

Figure 60: The prototype leg under 160 Newton force and the Maximum elastic strain that results

Next, we present the strain as demonstrated in Figure 60. Strain is the ratio of deformation to original length. The maximum strain for the leg was located at the bottom of the foot and 0.00137 mm/mm in an area measuring less than 2 mm cubed. The minimum strain expected is 0.25469 microstrain, occurring throughout the flat sections of the leg. This illustrates that the deformation is not only nominally small, as shown above, but is also a very small percentage of the original length. The low strain predicted in this simulation is a key factor in validating the proposed rover design before fabricating.

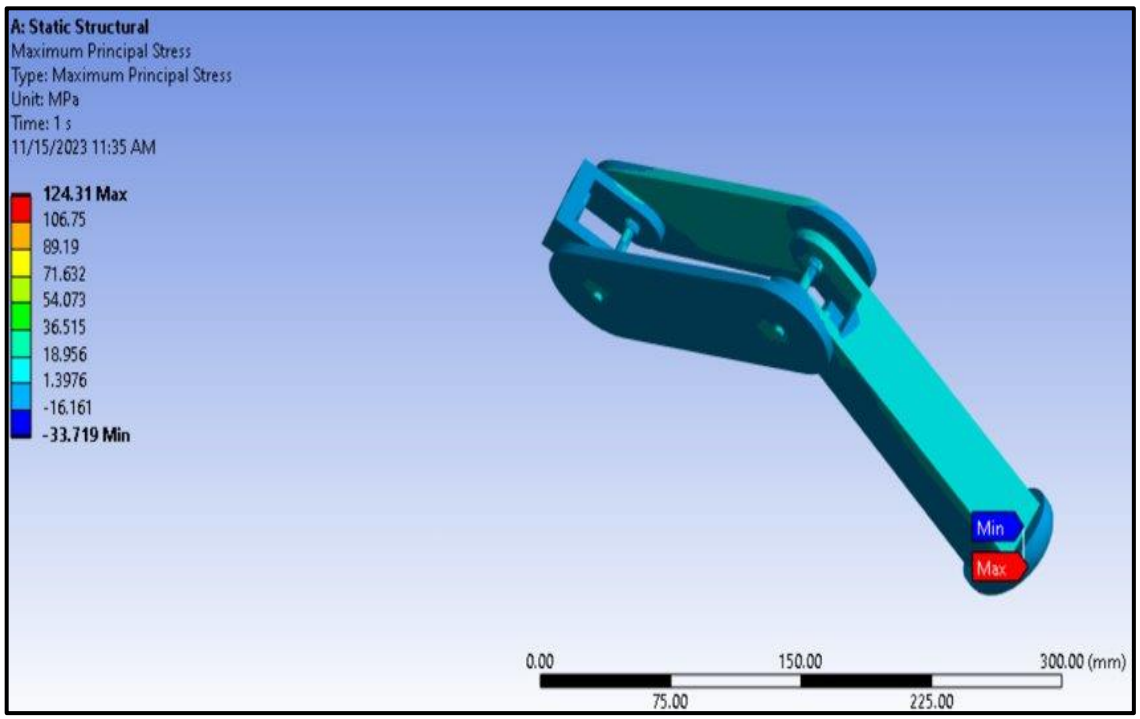

Figure 61: The prototype leg under 160 Newton force and the Maximum stress that results

Next, the maximum principal stresses are displayed. These principal stresses represent the maximum stress that could be experienced by the element on any plane passing through that location. As shown in Figure 60 the maximum stress experienced is 124.31 Megapascals. The stress limit for this material is approximately 240 megapascals. Therefore, the parts should not fail. The vast majority of the rover is compressed by 16 megapascals easily under the 240 Megapascal threshold. In conclusion, the principal stresses appear to be well within the limits of the chosen material for the prototype rover. The team concludes that the prototype is able to stand statically under its own weight with a reasonable safety factor of 2 as displayed in Figures 59 to 61.

A separate simulation was run to assess the structure of the proposed rover. The static structural simulation for the proposed rover was created through a similar process to the one used for the prototype. The simulation for the proposed rover used titanium instead of aluminum

because of the increased budget for this design. The overall proposed rover mass is 343.33 kilograms as calculated in the SolidWorks model. The weight of the rover on Earth distributed over 3 legs is a force of 1121.54 Newtons for each, which was applied to the modeled leg. While the rover is intended for use on the Moon, simulating under Earth's six times stronger gravity ensures a high factor of safety. If this design were intended to undergo significant testing on Earth, it would likely be important to increase the safety factor through small design changes. Figures 62 through 64 below show the results of the static structural simulation for the proposed rover leg.

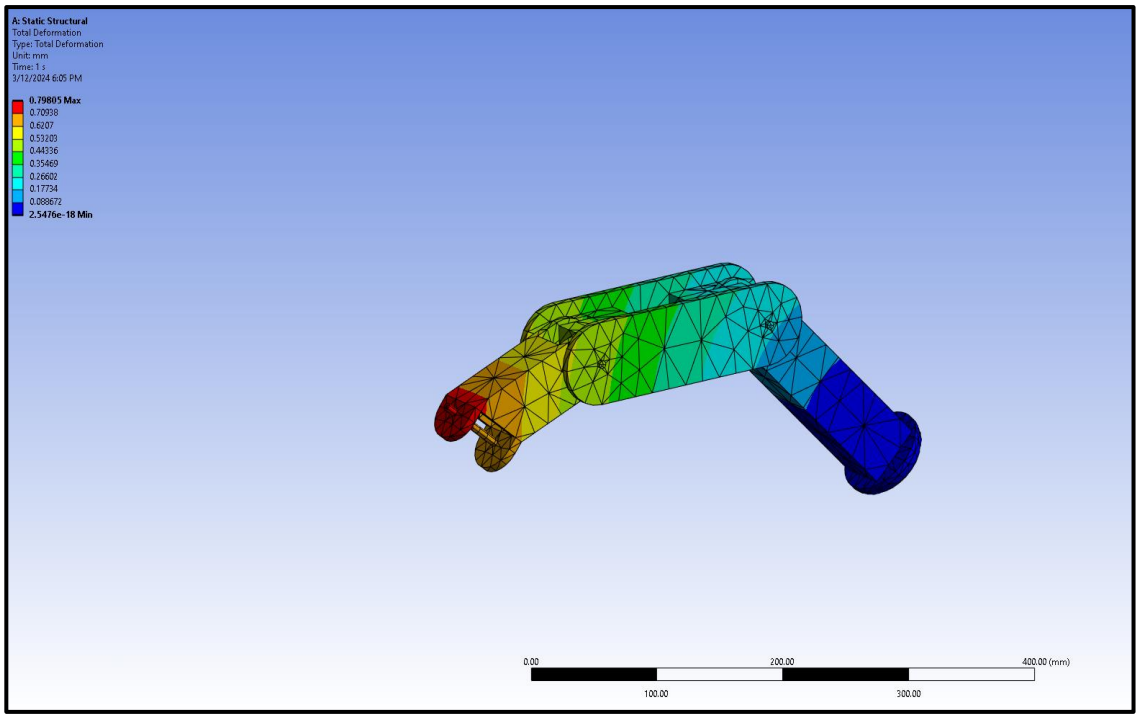

Figure 62: The proposed leg under 1121 Newton force and the Maximum deformation that results

As a result of a 1121 Newton gravitational force as the rover would experience on the surface of planet Earth Figure 62 demonstrates the expected deformation that would occur during a static standing test, with the most extreme deformation being 0.798 millimeters. This is below

the design objective of deformation below one millimeter. In the rest of the simulation, the deformation throughout the leg is all relatively small, and most of the deformation is less than half a millimeter. The strain was also calculated for this in Figure 63.

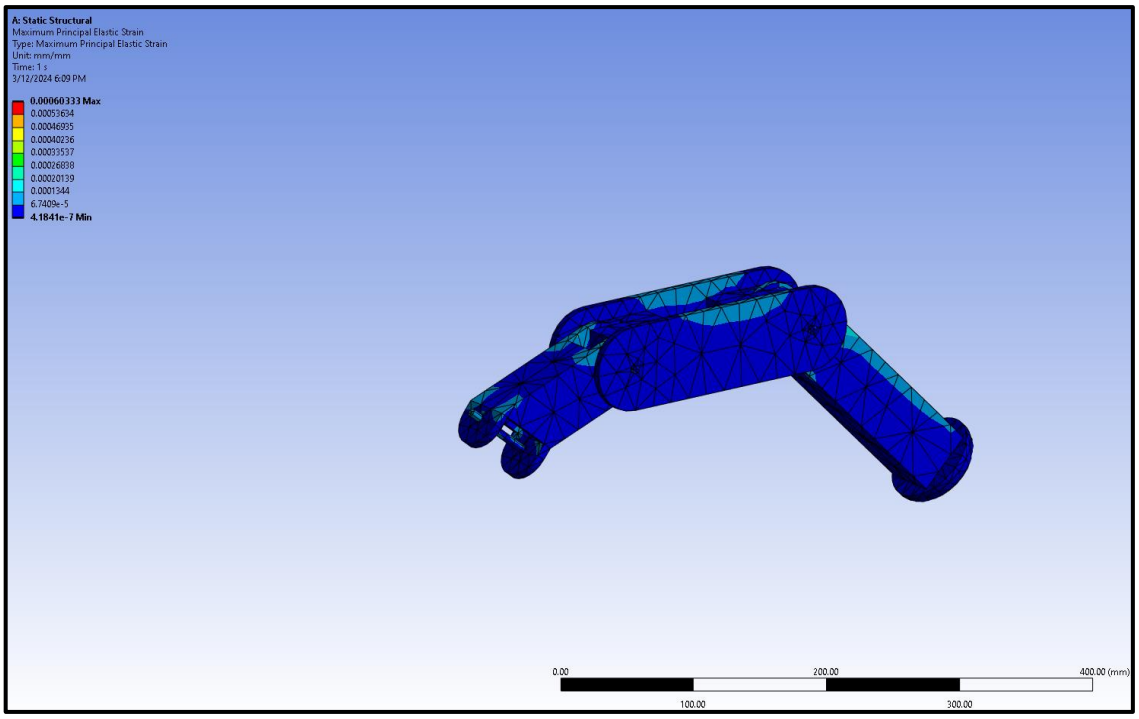

Figure 63: The proposed leg under 1121 Newton force and the Maximum strain that results

The strain calculated in the simulation is displayed in Figure 63. A result of the simulation is that the proposed rover leg is within tolerance with the maximum strain being on the axles at 0.0006 mm/mm while most of the rover experiences a microstrain of 0.4184. These values show that the rover's deformation makes up a small amount compared to the original dimension. These results would be within the elastic region of the material, indicating that the structural components would not experience plastic deformation and would experience less deformation after loading decreased from the maximum. Through this simulation the maximum stress was also calculated in Figure 63.

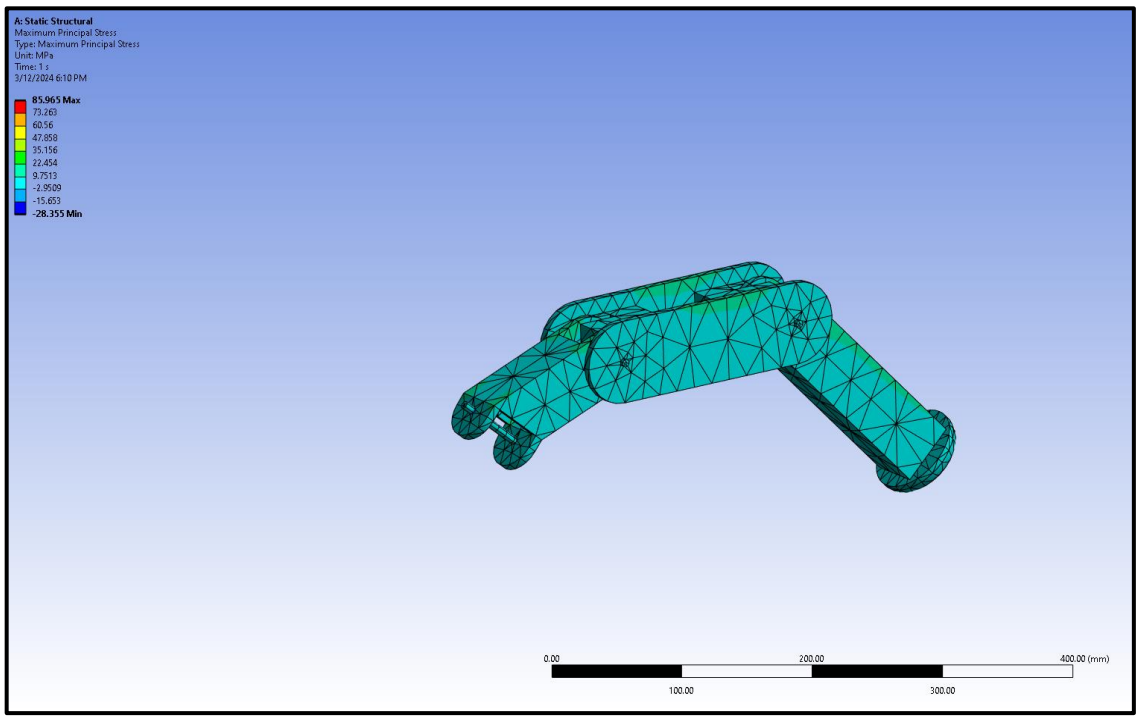

Figure 64: The proposed leg under 1121 Newton force and the Maximum stress that results

Figure 64 demonstrates the maximum principal stresses the leg experiences. The maximum allowable stress for the Titanium used is 293 Megapascals. The parts are compressed at 2.95 Megapascals. Therefore, the leg will not fail under a load of 1127 Newtons. There are several noticeable areas of improvement for future projects using a similar static structural simulation. First, the simulations could be improved through the usage of a more powerful computer, because with more power the simulation can evaluate a finer mesh without unreasonable time requirements. A finer mesh would result in more accurate analyses of the system. Additionally, a more complex model of the system could be used to further improve accuracy.

7.2 Dynamic Simulations

Dynamic simulations were performed on both the proposed and prototype rovers in order to evaluate the performance of the system under dynamic conditions. The team used ANSYS explicit dynamics to run these simulations. Neither version of the rover is expected to experience a drop greater in distance than roughly a foot and a half on Earth, so the simulation was run under these conditions. As with the static simulation, the dynamic simulations were run on a simplified version of the models to prioritize the key aspects of the model given the limited computational resources available. This allows the simulation to obtain more accurate results about key areas of interest. The simplifications to the models included removing connection hardware and simplifying the geometry. The remaining parts were classified as bonded together, the gears were assumed to always be in contact with no slippage, the feet were considered anchored to the ground, and the gravitational force was applied directly to the surface of the lower shoulder joint.

The simulations for both the prototype and proposed rovers required first a simplified model to be imported into ANSYS explicit dynamics. Then the material was selected, for the prototype it was Aluminum 6061 and for the proposed rover it was Titanium. The connection between the “ground” plate must have its connection to the leg suppressed and a joint must lock the upper shoulder to the plane it is on. Next a velocity must be applied to the foot of 3000 mm/s. When triggered this will send the “ground” speeding into the foot generating as if there was an impact with the ground at such a speed. The time was kept constant at 1*e-4 seconds.

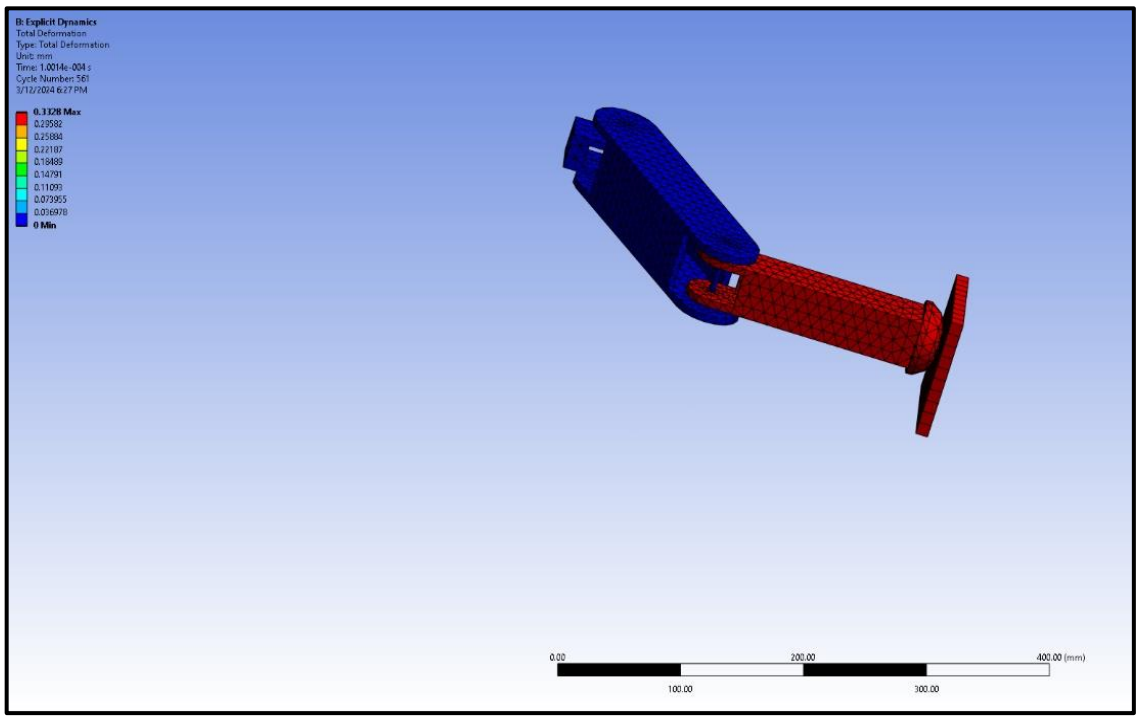

Figure 65: Total deformation of the leg of the prototype rover from a 1.5-foot Earth drop

Most of the rover was made from wrought Aluminum 6061 with a few exceptions such as the axles with are made of structural steel. The simulation calculated the total leg deformation to be 0.3328 millimeters upon impact with the surface. This shows that the leg deforms less than the 1 millimeter maximum dictated by the team's design objectives. In the simulation the lower leg experienced the largest deformation, while the upper leg segment didn't deform at all. The maximum elastic strain was also calculated from this simulation.

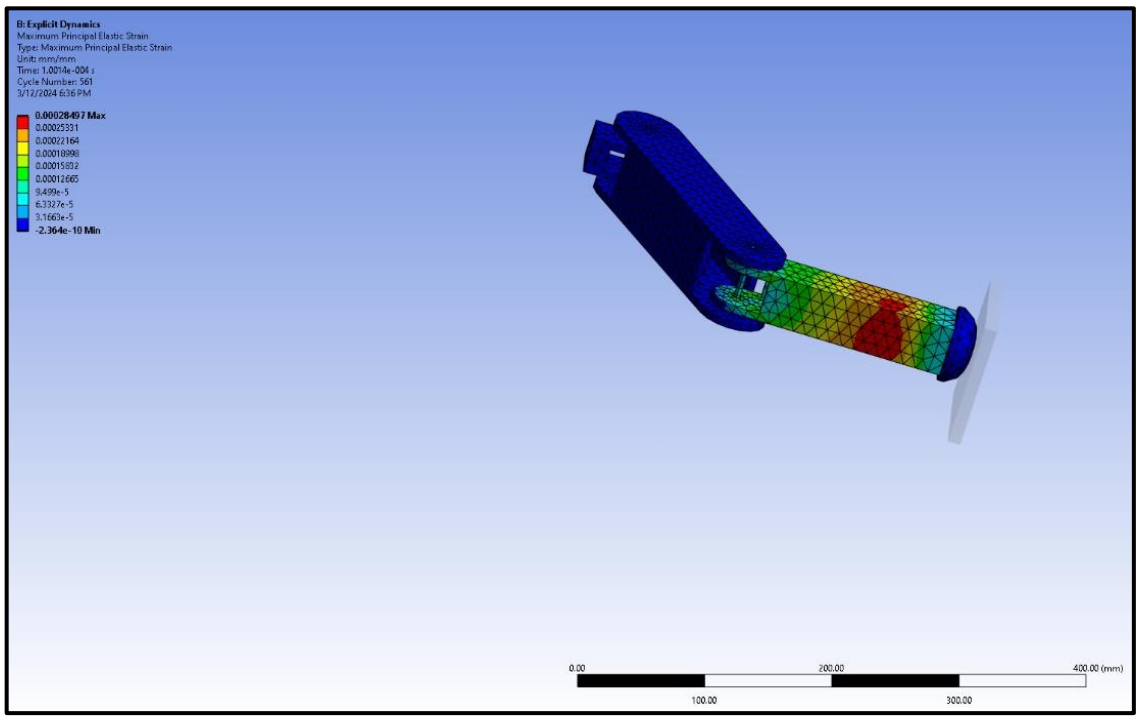

Figure 66: The maximum strain on the prototype rover from a 1.5-foot Earth drop

The strain simulation utilized the same simplified model as other dynamic prototype simulations. The maximum strain expected is 0.000284 mm/mm and the minimum strain during this simulation is shown to be 2.36 * e-4 microstrain this indicates that the expected deformation is small when compared to the original part. Additionally, this is within the elastic regime of the material, so the modeled components should survive after impact without permanent damage. Next, the stress on the prototype rover leg is calculated in Figure 67.

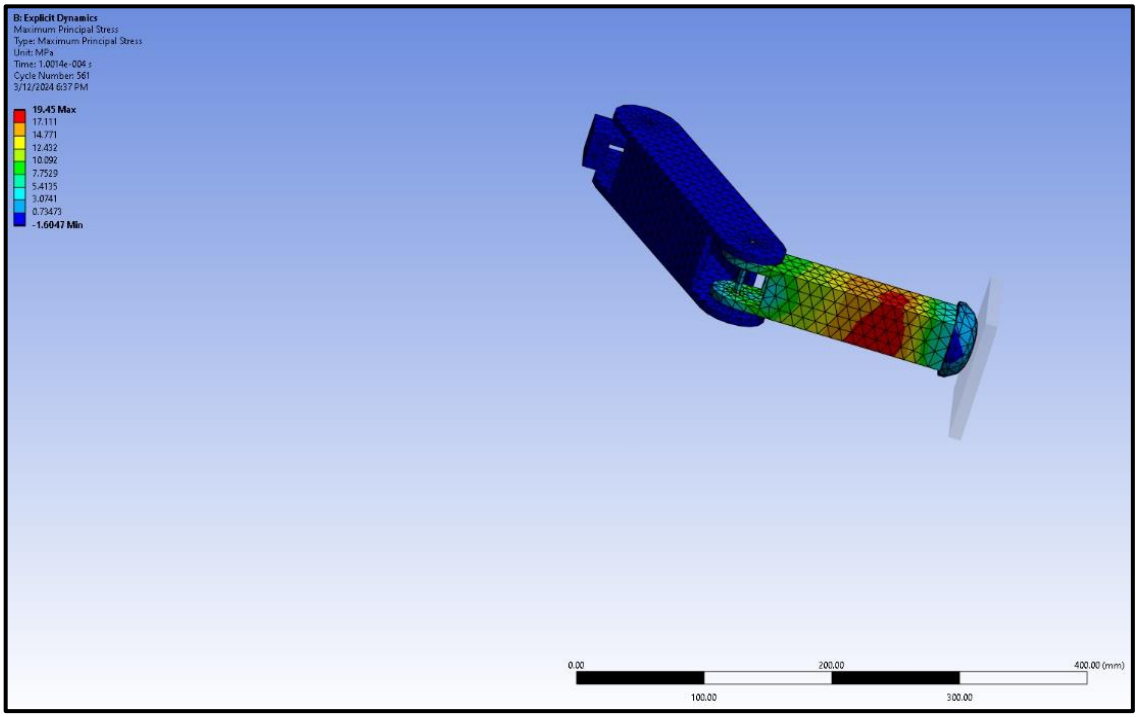

Figure 67: The maximum stress on the prototype rover from a 1.5-foot Earth drop

In Figure 67 the maximum principal stresses throughout the leg are found. The maximum stress in the leg is 19.45 megapascals of tension is applied to rover and at minimum is compressed 1.60 Megapascal both fall within Aluminum's maximum tensile strength of 240 megapascals. Therefore, the leg is not expected to fail and will perform as intended when impacting the ground from 1.50 feet on Earth.

These values demonstrate that the leg is expected to withstand such a fall without any permanent damage to the rover. These values also provide a baseline for the proposed rover. If kept to a similar weight, similar results can be expected from a drop of a similar height.

The proposed rover, while being much stronger material can survive similar distance falls to the prototype on earth. This is because the stronger material comes with lots of excess weight of parts.

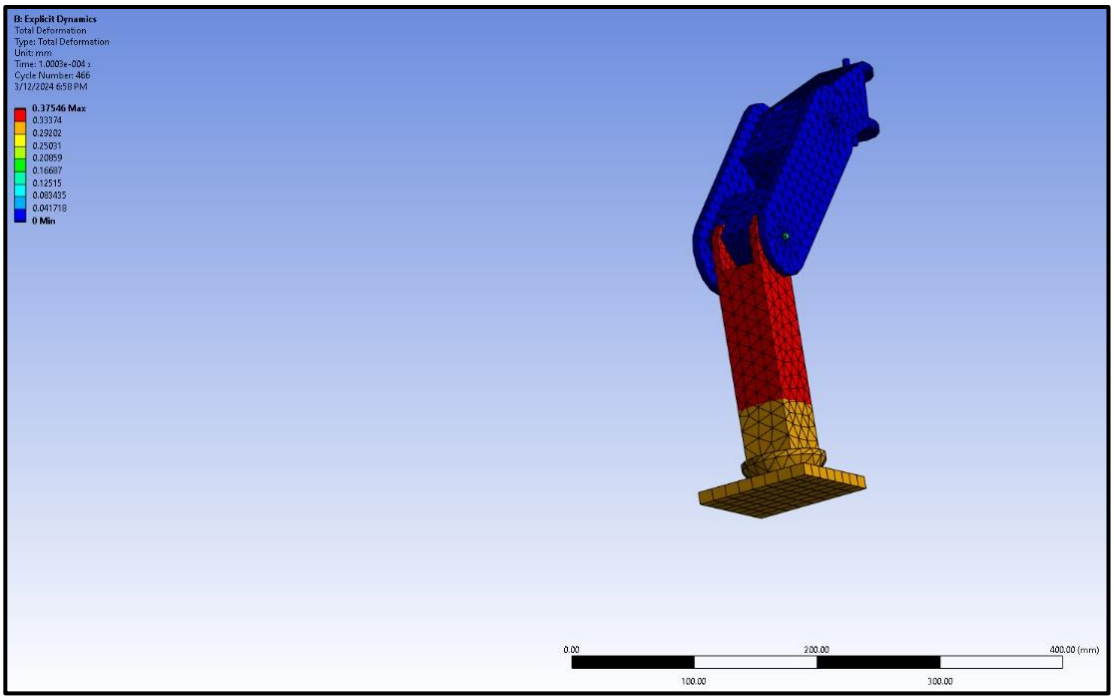

Figure 68: The maximum stress on the proposed rover from a 9-foot Lunar drop

In Figure 68 The deformation of the proposed rover is displayed after the simulation was run. The maximum deformation found was 0.37546 mm, which occurred at the bottom of the lower leg and the foot, as expected. The minimum deformation is zero, occurring in the upper leg. These values are beneath the required threshold one millimeter of deformation therefore the proposed rover should survive a 1.5-foot drop on Earth or the equivalent 9-foot drop on the Moon. During this simulation the strain is calculated as well.

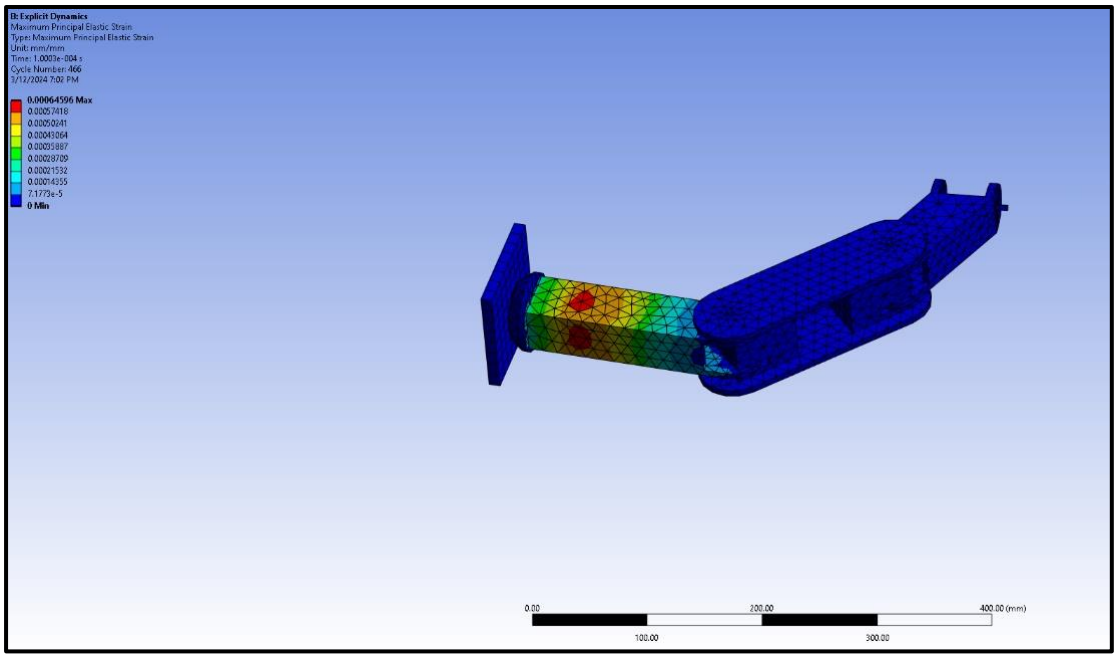

Figure 69: The maximum stress on the proposed rover from a 9-foot Lunar drop

Figure 69 demonstrates the strain experienced by the proposed rover after dropping 9 feet on the Moon. The maximum strain expected is 0.000645 mm/mm, which occurs in the lower leg, and 0 at minimum, which occurs in the upper leg. This matches the expected results based on the deformation simulation, shown above. This shows the strain will be elastic allowing any deformation in the titanium to recover without permanently damaging the structure. The stress in the simulation is calculated in Figure 70.

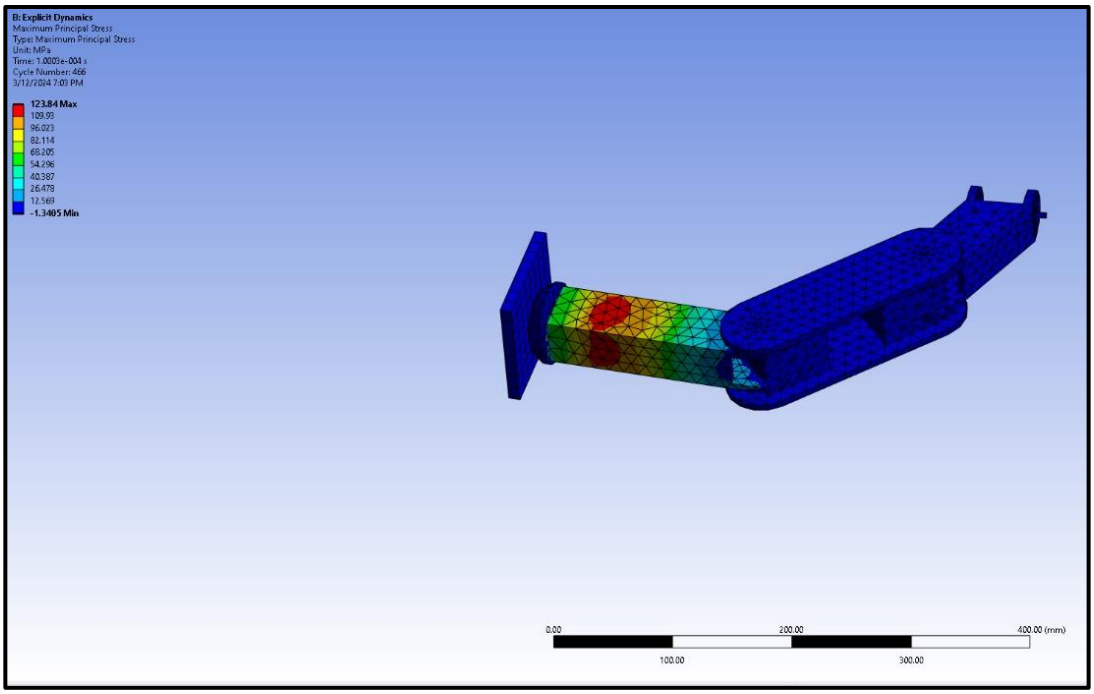

Figure 70: The maximum stress on the proposed rover from a 9-foot Lunar drop

The stress experienced in this simulation at maximum is 123.84 Megapascals while the minimum 1.6 Megapascals. This is far less than Titanium's 293 Megapascal tensile strength. Therefore, the leg is expected to perform as intended on the Moon without the leg breaking when falling from 9 feet on the Moon.

The simulation can be improved by running more detailed models. The models used for this simulation require defeaturing on much of the assembly to successfully run the simulation. If more computing power was available, the simulation would be able to run a more detailed model that would provide better results for both prototype and proposed rovers. Another way this system could be improved is having the leg of the rover impact the ground instead of having the ground impact the leg this would provide results more accurate than the current method of using the ground piece like a hammer to simulate the impact.

7.3 Thermal Simulations

Verification of the rover's temperature was required to ensure system survivability in the extreme conditions on the Moon. Under the harshest daytime conditions, the Lunar surface is approximately 395 K and the solar radiation is 1361 W/m^2 (NASA, 2024). The rover model was simplified to allow for rapid thermal modeling in COMSOL, and only the proposed rover was analyzed with a thermal simulation. Simulations included both conduction and radiation heat transfer. The sun was simulated as a radiative source vertically positioned at an infinite distance from the system, while the Lunar surface was simulated using Apollo Lunar samples whose properties were included in the COMSOL material library. Under the harshest nighttime conditions, the Lunar surface is approximately 140 K and there is no substantial source of radiative heating for the rover. Figures 70 and 71 below show the predicted thermal state of the rover in both daytime and nighttime conditions.

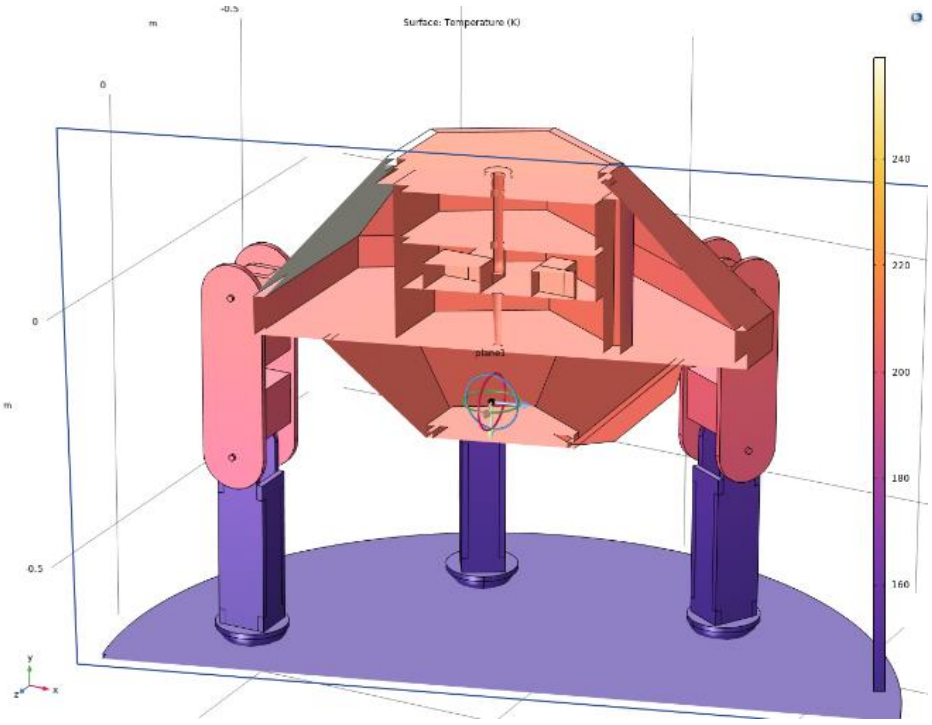

Figure 71: Thermal simulation of the rover in daytime conditions

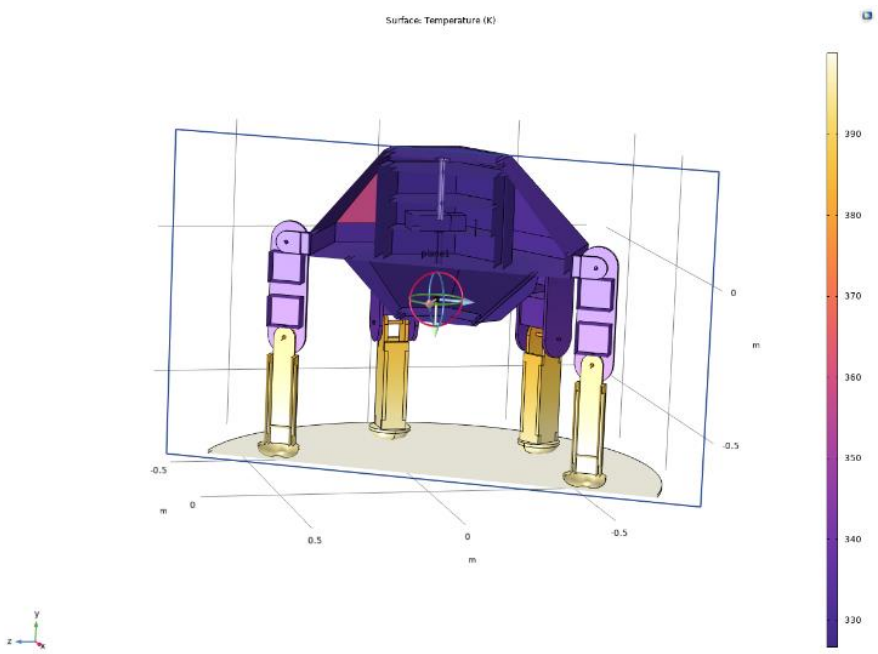

Figure 72: Thermal simulation of the rover in daytime conditions

For both situations, the materials on the rover were simulated using the same materials listed in the proposed rover design section of the report. Under daytime conditions, the temperatures inside the rover computing core reached values as high as 320 K. Under nighttime conditions the temperature in this section of the rover dropped to values as low as 265K. This was given a 50 W heater within the rover. The most stringent electronics selected for this rover have an operating range of –10 °C to 60 °C, or 263 K to 333 K. Using the simplified model, the rover is expected to survive in the harsh thermal conditions on the Lunar surface.

Given access to the research version of COMSOL, the simulations could be improved by reducing simplifications and increasing the number of elements in the rover mesh; however, these would only provide slight improvements to the results. The most significant improvements to the thermal analysis would come from validation of a constructed version of the proposed rover in a vacuum chamber. Such a physical verification will greatly improve confidence in the results.

8. Prototype Rover – Fabrication and Assembly

For fabrication and assembly, the team had numerous resources available through WPI and was able to fabricate many of the major components on site. A combination of laser-cutting, metal CNC, 3D printing, and waterjet-cutting were used to manufacture the structure of both the rover body and its legs. This helped reduce the purchasing of hardware and electrical components. A more detailed overview follows. Note that as testing of the prototype was conducted, several alterations to the assembly were made to improve functionality as described in the validation section of this report.

8.1 Body

The rover body was designed as a hexagonal shelf with a truncated hexagonal shell to protect the internal components. The shell was constructed out of a single piece of sheet aluminum, cut into a hexagonal pattern with the trapezoidal and rectangular side panels directly attached. It was then bent along the seams to form the truncated hexagonal pyramid shape we modeled in SolidWorks. To maintain shape, brackets were installed on each seam where two of the side panels met. This held the folded aluminum in place securely. Figure 73 shows this fabricated upper shell.

Figure 73: Image of the prototype rover's upper shell

The shelf was fabricated using a ¼-inch acrylic sheet and a custom aluminum bracket (Figure 74). Due to the size of the acrylic available, the shelf was laser-cut in two trapezoidal sections, so that they met along a major diameter of the hexagon. The hole for motor mounts and axles were simultaneously cut into the shelf. A 3.5-inch-wide aluminum bracket was constructed from two plates of ⅛-inch aluminum using a bandsaw. It was used to fit over the mating edge of the acrylic sections to hold them together. The two plates were then clamped on the top and bottom of the shelf sections and a drill press was used to drill the attachment holes. Upon being bolted together (bracket plate, then shelf, then bracket plate) the shelf was both assembled and reinforced along the centerline. Figure 75 shows an image of the completed shelf for the prototype.

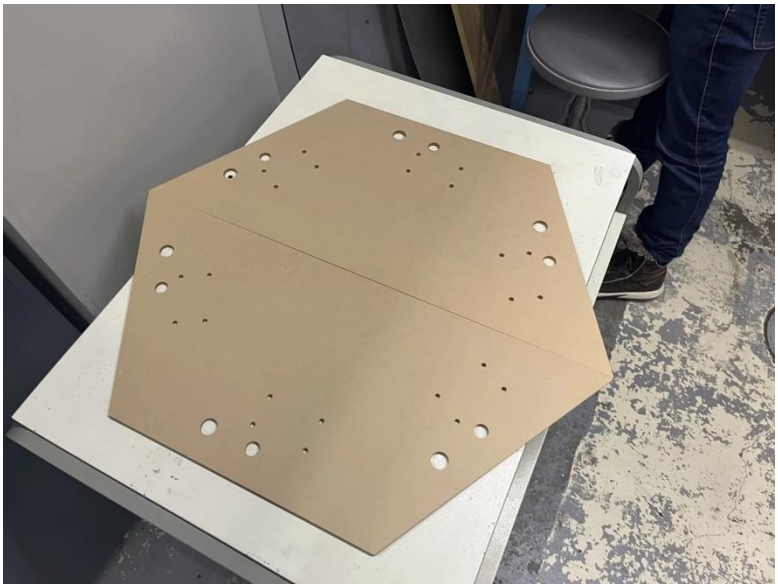

Figure 74: The acrylic shelf being fabricated in a laser cutter with the protection still attached

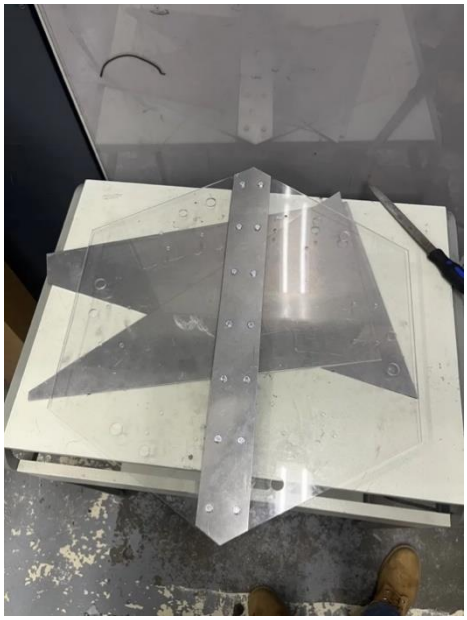

Figure 75: The final acrylic shelf for the prototype rover

When it was determined that the resistors in the electrical system required active cooling, two aluminum brackets were added to help siphon heat from them. These brackets were constructed by cutting two strips out of sheet aluminum and bending two feet into each strip. Holes were drilled into each of the feet to align with the mounting bolts of the acrylic plate

brackets. To ensure good thermal contact between the resistors and their brackets, a silicon thermal paste was applied to all mating surfaces. This thermal paste was also applied to the bottom of two large, prefabricated aluminum radiative heat sinks. These heat sinks were then mounted on the top of the resistor brackets using a small amount of epoxy resin on the edges to secure them.

In addition to the primary structure of the shelf, the mounting of the legs and motors also required fabrication. 6 motor mounts were 3D-printed, using standard black and white PLA, to house each leg's uppermost motors. The team recognizes that black and white PLA often have different material properties, but because these parts were not load-bearing, the differences were deemed negligible. These motor mounts are shown in Figure 76. These were bolted directly into holes which were laser-cut into the acrylic of the shelf. Additionally, 6 radial bearings were epoxied into the shelf so the legs could be properly mounted. Finally, two 12V DC fans were epoxied onto motor mounts so that each one was oriented directly across the fins of the heat sinks.

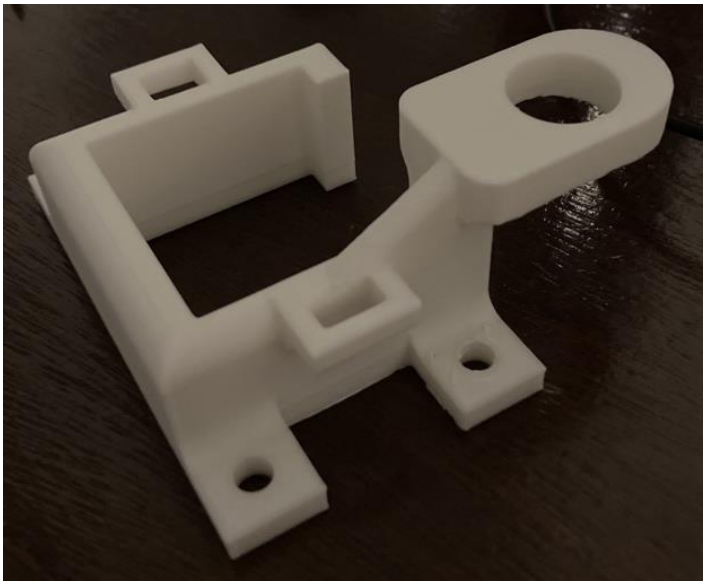

Figure 76: Image of the 3D printed motor mounts used in the prototype rover

8.2 Leg Fabrication

As previously discussed, the legs of the prototype require a significant number of components. This includes 10 major structural components and 19 small components for each leg, which were purchased. The total number of components for all six legs is 174, excluding mounting hardware. The major structural components include four segments of the lower leg, two plates on the upper, two motor mounts inside the upper leg, one shoulder mount, and a foot. All of these structural components were designed and fabricated by the team as described in the next section. The small components include motors, axles, flanged shaft couplings, gear sets, shaft collars and bearings. All these small components were purchased from outside vendors. Figures 77 through 79 show pictures of the small components the team used on the legs of the rover prototype.

Figure 77: Axles used in the prototype rover's legs

Figure 78: Image of the bearings used in the prototype

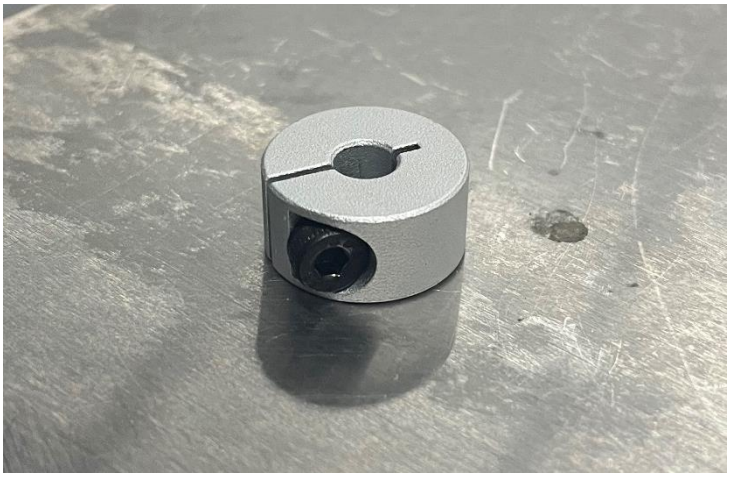

Figure 79: Image of the shaft collars used in the prototype

For the initial fabrication of the leg assembly, the team laser cut 1/8th inch plywood to test the fitment of parts and motors. An image of this model is shown in Figure 80 below.

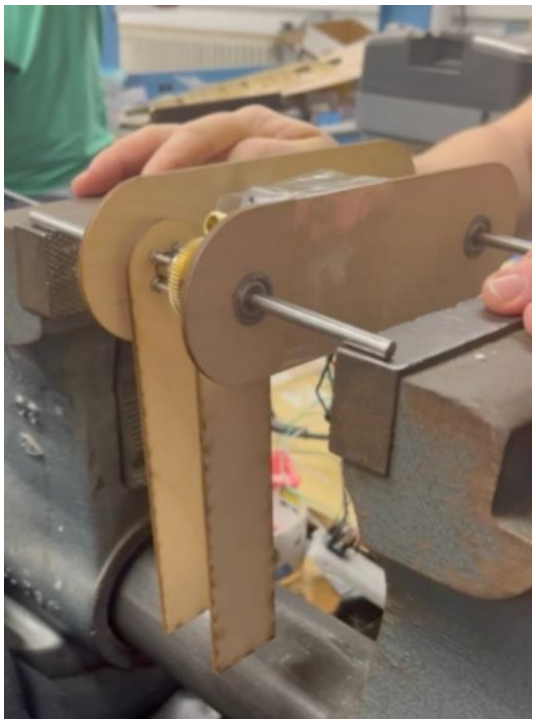

Figure 80: Image of the test leg made from laser cut plywood

The prototype's structural leg components were manufactured out of 6061-T6 aluminum alloy. The flat structural components were cut using a ProtoMax waterjet machine and the set up for cutting the flat plates are shown in Figure 81. The cut outs for the final parts are shown in Figure 82. The plate of six-millimeter thick 6061 aluminum alloy was clamped inside the machine. These clamps are pressed into place on a shaft that is screwed into a rail on the machine. The machine path is programmed with a .dxf file that shows the outline of the flat plate to define a tool path. Combined with material information, the software calculates the required flow rate of water and garnet to cut through the material. The process of cutting all forty-eight flat parts took roughly ten hours. This was a fraction of the time it took for the far more complicated parts, which had to be machined.

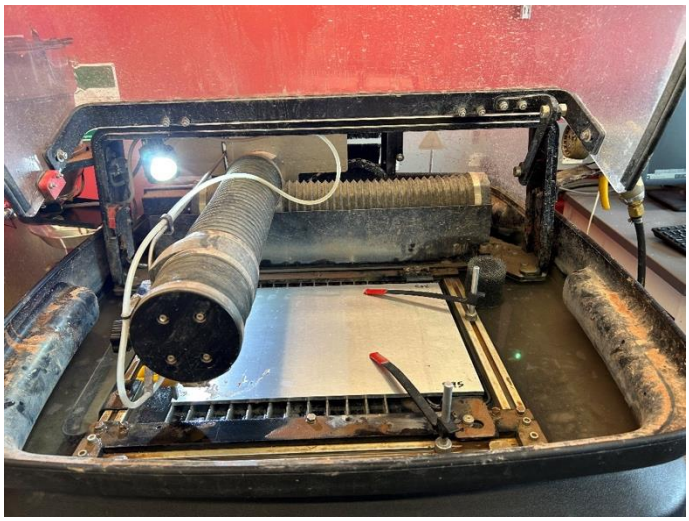

Figure 81: ProtoMax Waterjet setup

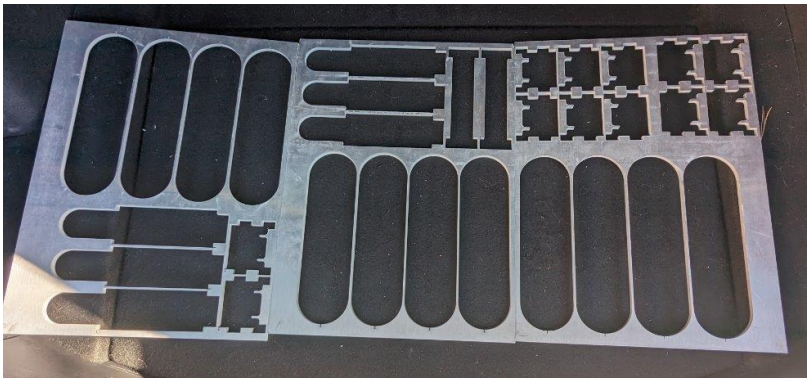

Figure 82: Cut out of final parts from the waterjet

The shoulder mount had to be machined due to the complex curves, tight tolerances, and the presence of features on all sides of the part. This was done in WPI's Washburn Machine Shop on Haas MiniMills and a VM-2, which are operated similarly. Images of these machines can be seen in Figures 83 and 84 respectively. Since a CNC mill was chosen, a CAM program had to be created to define the operations precisely and generate the complex toolpaths. This was done in Autodesk's Fusion 360 program in combination with predefined tool libraries from WPI's Washburn Machine Shop. Once a satisfactory program was created, it was loaded onto the

machine and run using a block of Al 6061-T6 material. This general process became more difficult due to the complex nature of the parts and the fact that there was no budget for additional tooling. The CAM process was further complicated by the use of scrap material that had drastically different starting dimensions.

Figure 83: Picture of the Haas MiniMill that was used in fabrication

Figure 84: Picture of a Haas VM-2

The first step in the process was to find stock for machining. Due to budget constraints, the team was able to find suitable stock for free which was cut into four separate parts with the bandsaw for the shoulder mounts. However, these segments had drastically different starting dimensions which complicated the CAM. The team also used two additional pieces of round stock material for the remaining two mounts. The stock then had to be prepared by squaring, cutting, and re-squaring along the cut sides. The squaring was done on the Haas MiniMill using a three-inch shell mill with carbide inserts. Figure 85 shows the large piece of stock after some squaring was done and after it had been cut into four pieces. Figure 86 shows a piece of stock after it was fully squared to within a degree of parallel. The different sized stock meant that either all the parts had to be cut with the CAM program for the largest piece of stock, resulting in

unnecessary air cutting and a slower process, or a separate CAM program would need to be used for each size of stock. The team decided to create different CAM programs for each size of stock. These programs had the same operations, but different toolpaths. There were some small changes, such as using different tooling for stock that needed more material removed, but they were largely the same.

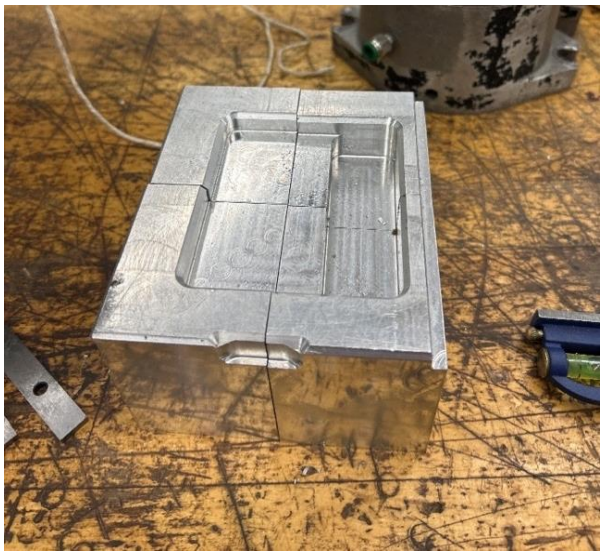

Figure 85: Large piece of stock after cutting

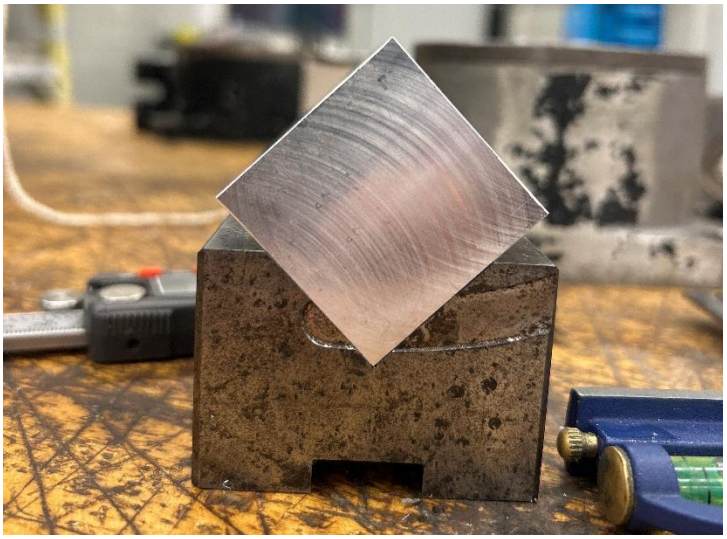

Figure 86: Piece of stock after squaring for the final time

The program for each piece of stock was broken into four different operations, with each operation using multiple tools to take multiple cuts. This was done because the machine was a three-axis machine and could not create all the features in a single setup. This meant that the parts had to be rotated in the fixture by hand between operations. Due to tooling constraints, each part was machined in five separate operations, with the last two operations being identical. These operations included facing, drilling, adaptive clearing, and boring. The tools used were primarily a three-inch shell mill, a 3/8-inch bull nose endmill, a ¼-inch bull nose endmill, and an 1/8-inch drill. Fixturing was done in a Haas machinist's vice for all operations. There was some postprocess filing and deburring required to square off the interior fillets naturally formed by the rounded tools and to finish off the part. The total time for CAD refinement, CAM, and machining was approximately 200 hours due to the team's lack of machining experience prior to starting the prototype. Pictures from various stages of the machining process are shown below in Figures 87 through 90.

Figure 87: First operation being executed on the shoulder mount

Figure 88: Shoulder mount after the first operation

Figure 89: Single shoulder mount with two operations remaining

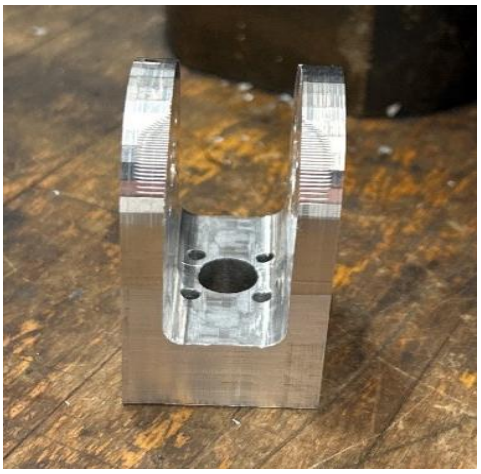

Figure 90: First finished shoulder joint

The flat plates were put together using epoxy, and the smaller, purchased components were secured using bolts. Due to inaccurate tolerances of purchased parts, some components needed to be heated while their mate was cooled to properly fit together.

Assembly time for all six of the prototype legs was approximately twenty hours. Figure 91 shows an image of the team assembling the legs.

Figure 91: The team assembling the rover legs

8.3 Leg Assembly

The assembly of the legs required a precise order of operations to prevent interference during the installation process. Firstly, two radial bearings were epoxied into each of the upper leg plates with the flange on the outside of the plate. Next, the flanged shaft mounts were installed. Three of these mounts were installed on the shoulder joint with the flanges on the outside and the hollow shaft pointing inwards. Prior to its installation, an axle was inserted into the vertical shaft mount and the setscrew was tightened down. This was done because the installation of the mount blocked access to the setscrew. The shaft mounts were then screwed in place to prevent them from rotating in their housing. Two more of these mounts were installed on the lower leg plates. Thirdly, the lower leg was assembled by epoxying two of the outer plates to two of the inner plates, with the plates fitting together like puzzle pieces.

After the epoxy was set, the axles were added. First, they were set into the bearings of a single upper leg plate. Then the lower leg was slid partway onto the lower axle, with the axle

only passing through the first of the attached flange mounts. The worm wheel was then slid onto the axle before sliding it the rest of the way through the lower leg segment. This procedure was then repeated with the shoulder joint and worm wheel installation on the upper axle of each leg such that the worm wheel was situated between the two flanges of the shoulder joint.

Next, the motor mount plates were inserted into the slots on the upper leg plate. This allowed the second upper leg plate to be attached to the leg, thus securing the motor mounts, axles, gear wheels, shoulder joint, and lower leg segment in place. The mating surfaces between the upper leg plates and motor mount plates were epoxied to ensure security. Also, all setscrews on the exposed flange mounts and gear wheels were tightened to prevent axle slippage.

The cylindrical worm gears were then installed onto the stepper motor shafts, with the setscrews being tightened down to prevent slippage. These motors were then installed onto the motor mount plates in two steps. First, they were loosely screwed onto motor mounts to allow them to slide freely. Second, the motors were positioned such that the cylindrical worm gears fit tightly against the worm wheels and the screws were tightened.

With the leg assembly completed each leg was installed on the main rover body as follows. First, a gear wheel and shaft clamp were stacked between the two bearings for each leg, with the shaft clamp being the lower of the two. Next, the vertical axle for each leg was inserted through the bearing in the acrylic shelf, the shaft clamp, the gear wheel, and finally the upper bearing in the corresponding motor mount. While holding the leg in place, the setscrews on both the worm wheel and shaft clamp were tightened, fixing each leg to the rover body.

9. Controls and Navigation

As one would expect, the guidance, navigation, and control systems software for the proposed rover would be of much larger scope and would strive to create a semi-autonomous rover. The code created was only designed according to the prototype and its necessities. Much of this code was used to simply communicate with the on-board computer, in this case a Raspberry Pi. For actual rover applications, this is largely not an issue, since it has been adequately implemented on earlier rovers. Beyond this, the team focused on researching and testing the kinematic model for the prototype rover, which was necessary to calculate movement instructions, and the basics of a navigation system, which would help direct the rover's path through obstacles.

9.1 Rover Kinematics

Inverse kinematics for a hexapod rover involves determining the joint angles needed to achieve the desired foot position and orientation. Forward kinematics, on the other hand, computes the position and orientation of the foot based on known joint angles. These kinematic models were created by deriving the equations with respect to the rover's dimensions. Deriving the inverse kinematic equations was necessary to convert desired positions and movements into information capable of moving the motors, since the movements of the legs are all dependent on motor angles. Data of all motors' angle changes over discrete time allow the rover to move precisely and navigate in a variety of terrains.

9.1.1 Leg Kinematics

To create a kinematic model for the entire robot, it was first necessary to derive a simplified model for an individual leg. This sub model uses the angle of each joint to estimate the foot position relative to the attachment point of the leg. Each leg has three linkages to connect three joints, each with one degree of freedom.

As done in (Lubbe Et al., 2015), the link and axes are assigned following the Denavit-Hartenberg notation. The hip, shoulder, knee, and foot are assigned a number ‘m’, 1-4 respectively. The foot and each joint are made the origin of reference frame m with unit directions X_m, Y_m, and Z_m. As shown in Figure X, for each axis, the X_m direction is parallel to the m^{th} linkage. The joint angle is simply the angle between X_{m+1} and X_m.

The primary point of focus for the movement of the rover revolves around foot position. The path of the foot through the air and on the ground, combined with timing, is entirely what moves the robot. Once the necessary physical positions of each foot are determined, the angles of the joints required to represent these positions must be calculated. These joint angles, and more specifically their changes through time, are what is fed to the different motors. Inverse kinematics is the mathematics behind the conversion of the joint positions to their angles.

Inverse kinematics are described as inverse due to how they ‘work backwards’ from a result (foot position) to find the cause (joint angles). To calculate forward from angles to positions, one would use joint angles and simple trigonometry to find the joint positions in 3-dimensional space. Inverse kinematics, rather, involves using the link lengths of the legs to find each angle using, primarily, the law of cosines since no angles are initially known. The order of these calculations starts with finding the second angle (shoulder) and then determining the third

angle (knee). The first angle is already determined since the forward-and-backward angular motion of the leg in the body frame is already pre-specified.

The figure below displays the equations used for these calculations based on the dimensions of our rover. The problem is initially 2-dimensional as the hip angle can be neglected at first. The horizontal distance from the hip to the foot is represented as, while the direct distance from hip to foot is 'Lr'. This forms a right triangle with the length of each side known (Figure 91). The law of cosines is done twice, once with respect to θ_3 (knee) and next with respect to θ_2 (shoulder).

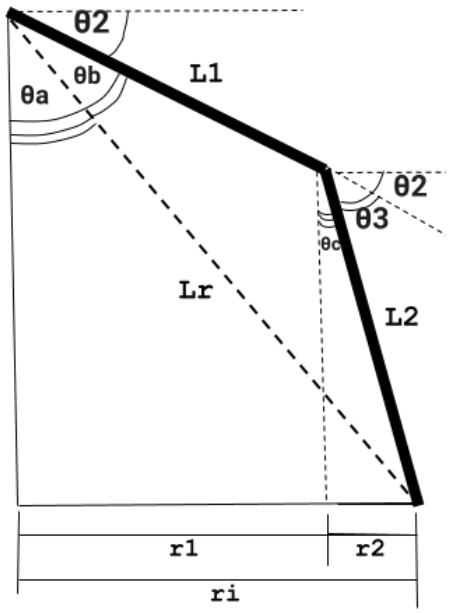

Figure 92: 2-dimensional geometric representation of the leg

Subcomponents such as horizontal distance from shoulder to knee and from knee to foot are represented by r1 and r2. In addition, there are three extra angles (θ_a, θ_b, and θ_c) used for the purposes of trigonometric calculations.

Below are the equations used for 2-dimensional hip and knee angles based on the dimensions of our rover.

$$l_r = \sqrt{ri^2 + zi^2}$$

$$\theta_a = cos^{-1}\left(\frac{zi}{lr}\right)$$

$$\theta_b = cos^{-1}\left(\frac{zi}{lr}\right)$$

$$\theta_c = tan^{-1}\left(\frac{r_2}{z_2}\right)$$

$$\theta_2 = \left(\frac{\pi}{2}\right) - \theta_b - \theta_a$$

$$\theta_3 = \frac{\pi}{2} - \theta_2 - \theta_c$$

$$z_1 = l_1 * sin(\theta_2)$$

$$z_2 = z_i - z_1$$

$$r_i = \sqrt{xi^2 + yi^2}$$

$$r_1 = l_1 * \cos(\theta_2)$$

$$r_2 = r_i - r_1$$

For normal kinematics (angles to positions), the hip angle θ_2 is incorporated to account for the x and y axes, rather than just the radial positions from above. The below equations display how the calculated angles are used to find positions in 3 dimensions.

Below are the equations for the knee coordinates.

$$k_{xi} = l_1 * \cos(\theta_{2\,new}) * \cos(\theta_{1\,new})$$

$$k_{yi} = l_1 * \cos(\theta_{2\,new}) * \sin(\theta_{1\,new})$$

$$k_{zi} = l_1 * \sin(\theta_{2\,new})$$

Below are the equations for the foot coordinates.

$$x_i = r_{foot} * \cos(\theta_{1\,new})$$

$$y_i = r_{foot} * \sin(\theta_{1\,new})$$

$$z_i = \left(12 * \cos(90) - (\theta_{2\,new} + \theta_{3\,new})\right) + k_{zi}$$

The determined angles, radial distances, and x-y-z distances from the shoulder are referenced from the shoulder frame of reference. The foot position relative to this hip x-y-z frame is represented by ^{0}p. Another mathematical form of converting the foot position through reference frame (foot frame to knee frame to shoulder frame to hip frame) involves using transfer matrices, notated by T_m^{m-1}, that convert ^{m}p to $^{m-1}$p (foot position relative to the preceding coordinate frame) (Sun Et al., 2017). Multiplying all transfer matrices for each joint by the foot position in its original coordinate frame gives ^{0}p. Figures 92 below shows how the body frame would incorporate the leg frames, and Figure 93 provides the transfer matrix used to convert the foot position through the coordinate systems of the leg to find p0 (Sun Et al, 2017),

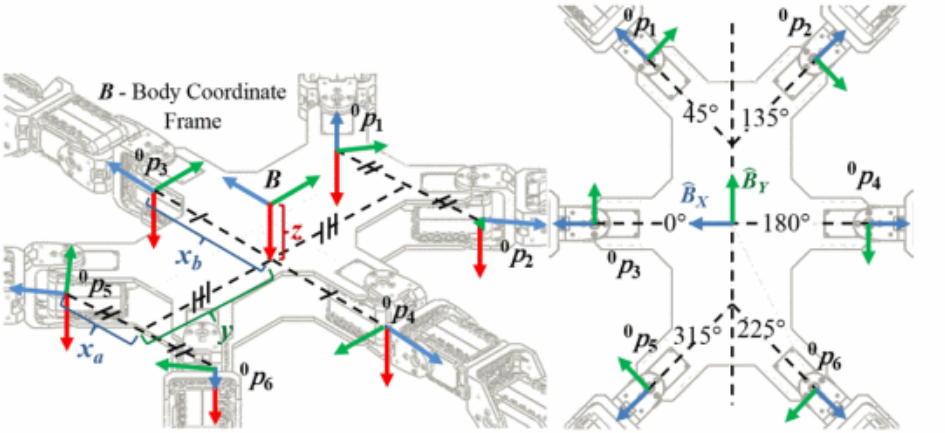

Figure 93: The relationship between the body coordinate frame and the origin of the legs. © 2024 IEEE

$$
{}^{m-1}_{m}T = \begin{bmatrix} c\theta_m & -s\theta_m & 0 & a_{m-1} \\ s\theta_m c\alpha_{m-1} & c\theta_m c\alpha_{m-1} & -s\theta_{m-1} & -s\theta_{m-1} d_m \\ s\theta_m c\alpha_{m-1} & c\theta_m c\alpha_{m-1} & c\theta_{m-1} & -c\theta_{m-1} d_m \\ 0 & 0 & 0 & 1 \end{bmatrix}
$$

Figure 94: The general form for the transformation between neighboring links is given (Sun Et al., 2017), © 2024 IEEE

9.1.2 Step Motion

With the ability to determine angle positions for the legs' orientations, it was then possible to discretize a desired foot path and convert the changes in position to changes in joint angles over time. The first step in this process was to create a desired foot path and define it mathematically. Originally, a simple parabolic curve was used, since it appeared to be the most optimized path, in terms of having smooth motion with minimal exertion (Ma Et al, 2022). However, this was not simple to implement and added complexity with changes step parameters such as height and distance. Success was achieved using a simple up-over-down-back rectangular path. This path was easier to code for the motors and decreased the need for all motors to be running at once.

The discretization was done by starting with an initial value, an increment value, and a final value in MATLAB. The step motion was broken up into four parts, one for each direction. Each phase of the step for each joint was discretized by its initial and final angles, creating a vector of angles in between these two values. The four vectors were then vertically concatenated to form a vector of all angles throughout a step for each specific motor. Applied to all motors, the result was a matrix with eighteen columns, corresponding to the 18 motors, and a number of rows dependent on the discretization.

Next, these angles needed to be converted to angle changes so that it could be given to the motors in terms of the number of stepper motor increments. This was done by simply subtracting each row by the row before it. To convert these angle changes to stepper motor increments, multiplying the stepper motor's steps per revolution by the gear ratio gave the total number of motor steps required for a full revolution of a joint. This was then divided by 360 degrees to get the number of steps per degree.

9.1.3 Gaits

For the rover's mobility and having the legs move, there are a few gait options available for hexapod robots that are commonly used: wave, ripple, and tripod. Each is functionally distinct, providing different speeds and stability, though all are adaptable for obstacle avoidance and non-linear paths (Gurel, 2017).

Wave gait provides the lowest speed but highest stability by moving one leg at a time. The ripple gait meanwhile follows a more insect-like pattern and could be considered as moving 'one and a half legs' at a time in a ripple-like fashion as shown below. Lastly, the tripod gait moves three legs at a time while pushing with the other three. It is the fastest, though it has only 3 legs on the ground at a given time hence it is less stable (Gurel, 2017).

For our prototype design we decided to primarily use the wave gait due to its simplicity and better weight distribution, a significant problem for our lower-budget motors, which had torque limitations. An actual Lunar rover could naturally swap between different gaits and vary step height and distance according to obstacles in its local environment. It would likely have some form of artificial intelligence capable of adapting the rover's gait to step over or on top of obstacles. This type of intelligent programming was beyond the scope of our time and hence we

focused on optimizing our prototype's use of RRT* pathfinding for navigation using one specific gait at a time.

To mathematically convert the stepper motor changes for a full leg step, as described in the previous section, to behavior matching the selected gait, it was necessary to reform the order of the columns (motors) so that the stepper increments would take place at the right time. For instance, the tripod gait always has three legs going up/forward while the other three are going down/back. This was created by taking the columns representing half of the motors and shifting the four phases of each in the order of down-back-up-over (rather than up-over-down-back). The timing therefore would occur so that the movements are happening for all legs according to that specific gait.

To create a 3D simulation for the rover's walking in MATLAB, the rover's kinematic model was implemented in conjunction with the leg model applied to all six legs. The rover's body frame, specifically its X-axis (representing a heading of zero) and origin were established. From this, the location of all six hip joints relative to this coordinate system were found. The 0.263 meter offset of the hip joints from the rover's center and the 60-degree angular increments of each leg from the X-axis were applied to the kinematic model to add the start of each leg to the overall model. From this point, the knee and foot points were converted to the body frame using the transfer matrix from before (Lubbe, 2015). It is important to note that the plotting did not require any of the previous inverse kinematics, since plotting in MATLAB is just in coordinates.

To form the 3D MATLAB plot, the body frame was placed in an inertial frame with its origin at (0,0,0). Because the center of the robot was at zero in the Z-axis (height), all points below the robot had negative values. Other than this detail, the body frame and inertial frame

were identical which meant all points simply needed to be added to the plot. Lines connecting these points were included for better visualization and the changes in coordinates throughout a step were discretized and re-plotted continuously. To form the tripod gait, the steps for three of the legs were started halfway through the completion of the other three legs.

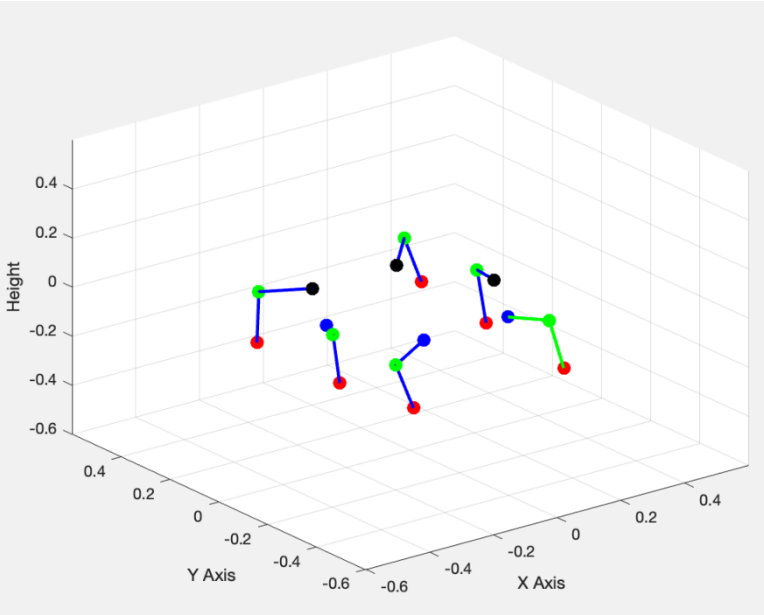

Figure 95: MATLAB simulation of the tripod gait

9.2 LiDAR

LiDAR (Light Detection and Ranging) is a remote sensing technology that measures distances. Real-time processing refers to the ability to process LiDAR data quickly in order to extract relevant information, such as detecting obstacles, localizing the vehicle, and updating navigation parameters (Yuwen, 2023).This is critical for ensuring the safety and accuracy of the navigation system. LiDAR is critical in providing real-time data for understanding the environment when it comes to controls and navigation. The team investigated three types of LiDAR: single-point, plane and cone. A single point LiDAR emits a single laser beam and measures the amount of time it takes for the laser pulse to return after hitting the object

(McManamon, 2019). Single-point LiDAR sensors are frequently used to measure basic distances. Plane LiDAR, also known as 2D LiDAR, emits a laser beam in the shape of a plane or fan. It scans a horizontal section of the environment and generates a 2D representation of what it senses. Plane LiDAR is commonly used in obstacle detection and collision avoidance applications (McManamon, 2019). Cone LiDAR, also known as 3D LiDAR, emits laser beams that cover a three-dimensional area in multiple directions. It provides detailed spatial information and is used for mapping and localization in advanced applications such as autonomous vehicles and robotics.

9.3 Navigation

A* and RRT* are two well-known path planning algorithms used in robotics. A* is a popular search algorithm for determining the shortest path between two nodes in a graph or grid. It is commonly used in applications such as map route planning and video games. A* is based on a combination of two cost functions: the actual cost to reach a node from the start node (called "g" cost) and an estimated cost from the node to the goal (called "h" cost). The algorithm aims to minimize the sum of these two costs (Yuwen, 2023). A* uses a priority queue to explore nodes with the lowest total cost, making it a best-first search algorithm. It is complete and optimal, meaning it is guaranteed to find the shortest path if one exists.

RRT* (Rapidly Exploring Random Tree Star) is a tree-like structure that builds possible paths from a starting configuration to a goal configuration. It accomplishes this gradually by adding new nodes to the tree. Unlike A*, RRT* randomly samples the configuration space, making it more suitable for problems where the search space is not known in advance. As it explores, RRT* tries to optimize the tree by rewiring it to find shorter and more efficient paths. This makes it useful in rapidly changing environments or when the surrounding space has not

been fully explored (Yuwen, 2023). Given enough time and samples, RRT* will eventually find a solution if one exists. In summary, A* is a deterministic, graph-based search algorithm that finds the shortest path in known environments, whereas RRT* is a probabilistic, tree-based algorithm that plans motion in unknown environments.**Error! Reference source not found.** The choice between these algorithms is determined by the nature of the problem and the environment in which they are used (Yuwen, 2023)

The team created a MATLAB simulation for path planning in a predefined environment using the Rapidly-exploring Random Trees (RRT) technique. Users can specify the map's dimensions and the positions and sizes of obstacles by using the code. The code allows the user to use RRT methods to develop a path that is suitable without having to manually choose the path. There are many useful capabilities built into this code that expand beyond basic RRT implementation. This includes the ability to add intermediate goals. This is a necessary capability for cases where there is a scientific need to develop a path that does not go directly to the endpoint. Beyond this, the code also allows the user to simplify the path to create more efficient movements than would normally result from an RRT. Some of this functionality is built directly into the code, while the user is also allowed to request further simplification. The code displays the progress made during path planning improvements and also allows users to save progress. The ability to save progress is useful for areas that require significant computation time, as the computation can be done ahead of time and the path can be loaded later when it is needed.

The built in path simplification algorithm was implemented to create more direct, linear paths for the rover to follow. This is necessary because the natural output of an RRT will be a convoluted and indirect path, which would usually not be ideal to follow. By checking many points throughout the path generated by the RRT to see if they can be connected more directly.

In doing this, the program checks obstacle locations and ensures that no obstacles are in the new path. By doing this, the algorithm will often reduce a complex path to a much smaller series of points that are more suitable for a rover to follow. The below code shows an implementation of the navigation system in a simple area. This path starts with intermediate goals, that require the RRT to navigate around an obstacle, despite the final objective being close to the starting point. This path was filtered to create linear segments that could be followed. The first output can be seen below in figure 96.

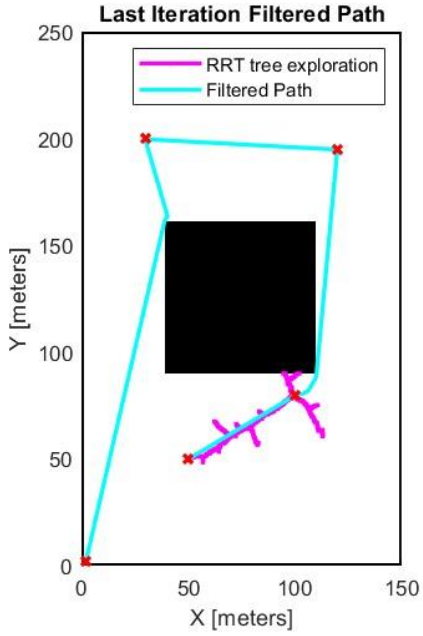

Figure 96: The MATLAB plot demonstrates the RRT path planning algorithm in a simulated setting.

As seen in Figure 96, the original path meets all intermediate objectives, marked by red "X". These paths are linear due to the filtering that was performed on the output of the RRT. However, if the user no longer needs the exact intermediate points, the path can be filtered again to yield a simpler path, which will still avoid obstacles. This is shown below in Figure 94.

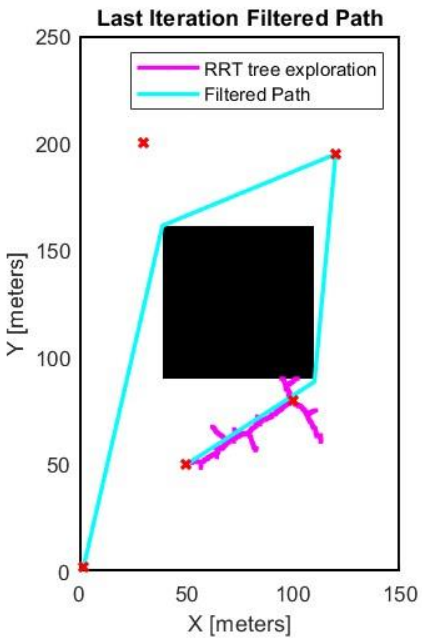

.

Figure 97: Path planning is shown in this MATLAB RRT plot, where four goal sites are shown by red 'x' markers.

As seen above in Figure 94, the new path is simpler than the first. However, the intermediate objectives were no longer met. Despite this, the path does still goes around the obstacle the long way due to the intermediate points in the path. The team believes that this is a likely beneficial outcome since the intermediate goals on the far side of the obstacle indicate some scientific objective that needed to be investigated. This same system can take any number of obstacles of varying size. Additionally, it can be run on larger areas, but requires the tolerances of the RRT to be changed, which is a simple matter. The team believes similar methods that were used for this algorithm could be useful to more complex rover implementations, since it enables the relatively simple RRT algorithm to be adaptable to different mission requirements. A notable improvement to the methods presented here would be to use a three-dimensional RRT. This would likely need to compute valid paths for both the body and the individual legs. This algorithm would be much more complex and would require greater computational capabilities or the ability to calculate the paths in advance for a given mission.

10. Validation

A key aspect of this project was to validate the feasibility of the proposed rover by testing a simplified prototype. As previously discussed, the prototype rover was constrained by budget and time. As a result, some capabilities that would be required for a real Lunar rover were only able to be tested in a diminished capacity. By testing and validating most of the major capabilities on the prototype, the team believes that the proposed design would be able to adequately extend to many computational tasks with better hardware.

10.1 Structural Validation

As previously discussed, the team performed structural simulations, both static and dynamic, on the proposed and prototype rover designs. Since the proposed design had no tangible product, it was not possible to physically validate the results of these FEA analysis and results. However, because the FEA for both designs were conducted so similarly, it can be confidently asserted that any successful validation of the prototype structural simulation lends some credibility to the FEA that was done for the proposed design, although it is not a definitive validation. The FEA simulation that was performed on the prototype design showed that all major structural components should have experienced minimal deformation at higher-than-expected loads while standing on three legs. The team successfully tested this by standing the prototype on the ground with only three legs supporting it. During numerous tests, the team observed no noticeable deformation on any of the structural aluminum parts, indicating that they performed as expected. However, testing highlighted one major inaccuracy of the ANSYS structural simulation resulting from the simplification of the rover design. The simulation assumed the worm gear components to be in contact with their counterpart throughout loading, but during testing this was not necessarily the case. During certain configurations loading could

cause gears to lose contact because of slight tolerance differences and slip, resulting in leg placement errors that frequently caused the rover to fall. This specific issue will be discussed further in the rover operation section, but, in short, tested conditions were changed to avoid configurations in which the gears would slip. Going forward, the rover was mostly tested in configurations with more than three legs supporting it, resulting in the load per leg being lower than simulated. It should be noted that the aluminum components never experienced visible deformation as a result of the applied load. Therefore, the team considers the simulations to be valid implementation of FEA for the structural aluminum components only and believes that a more complex model should be used for future applications. The team believes that these results indicate the proposed model would likely not experience any significant structural failures of the modeled components, and with precision tolerances, this gear slippage, and other related issues may not be nearly as significant.

The other major structural simulation was the dynamic test, which modeled a drop test. This was not validated for either the proposed rover or the prototype rover. The team could have conducted a similar drop test with the prototype rover but elected not to because some of the unmodeled components such as gears and epoxy would have failed during a drop test. The team believes that the gears would easily slip and some of the epoxy that was used for assembly would have broken, leading to complete failure of the prototype rover, and the inability to conduct the necessary tests on a budget. Had the gears been rigid enough to support the rover during maximum expected loading, the team would have considered performing a drop test to further validate the methods used to perform FEA and the generated analyses.

10.2 Electrical and Thermal Validation

Before performing extended testing on the prototype rover, the team conducted tests of the electrical and thermal systems. These tests were exclusively limited to the prototype's electrical system and provided no validation for the proposed rover. In order to perform component compatibility tests, the team constructed one leg using smaller quantities of electrical parts. We used simple scripts to operate the motors over I2C addressing with low voltage batteries to confirm that it was possible to send commands to multiple motor controllers at the same time. These tests also confirmed the importance of using high voltage batteries for motor operation because there was a significant difference in motor speed when using the Raspberry Pi's 5V source and the nine-volt battery. With this knowledge, the team chose to expedite the purchase of higher voltage batteries that would be used to power the motors.

Upon integrating the higher voltage batteries, the team tested the operation of multiple motor controllers over I2C addressing and found that the motors could be run roughly 30 percent faster. When testing the electrical system, one of the motor control boards suffered a failure because there was not enough resistance in the system and too much current was put into the motor controllers. This resulted in the loss of one motor controller, which had to be replaced. The solution to this problem was to add resistance to the system to reduce the current. The additional resistance generated a significant amount of heat, which had the potential to negatively impact the other electronic components.

The team encountered a few thermal issues during testing, some of which were solved with simple alterations while others required the addition of components to the system. The first of these occurred when testing the motors with nine-volt batteries. Multiple nine-volt batteries had to be used to provide enough current for all motor controllers. This current was too much for

the smaller wires that had been used for initial testing. To solve this, the team instead used twelve-gauge wire for connecting the batteries. However, even this thicker wire heated a significant amount when connected to the final, larger batteries. This required the team to remove the terminal covers, which acted as insulators to cause excessive heating over extended periods of time. The final heating problem came from the large resistors that were added to the wiring to reduce the current leading to the motor control boards. These resistors could heat excessively during operation, which was partially software driven. In order to solve this issue, the team added heat sinks to the rover and fans to help dissipate excessive heat. The resistors were attached to the rover's central aluminum bracket using thermal paste to help with heat conduction. Then, a commercial heat sink was attached to a large metal bracket that covered and secured the resistors. This system was validated during testing by checking the temperature of the resistors using a thermistor and an infrared temperature sensor. This showed that the resistors would eventually reach levels beyond the capacity of the electronics (one hundred fifty degrees Fahrenheit), if the rover was run continuously for more than ten minutes. This could be extended by improving the software, which will be discussed further in the following section.

The final element of electrical validation occurred in the form of motor tests. As will be further discussed in the following section, there were significant software elements that pertained to operating the electrical components. However, the team also had to test the components themselves to ensure they were working properly, so that any errors later in testing would not be wrongfully attributed to the equipment. While testing this, the team found significant manufacturing quality problems with the stepper motors that were purchased. After being operated numerous times, five motors stopped functioning. When investigated, the team found that the solder inside the motor had come loose, most likely due to excessive vibration, causing

one of the phases of the motors to fail. The team was able to re-solder the motor connections and correct this issue to continue using the components on the rover. Also, the team encountered a failure on one of the Raspberry Pi power supplies, which led to the failure of one Raspberry Pi unit. Luckily, the team had two Raspberry Pis that remained operational and were used for the remainder of the project.

10.3 Software Validation

The primary forms of software validation that were performed during the course of this project involved confirming expected performance, controlling heating, and adding functionality necessary for testing. The first of these took the form of operating the primary motor code either with or without the rate filter to confirm that the expected movements were occurring. Heating control was done by including releases for the motors that were not being run. This limited the current that was running through the resistors and significantly reduced heating. Additionally, as testing progressed, the team found that certain functionality could be added to allow for easier testing.

Confirming expected motor performance was necessary to validate the accuracy of the motor control function, which was written in Python. This function was crucial to the project since operating all motors according to instructions was the basis for all rover operations. This was done repeatedly by determining commands for a specific action and observing the reaction of the motors. As with most code, some bugs were found and fixed during testing, but the team also encountered some errors that appeared to trace back to third party software or firmware. The simplest of these was a failure with I2C addressing which occurred numerous times at seemingly random intervals. When the code failed to send the I2C command, the code would error and then fail, making it impossible to run the motors. The team used simpler Python scripts to run the

motors in a for loop with error catching functionality to count I2C errors. The results of this test showed that depending on the wait times used in the code, I2C errors could occur between roughly four percent of the time and fifty percent of the time. The team also found that there was an ideal wait time to account for this error, but it depended on the specific code being run. The findings from this testing allowed the team to use similar error catching in the main motor operation code to avoid missing steps and to tune the wait times for optimal performance.

With improvements to the motor code to avoid I2C addressing issues, the team continued testing to confirm that the motors moved as expected both with and without passing the instructions through the rate filter. The team found that this function operated as intended, although some rare motor issues persisted. During testing the motors would still fail to step properly at times, but the results could not be replicated. The team determined that this was still due to issues using I2C addressing, either due to the third-party software or the firmware, likely the clock desynchronizing. The team was not able to correct this issue, but, due to its relatively rare occurrence, the team continued testing the full prototype rover.

10.4 Rover Operation Validation

Over roughly seven weeks, the team tested the prototype’s ability to operate successfully and consistently and made adjustments accordingly. The main objective of these tests was to prove the functionality of components needed for the rover to walk under its own power. Originally, the team’s objective was to demonstrate the ability for it to walk using multiple gaits, over various terrain, up inclines and stairs, as well as operate remotely while gathering data. As discussed in prior sections, there were difficulties encountered during the prototype's fabrication and testing. For this reason, the team had to narrow the test objectives to maintain realistic goals.

The first issue that the team encountered after fully assembling the prototype was the fitment of the motors. The gears used on the prototype, particularly its teeth, were very small, meaning the cylindrical worm gear on the motor shaft had to be precisely aligned with the worm wheel so as to avoid slipping. The team anticipated this issue and designed the lower motor mounts with elongated mounting holes to help adjust the motor fitment. However, the fit was looser than anticipated. Throughout testing, the team had to readjust the motor fitment, occasionally after long periods of testing or excessive vibration from the motors. The lower motors were adjusted by realigning and tightening the mounting screws. The upper motors were adjusted using shims to keep the motor aligned with the gear. In addition to this, the team had to redesign the upper motor mount, which was made out of PLA, because the upper shaft was not rigid enough. To solve this problem, the team added a shaft collar, an additional bearing, and an extended motor mount to hold the shaft. This worked well and the team rarely had to adjust this upper system throughout the project.

Another problem encountered during testing was the fit of the cylindrical worm gears, the worm wheels, and the flanged shaft couplings to their respected rounded shaft/axles through set screws. These components were secured by small set screws, but the poor manufacturing quality of the purchased parts led to fitment issues. To tighten the fit, tape and epoxy were used to securely fit the cylindrical worm gears to the motor shafts. Additionally, shafts had to be filed to create a flat section for the set screw to sit against. This proved useful but did not completely solve the issue. The team then drilled small divots into the shaft to hold the set screw, which further improved the fitment. Despite these efforts, the fit of the motors still had to be extremely precise and, when combined with loads near the maximum expected values, they could still slip out of position and cause the legs to buckle. This generally happened when the rover was moving

three legs at once. After trying to fit the motors better and continuing to find that slipping could occur, the team decided that the prototype would not be able to perform a tripod gait. The prototype stood in a tripod, but when shifting the center of mass by moving the legs was combined with the sudden movements of the motors, three legs could not support the prototype, thus highlighting the issues of the FEA simulation. The tripod gait was still tested on the test stand and through MATLAB but could not be attempted on the ground. Additionally, this issue made walking up stairs and significant slopes impossible given the current condition of the rover. Despite this, the team continued to pursue a demonstration of the rover walking on flat ground using the wave gait.

At this stage, the team knew walking would need to occur from a squatted position, such that the legs of the prototype were not completely vertical. Before trying to walk, the team sought to have the prototype transition from a standing position with straight legs to a standing position with the only the lower leg vertical and the upper leg at an ideal angle. The team often used a squatted position with the top leg section at sixty degrees from the horizontal and the lower leg an additional thirty degrees to make it vertical.

Many tests on the squatting motion were needed to troubleshoot problems with the motor fitment. One of the notable lessons learned from this testing was the need for ensuring that feet had completely cleared the ground while moving. A video of the prototype squatting under its own power and a simulation of how it is supposed to do this are available in the video repository linked in Appendix B. As can be seen in the video, the lower legs move inward when a leg lifts up. This is done to keep the lower leg from dragging on the ground because it would lead to more gear slipping.

Often this slipping was small and would not cause the rover to fall on a single leg; rather, it would cascade to where the final legs would fully buckle because the rover was not positioned correctly. The team carried this lesson through to walking and continued to have the legs move such that there was no contact with the ground when a leg needed to move outward or forward.

Additionally, the team was able to confirm the necessity of the rate filter for motor movements. We were able to run the instructions for squatting both before and after using the rate filter and the team observed that there was a significant difference in performance. The team evaluated that the squatting instructions would only have worked with the rate filter, as expected, and continued to use it for all future motor movements. With these basic operation tests done, the team moved on to walking tests.

10.5 Walking Tests

The team's initial functionality goals for the prototype rover were for it to walk with three different gaits, over various terrain, up inclines and stairs, operate remotely while gathering data, and avoid obstacles through map updating. As previously stated, the team refined these goals throughout the project as new problems arose to inhibit the feasibility of the initial objectives. By the end of the project, the team decided to establish the final goals as demonstrating the rover's capability to walk several steps to achieve a noticeable displacement using the wave gait, demonstrate the tripod gait and zero radius turn on the test stand, and simulate the inverse kinematics for both the wave and tripod gaits.

One of the main differences between the final and the initial walking methods was the position of the initial leg conditions on the rover. The team designed the rover as a hexapod so that the legs could be initially oriented perpendicularly to the hexagon's edges. This would allow the rover to begin walking in any direction and would, therefore, be beneficial for a Lunar rover.

The team had some difficulty instructing the rover to take successful steps in the initially intended walking conditions, due to previously discussed mechanical issues. By simplifying the initial leg orientation so that there were two sets of three parallel legs, the number of axes of symmetry was reduced from 3 to 1 as shown in Figure 98. Therefore, the instruction matrix uploaded to the rover to initiate a walking motion was much simpler and symmetric.

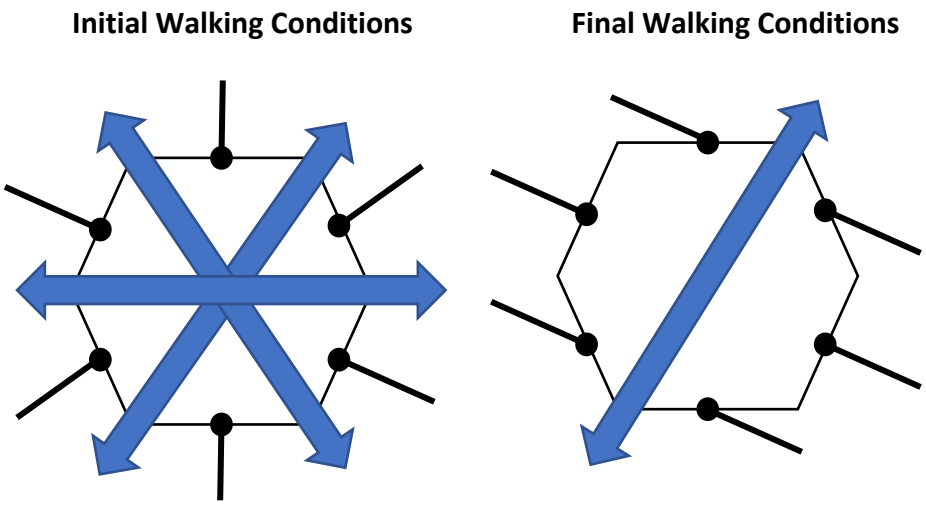

Figure 98: Initial and final walking conditions.

In this orientation it was also much easier to visualize when gears had slipped or motors had not functioned as intended, thus allowing for more precise adjustments. Using this orientation and the information learned from basic rover operation tests, the team created an n-by-20 matrix (as explained in earlier sections) where columns 3-20 instruct each of the 18 motors how many steps and when to take them. This matrix was then run through the rate filter to ensure that all motors run at an appropriate rate over time ensuring that motors follow the step increments with the correct timing. The team began testing this walking code by uploading the instructions to the prototype, incrementally increasing the complexity.

First, a single step for the front right leg was coded into a matrix and tested on the prototype. The team observed the results to see if they matched what was expected. If results

were not as expected, the team adjusted the software to re-test, and if the results were as expected, the team moved on to creating instructions for the next leg. All the legs were instructed to lift and rotate toward the front of the rover, with the right legs each rotating clockwise and the left legs each rotating counterclockwise. Once all the new foot positions were established, the rover was instructed to rotate using all the upper shoulder motors to shift the body over the new position.

This process was repeated to complete as many steps as was desired. We tested this code first for one step to evaluate its effectiveness and to identify the motor specific adjustments that needed to be made because of individual fitment differences. Then, once this was verified, we tried two steps to check the repeatability of the stepping motion code and made adjustments as necessary. This process was repeated until 5 steps, at which the team determined the code was now theoretically repeatable for any number of steps. There was a significant amount of trial and error involved in this process, but in the end, the team made the rover walk 6 full steps in this way, covering about 8 inches. A video of these steps and a SolidWorks simulation of what was expected is shown in the video repository linked in Appendix B.

After these 6 steps, the resisters heated up significantly to the point where it became unsafe to continue running the code. This was because none of the motors were released when they were inactive. Prior versions of the motor execution code had included more frequent motor releases, which allowed for much larger operational periods, but this seemed to contribute to motor movement errors. After testing this, the team decided this was likely due to a third-party software or firmware error and could not be solved, resulting in less frequent motor releases and more heat generation. To remedy this, a pause functionality was added to the software to release inactive motors and allow the resistors to cool.

Additionally, this code allowed users to send adjustment matrices to fix any discrepancies that may impact its future path. Although this was not how it was initially visualized, the adjustment code serves as a demonstration of the rover's ability to update its path upon new conditions or obstacles, so long as there is a user to send new instructions. In the future, this method could be improved so that it is an autonomous process based on a point cloud generated by the LiDAR.

The other way the team enabled the rover to take additional steps without overheating was to run a full code of 5 steps and then let all the motors release after the termination of the commands. Then the code was re-run so that the rover took 5 more steps in the same manner after cooling down. One other problem that the team noticed was that the middle legs on each side of the rover were not lifting completely off the ground due to the bending of the acrylic shelf after rigorous testing. To resolve this, the team added a cable brace across the shelf perpendicular to the aluminum support brackets. After testing with these adjustments, the rover walked more successfully due to more consistent ground clearance.

The successful six-step walking test took about ten minutes to complete, which the team recognizes is a very slow process. In response, we decreased the wait times in the Python code and increased the step size in the instruction code. However, doing so too much resulted in motor errors and gear slippage, causing the rover to fall before fully executing all steps. As mentioned, there is an ideal wait time for a given set of movements, which was caused by code execution speed combined with the specific motors being used. The team was able to slightly speed up the process by finding a lower wait time that yielded acceptable levels of error.

The team also tried increasing the step size, during which the rover fell over on the initial test. After running this test, it was determined that increasing the step size too much caused the

rover to collapse, but the team continued testing smaller increases to the initial step size. By increasing the step size, the prototype would be able to translate at a faster rate since fewer intermediate motor movements would have to be run. The team was able to double the initial step size. These larger steps yielded a faster translation but were also rougher than the originally tested step size.

The team also conducted simulated walking tests by operating the rover while raised on a test stand. Doing so, we were able to test significantly larger step sizes for the wave gait, as well as testing the tripod gait and zero radius turn. The wave gate was able to successfully operate on the test stand with the initial position of a 45° angle squat of the legs from the vertical. At this squat level, the rover achieved a 26 cm step length. This same step length was demonstrated with the tripod gate. Running the tripod gait requires nearly half the runtime as the wave gait. In addition, the zero-radius turn was operated on the test stand, successfully demonstrating a coordinated movement which would have achieved a stationary turn of the rover on the ground. We were unable to perform these tests on the ground due to stepper motor slippage under larger torque loads, however these tests demonstrate that the inverse kinematics for these movement modes were successful.

10.6 Results

In creating a simplified prototype, the team successfully demonstrated the viability and potential usage of the most basic functionalities that would be implemented on the proposed Lunar rover. We demonstrated the success of the python codes to control specific motors with reasonable precision, especially when run on the test stand. Any step-based instruction can be sent to any of the 18 motors as instructions to actuate the desired leg segment. The upper shoulder motors can rotate the legs by 360 degrees (but wire tangling can occur), the lower

shoulder motors can rotate the legs so that its upper section forms an angle between 0 and 90 degrees, and the knee motors can rotate the legs lower section so that it forms an angle between about 0 and 180 with the secondary rotational plane. The success of the basic function tests as described in the validation and testing section of this report demonstrates the success of the software and electrical systems to support the necessary rover capabilities.

The team also validated the structural simulations by placing the prototype on the ground in a squatted position. It successfully held this position, and there was no noticeable deformation to the components. The team developed a code that produces an instruction matrix to transition the rover from a straight legged configuration to a squatted position of any desired angle. This squatting functionality was simulated in SolidWorks and physically demonstrated in the video repository of Appendix B. Instructing the rover to squat was a necessary functionality because this is the optimal initial position for walking.

The team demonstrated that the prototype could walk using the simplified initial leg orientations and the repeated step code. However, it did need to take cooling breaks to protect the electronics from overheating. To date, the best walking test allowed the rover to successfully take six full steps with each of the legs which corresponded to a total displacement of about eight inches. The team hopes to improve these results by successfully running a walking test where the prototype takes more steps and travels a farther distance. These updated tests will be outlined in the video repository linked in Appendix B as needed. Even though the walking tests did not complete the goals initially established, they proved the rover's capacity to walk as intended to the point where it can be expanded upon for functionality and efficiency improvements.

The team calculated the inverse kinematics of the prototype rover in the initial leg configuration and generated a code to instruct the motors to execute a walking motion. Using this

code, the rover was also able to walk. To date, the rover has been able to take two full steps with this code, but the step distance was too large for the rover to maintain its walking motion. It was also proven to work on the test stand. Therefore, the rover kinematics were validated through these tests. Additional walking tests will be conducted using this code to improve the results, which will be updated in the video repository linked in Appendix B.

Analysis of the FEA simulations stated that the protype would be able to stand on three legs in a tripod configuration. This was validated by placing the rover, under its own weight, in a squatted tripod configuration. However, when dynamic tests were performed, the slipping gears proved to be too steep of a challenge for the legs to overcome. Since the tripod gait could therefore not be tested on the ground, this code was run on the test stand and proven to work under these conditions.

Ultimately, through extensive experimentation and refinement, we addressed the challenges posed by motor constraints by combining inverse kinematics and angle-to-step calculations. In addition to making significant progress in walking abilities, our team successfully validated squatting and turning capabilities into our rover. Despite encountering overheating issues during extended operations, we mitigated these concerns to expedite testing and ensure the reliability of our tests. Our efforts not only resulted in a successful demonstration of the prototype's walking capabilities, but also opened possibilities for improving its performance by adjusting step size and optimizing cooling mechanisms to prevent overheating during prolonged operation.

11. Broader Impacts

The results of this project go beyond the engineering decisions that included in the design of the team's proposed Lunar rover. Therefore, like all engineers the team has assessed the broader impacts of the technology and the stakeholders that may be most influenced by our actions.

11.1 Stakeholders

The scientific goal of the proposed mission is to explore complex Lunar terrain to gather information and potentially samples to inform future missions to the Moon. This could help discover water, ice, or other resources necessary for future exploration. Failure to adequately research the Lunar environment could result in vital information being missed or inaccurate information being used for future mission plans. Depending on the success of the mission, similar robotic systems could be used to improve life on earth by turning the rover into a six-legged rescue robot suited for many environments. Some other possible effects include an implementation of the technology to delivery robots, allowing for delivery of goods and services to remote or hard-to-reach locations. Another possible stakeholder effect could include a changed perception of space travel for either the positive or negative, which could impact the feasibility of future missions. This project can bring in stakeholders as diverse as governments, private space travel companies, industrialists, and more, should the Moon be found suitable for Human habitation. The results of the mission could have a significant and broad area of effect.

11.2 Other Considerations

Environmental concerns are a pressing issue within the entire aerospace industry. The act of propelling anything into orbit results in a very large amount of greenhouse gas emissions, which are poor for the atmosphere's health and contribute to global climate change. Space debris would also be produced during launch, the effects of which cannot be ignored. Increased debris means an increased risk of high-speed collisions with other satellites, as well as, while still very small, the risk of reentering debris harming someone or destroying property.

The team also considered many different materials and opted to make the prototype out of mainly aluminum 6061, a material known for being recycled in very high quantities especially relative to PLA plastic used in other designs. The machine shop that the team used for fabrication is committed to sustainability and commits to recycling or reusing byproducts of the machining process. The proposed rover is made up of Titanium and while this metal is not nearly as recyclable with less than 20% of production coming from recycled titanium recent advances in recycling methods are making it more sustainable (Garbarino, E et al., 2017). The long-term goals of establishing a human base of the Moon may provide sustainability benefits through the discovery and use of Lunar material, rather than exclusively material that is present on earth.

12. Conclusion

The purpose of this project was to help support the development of novel rover mobility solutions for Lunar exploration through terrains that have proven more difficult for traditional wheeled rovers. Background research was conducted on the factors impacting rover mobility on the Lunar surface, particularly at the poles, such as regolith, steep slopes, rocks, and darkness. This, along with an analysis of common rover mobility types, helped the team develop a problem statement to focus the research and a mobility method to test. Of the mobility methods considered, walking was selected for our rover because it proved the most practical option and is already a very well-established topic in robotics. While wheeled rovers generally have better efficiency over flat, even terrain, however, they struggle with excessively sloped, granulated, and rocky terrain. Using legs instead allows the rover to carefully step onto or over specific points to keep stability while moving past obstacles smoothly. Over the course of this project, the team followed the engineering design process to research, develop, fabricate, assemble, test, and improve a simplified prototype to demonstrate the viability of the more complex proposed Lunar rover and the basic implementations of required subsystems.

The team ultimately proposed the development of a walking hexapod rover that uses a periscope with LiDAR to track and avoid obstacles and high and low-res cameras for imaging. The proposed rover also incorporates a foot wheel to swap textures for better compatibility with the terrain. The upper shell opens to expose the solar panels on the undersides of the plates which allows for additional power generation and reduced battery power necessity.

After designing the proposed rover, the team simplified the model and constructed a testable prototype utilizing numerous manufacturing methods including 3D printing, laser cutting, waterjet cutting, and CNC milling. Once these parts were manufactured and the

prototype rover was fully assembled, testing of the basic functionality was conducted. The team was able to verify the simulations, demonstrate viability of the implemented software and electronics, prove squatting and walking capabilities, validate the rover's inverse kinematics, and identify areas for potential expansion.

The prototype served well as a first attempt at a proof of concept, demonstrating some very important capabilities on a limited budget. The team recognizes the need for further design changes and rigorous testing before future implementations but believes that this report serves as a suitable baseline for future work.

References

2022 Challenge Summary: Extreme Terrain Mobility. (2022). BIG Idea Challenge. Retrieved March 13, 2024, from https://bigidea.nianet.org/past-competition-themes/2022-forum-results/

Applied Motion Products. (2024). HT24-108 NEMA 24 High Torque Stepper Motor. Retrieved from https://www.applied-motion.com/s/product/step-motor-high-torqueht24108/01t5i000000xyxTAAQ?name=HT24-108-NEMA-24-High-Torque-Stepper-Motor

Artemis I - NASA. (n.d.). NASA. Retrieved from https://www.nasa.gov/mission/artemis-i/

B2B Applied Motion. (n.d.). Retrieved March 16, 2024, from https://www.applied-motion.com/s/product/40-mm-servo-motor-100-wj01003013000/01t5i000000y08YAAQ?name=J0100-301-3-000-40mm-Servo-Motor-100W.

Bartsch, S., Birnschein, T., Römmermann, M., Hilljegerdes, J., Kühn, D. and Kirchner, F. (2012), Development of the six-legged walking and climbing robot SpaceClimber. J. Field Robotics, 29: 506-532. https://doi.org/10.1002/rob.21418

Beck, K. (2021). Every Rover Landed on the Moon and Mars and the Distance Traveled. Retrieved from https://mashable.com/article/Moon-mars-rover-distance-driven

BETU Servo. (n.d.). BETU 50kg Waterproof Servo. Retrieved from https://betuservo.com/prosdetail_4593303.html

Boston Dynamics. (n.d.). "Spot." Boston Dynamics. Accessed March 16, 2024. https://bostondynamics.com/products/spot/

Bloesch, Michael & Hutter, Marco & Hoepflinger, Mark & Leutenegger, Stefan & Gehring, Christian & Remy, C & Siegwart, Roland. (2012). State Estimation for Legged Robots - Consistent Fusion of Leg Kinematics and IMU. 10.15607/RSS.2012.VIII.003.

Blue Origin. (2023, October 27). Blue Moon Mark 1 Lunar Lander | Blue Origin. Retrieved from https://www.blueorigin.com/blue-Moon/mark-1

Bullet Series 35 Cal. Linear Actuators | Firgelli. (n.d.). Retrieved March 16, 2024, from https://www.firgelliauto.com/products/bullet-series-35-cal-linear-actuators?variant=39510224633927

CLPS Providers - NASA. (n.d.). NASA. Retrieved from https://www.nasa.gov/commercial-Lunar-payload-services/clps-providers/#spacex

Collins, C. L. (2007, September 4-7). Stiffness Modeling and Force Distribution for the All-Terrain Hex-Limbed Extra-Terrestrial Explorer (ATHLETE). Retrieved from https://citeseerx.ist.psu.edu/document?repid=rep1&type=pdf&doi=a18e9d66a3a03b3e5869ba24401f22e1c3a6e82aco

Cyrus, F. (2023, April 12). *NASA Ames Research Center Trajectory Browser*. Retrieved from https://trajbrowser.arc.nasa.gov/example_queries.php

Designing Rovers for the Moon's Extreme Environment. (2022, December 19). Let's Talk Science. Retrieved from https://letstalkscience.ca/educational-resources/backgrounders/designing-rovers-Moons-extreme-environment

Du, Y. (2023). Multi-UAV search and rescue with enhanced A∗ algorithm path planning in 3D environment. International Journal of Aerospace Engineering, 2023 doi.org/10.1155/2023/8614117

Edmund Optics. (n.d.). GS3-U3-89S6C-C 1" FLIR Grasshopper®3 High Performance USB 3.0 Color Camera. Retrieved from https://www.edmundoptics.com/p/gs3-u3-89s6c-c-1-inch-grasshopper-usb-30-color-camera/33125/

El Hansali, H., & Mohammed, B. (2017). Gait Kinematic Modeling of a Hexapod Robot. International Review of Mechanical Engineering (IREME), 11, 200. doi:10.15866/ireme.v11i3.10987

Firefly Aerospace. (2024, February 15). Blue Ghost - Firefly Aerospace. Retrieved from https://fireflyspace.com/blue-ghost/

Garbarino, E., Ardente, F., Blagoeva, D. et al. (2017). Critical raw materials and the circular economy – Background report.

Government of Canada. (2023, July 12). The Artemis II mission. Retrieved from https://www.asc-csa.gc.ca/eng/missions/artemis-ii/mission.asp

Gupta, P. A. (2023, May 10). I2C Communication Protocol. Retrieved from https://www.geeksforgeeks.org/i2c-communication-protocol/

Gurel, Canberk Suat. (2017, June 29). Fundamentals of Hexapod Robot. *Hackaday.Io*, Hackaday, hackaday.io/project/21904-hexapod-modelling-path-planning-and-control/log/62326-3-fundamentals-of-hexapod-robot.

Haidar, J. (2020). Terrain Mapping and Pose Estimation for Polar Shadowed Regions of the Moon.Retrieved from https://www.hou.usra.edu/meetings/isairas2020fullpapers/pdf/5070.pdf.

Hambleton, K. (2022, November 16). Liftoff! NASA's Artemis I Mega Rocket Launches Orion to Moon. Retrieved from NASA: https://www.nasa.gov/news-release/liftoff-nasas-artemis-i-mega-rocket-launches-orion-to-Moon/

Hou, J., et al. (2022). A heuristic control framework for heavy-duty hexapod robot over complex terrain. IET Cyber-Systems & Robotics, 4(4), 322–330. doi:10.1049/csy2.12064

Hu, N., Li, S., Zhu, Y. et al. Constrained Model Predictive Control for a Hexapod Robot Walking on Irregular Terrain. J Intell Robot Syst 94, 179–201 (2019). https://doi.org/10.1007/s10846-018-0827-3

J. Sun, J. Ren, Y. Jin, B. Wang and D. Chen, "Hexapod robot kinematics modeling and tripod gait design based on the foot end trajectory," 2017 IEEE International Conference on Robotics and Biomimetics (ROBIO), Macau, Macao, 2017, pp. 2611-2616, doi:10.1109/ROBIO.2017.8324813.

Jones, A. (n.d.). What Is the Moon Made Of? Retrieved from NASA: https://Moon.nasa.gov/inside-and-out/composition/overview/

Kim, H. W., & Jung, S. (2020, October 21). Design and Control of a Sphere Robot Using a Control Moment Gyroscope Actuator for Navigation. Retrieved from Springer Link: https://link.springer.com/article/10.1007/s12555-019-0526-2

Kolenkiewicz, R., & Putney, W. (1965, November). Injection Conditions for Lunar Trajecties. Retrieved from NASA: https://ntrs.nasa.gov/api/citations/19660007973/downloads/19660007973.pdf

Lubbe, E., Withey, D., & Uren, K. R. (2015). State estimation for a hexapod robot. In 2015 IEEE/RSJ International Conference on Intelligent Robots and Systems (IROS) (pp. 6286-6291). Hamburg, Germany. doi:10.1109/IROS.2015.7354274

Lunar Landers | Astrobotic Technology. (2024, January 12). Astrobotic. Retrieved from https://www.astrobotic.com/Lunar-delivery/landers/

Lunar Rocks. (n.d.). Retrieved from Smithsonian: https://airandspace.si.edu/explore/stories/Lunar-rocks

McManamon, P. F. (2019). LiDAR technologies and systems. Society of Photo-optical Instrumentation Engineers.

Merancy, N. (2022, September 2). Houston We Have A Podcast: Artemis Mission Design. [Interview by G. Jordan].

Ma, J.; Qiu, G.; Guo, W.; Li, P.; Ma, G. Design, Analysis and Experiments of Hexapod Robot with Six-Link Legs for High Dynamic Locomotion. Micromachines 2022, 13, 1404. doi.org/10.3390/mi13091404

Microstepping Stepper Drive: 5.6A per phase, 2-phase output, 24-48 VDC, 400 to 25600 steps per revolution (PN# DM556E) | AutomationDirect. (n.d.). Retrieved March 16, 2024, from https://www.automationdirect.com/adc/shopping/catalog/motion_control/stepper_systems/stepper_drives/dm556e

NASA. (2003). Lunar Regolith. Retrieved from https://curator.jsc.nasa.gov/Lunar/letss/regolith

NASA. (2022). COBRA: Crater Observing Bio-inspired Rolling Articulator. Retrieved from https://bigidea.nianet.org/wp-content/uploads/Northeastern-University-2022-Big-Idea-Poster.pdf

NASA. (2023). NASA Selects Geology Team for the First Crewed Artemis Landing. Retrieved from https://www.nasa.gov/general/nasa-selects-geology-team-for-the-first-crewed-artemis-Lunar-landing/

NASA. (2024, March 8). Artemis - NASA. Retrieved from https://www.nasa.gov/humans-in-space/artemis/

NASA. (n.d.-a). About LRO. NASA. Retrieved from https://science.nasa.gov/mission/lro/about/

NASA. (n.d.-b). Earth Fact Sheet. Retrieved March 16, 2024, from https://nssdc.gsfc.nasa.gov/planetary/factsheet/earthfact.html

NASA. (n.d.-c). Hedgehog Systems. Retrieved from https://www-robotics.jpl.nasa.gov/how-we-do-it/systems/hedgehog/

NASA. (2009, April 20) Testing of the Lunar Reconnaissance Orbiter. Retrieved from https://svs.gsfc.nasa.gov/10425/

NASA. (n.d.-d). Weather on the Moon. Retrieved March 16, 2024, from https://science.nasa.gov/Moon/weather-on-the-Moon/

NASA. (n.d.-e). DuAxel. NASA Jet Propulsion Laboratory (JPL). Retrieved March 16, 2024, from https://www.jpl.nasa.gov/robotics-at-jpl/duaxel

National Aeronautics and Space Administration. (2020). NASA's Lunar Exploration Program Overview. In NASA APPEL. Retrieved March 13, 2024, from https://www.nasa.gov/wp-content/uploads/2020/12/artemis_plan-20200921.pdf?emrc=f43185

O'Brien, K. (2022, October 28). Space Launch System Engines: Launching Artemis Astronauts to the Moon. Retrieved from NASA: https://www.nasa.gov/image-article/space-launch-system-engines-launching-artemis-astronauts-Moon/

Online, F. (2023, October 5). High Reflective Coatings. Avantier Inc. https://avantierinc.com/resources/application-note/high-reflective-coatings/

Papež, N., Dallaev, R., Ţălu, Ş., & Kaštyl, J. (2021). Overview of the Current State of Gallium Arsenide-Based Solar Cells. Materials (Basel), 14(11), 3075. doi:10.3390/ma14113075

Peraire, W. J. (2008). Orbit Transfers and Interplanetary Trajectories. Retrieved from MIT: https://ocw.mit.edu/courses/16-07-dynamics-fall-2009/e6393974ce4ed22b095f2e1d1a6a8e81_MIT16_07F09_Lec17.pdf

Piher Sensing Systems. (n.d.). Contactless sensor PST-360. Retrieved from https://assets.alliedelec.com/v1591351426/Datasheets/cc0e21f967c6f7a051005eb7627798c6.pdf

Planetary Gearbox - 200:1 Ratio | J53-200. (n.d.). Retrieved March 16, 2024, from https://www.ondrivesus.com/in-line-gearboxes/in-line-spur-gear/j53-200

Rincon, P. (2015, March 19). Lava tubes safe enough for Moon base Published. Retrieved from BBC: https://www.bbc.com/news/science-environment-31953052

Sharp, T. (2023). What is the Temperature on the Moon? Retrieved from https://www.space.com/18175Moontemperature.

SpaceCloud iX5-106 | satsearch. (n.d.). Retrieved March 16, 2024, from https://satsearch.co/products/unibap-ix5100

Suomela , J. (2006). Ball-Shaped Robots: An Historical Overview and Recent Developments at TKK. Retrieved from https://link.springer.com/chapter/10.1007/978-3-540-33453-8_29

TeachEngineering. (n.d.). Design Process. Retrieved from https://www.teachengineering.org/populartopics/designprocess

the Moon. Retrieved from https://www.esa.int/Enabling_Support/Preparing_for_the_Future/Discovery_and_Preparation/En_route_to_exploring_Lunar_cavec

Urakubo, T., & Oki, M. (2012). Development of a spherical rolling robot equipped with a gyro. Retrieved from IEEE Xplore: https://ieeexplore.ieee.org/document/6284376

Velarray M1600. (n.d.). Retrieved March 16, 2024, from https://velodynelidar.com/products/velarray-m1600/

Weber, B. (n.d.). Hohmann Transfer. Retrieved from https://orbital-mechanics.space/orbital-maneuvers/hohmann-transfer.html

Whittaker, William. “Technologies Enabling Exploration of Skylights, Lava Tubes and Caves.” NASA Innovative Advanced Concepts (NIAC) Phase I, NASA, 14 Sept. 2012, www.nasa.gov/wp-content/uploads/2017/07/niac_2011_phasei_whittaker_lavatubesandcaves_tagged.pdf.

Why has it been 50 years since humans went to the Moon? (n.d.). National Air and Space Museum. Retrieved from https://airandspace.si.edu/stories/editorial/why-50-years-since-humans-went-Moon

Williams, D. R. (2021, December 20). Moon Fact Sheet. Retrieved from NASA: https://nssdc.gsfc.nasa.gov/planetary/factsheet/Moonfact.html

Williams, D. R. (2023, June 5). Earth Fact Sheet. Retrieved from NASA: https://nssdc.gsfc.nasa.gov/planetary/factsheet/earthfact.html

Zangrandi, Marco & Arrigoni, Stefano & Braghin, Francesco. (2021). Control of a Hexapod Robot Considering Terrain Interaction.

Appendix A: GitHub Repository

https://github.com/MikeDoesCodeKinda/Lunar-Rover-MQP.git

Appendix B: Video Repository

https://sites.google.com/view/vectorrepository/home